University of Rome "Tor Vergata"

Consiglio Nazionale delle Ricerche

UNIVERSITY OF ROME "TOR VERGATA"

Dr. Stefania Siracusano

Ph.D. course in *"Materials for Environment and Energy"*

(XXII cycle)

Development and characterization of catalysts for electrolytic hydrogen production and chlor – alkali electrolysis cells

A.A. 2009/2010

Supervisor:

Dott. Antonino Salvatore Aricò

Director:

Prof. Silvia Licoccia

Contents

SUMMARY

Development and characterization of catalysts for electrolytic hydrogen production and chlor – alkali electrolysis cells

The topics of this PhD thesis are concerning with Chlor alkali electrolysis and PEM water electrolysis.

- *Chlor alkali electrolysis*

The industrial production of chlorine is today essentially achieved through sodium chloride electrolysis, with only a minor quantity coming from hydrochloric acid electrolysis. The main problem of all these processes is the high electric energy consumption which usually represents a substantial part of the total production cost. Therefore, in order to improve the process, it is necessary to reduce the power consumption. The substitution of the traditional hydrogen-evolving cathodes with an oxygen-consuming gas diffusion electrode (GDE) involves a new reaction that reduces the thermodynamic cell voltage and leads to an energy savings of 30-40%.

My research activity was addressed to the investigation of the oxygen reduction at gas-diffusion electrodes as well as to the surface and morphology analysis of the electrocatalysts. Specific attention was focused on deactivation phenomena involving this type of GDE configuration. The catalysts used in this study were based on a mixture of micronized silver particles and PTFE binder. In this study, fresh gas diffusion electrodes were compared with electrodes tested at different times in a chlor-alkali cell. Electrode stability was investigated by life-time tests. The surface of the gas diffusion electrodes was analyzed for both fresh and used cathodes by scanning electron microscopy and X-ray photoelectron spectroscopy. The bulk of gas diffusion electrodes was investigated by X-ray diffraction and thermogravimetric analysis.

- *PEM water electrolysis*

Water electrolysis is one of the few processes where hydrogen can be produced from renewable energy sources such as photovoltaic or wind energy without evolution of CO_2. In particular, an SPE electrolyser is considered as a

promising methodology for producing hydrogen as an alternative to the conventional alkaline water electrolysis. A PEM electrolyser possesses certain advantages compared with the classical alkaline process in terms of simplicity, high energy efficiency and specific production capacity. This system utilizes the well know technology of fuel cells based on proton conducting solid electrolytes. Unfortunately, electrochemical water splitting is associated with substantial energy loss, mainly due to the high over-potentials at the oxygen-evolving anode. It is therefore important to find the optimal oxygen-evolving electro-catalyst in order to minimize the energy loss.

Typically, platinum is used at the cathode for the hydrogen evolution reaction (HER) and Ir or Ru oxides are used at the anode for the oxygen evolution reaction (OER). These metal oxides are required, compared to the metallic platinum, because they offer a high activity, a better long-term stability and less efficiency losses due to corrosion or poisoning.

My work was mainly addressed to a) the synthesis and characterisation of IrO_2 and RuO_2 anodes; b) conducting Ti-suboxides support based on a high surface area.

a) Nanosized IrO_2 and RuO_2 catalysts were prepared by using a colloidal process at 100°C; the resulting hydroxides were then calcined at various temperatures. The attention was focused on the effect of thermal treatments on the crystallographic structure and particle size of these catalysts and how these properties may influence the performance of oxygen evolution electrode. Electrochemical characterizations were carried out by polarization curves, impedance spectroscopy and chrono-amperometric measurements.

b) A novel chemical route for the preparation of titanium suboxides (Ti_nO_{2n-1}) with Magneli phase was developed. The relevant characteristics of the materials were evaluated under operating conditions, in a solid polymer electrolyte (SPE) electrolyser, and compared to those of the commercial Ebonex®. The same IrO_2 active phase was used in both systems as electrocatalyst.

CHAPTER 1
Introduction to Electrolysis Processes

1.1 Introduction to Chlor-Alkali Electrolysis

The production of chlorine and caustic soda by electrolysis of aqueous solutions of sodium chloride or brine is one of the most important electrochemical processes used in the industrial field. Chlorine and caustic soda are the base elements of 60% of Europe's chemical industry production.

Chlorine (Cl) can not exist naturally by itself because it is highly reactive, but it is one of the most plentiful elements in the world. It is required for the synthesis of various products in many chemical processes. It is used in industries for water treatment, plastics fabrication, acids production and many more.

Caustic soda (sodium hydroxide – NaOH) is a very versatile alkali and is used as a reactant in the manufacturing of various sodium compounds. It is used for the synthesis of sodium hypochlorite, which is utilized to produce various bleaches and disinfectants. Caustic soda is used in many industries: to control pH, to breakdown cellulose, in cleaning operations, etc. The main industries where it is used include rayon cellophane, soap and paper.

Hydrogen is the other major product formed in the chlor-alkali electrolysis process, which as well known has good potentialities as energy vector. Yet, to reduce the energy consumption oxygen can be fed to the cathode and oxygen reduction occurs instead of hydrogen evolution.

1.2 Chlor-Alkali Electrolyzer Technology

Chlorine is produced electrolytically using three types of electrolytic cells: mercury cells, diaphragm cells and membrane cells. The main difference in these technologies is attributed to the manner by which the anolyte and the catholyte streams are separated to ensure generation of pure products. Separation is achieved in a diaphragm cell by a separator, and in a membrane cell by an ion-exchange membrane. In mercury cells, the cathode is used as a separator by

forming an alloy of sodium and mercury (sodium amalgam) which is subsequently reacted with water to form sodium hydroxide and hydrogen in a separate reactor.

The anode in all technologies is titanium metal coated with an electrocatalytic layer of mixed oxides. All modern cells (since the 1970's) use these so-called "dimensionally stable anodes" (DSA)[1,2]. Earlier cells used *carbon* based anodes. The cathode is typically steel in diaphragm cells, nickel in membrane cells, and mercury in mercury cells.

1.2.1 Mercury Cells

The mercury cell has steel bottoms with rubber-coated steel sides, as well as end boxes for brine and mercury feed. Metal based anodes are on the top, and mercury (which forms the cathode of the cell) is in the inner of the bottom. The current flows from the steel bottom to the flowing mercury.

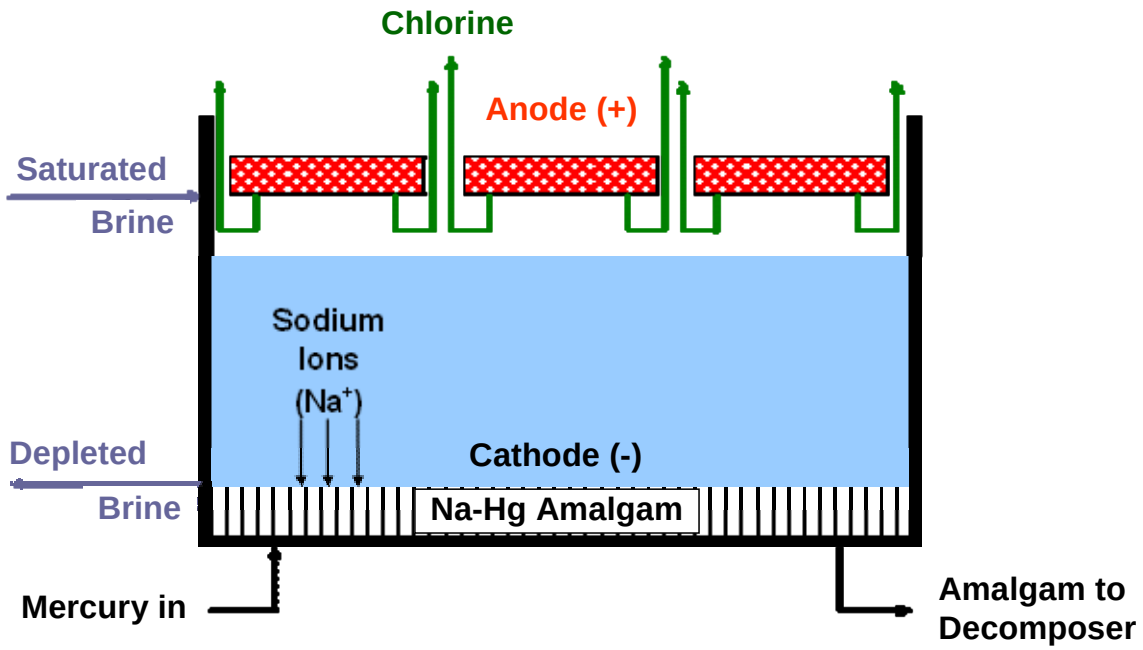

Figure 1. Mercury cell [3]

Satured brine, fed from the end box, is electrolyzed at the anode to produce the chlorine gas. The sodium ion generated reacts with the mercury to form sodium amalgam (an alloy of mercury and sodium), which flows out of the end box to a vertical cylindrical tank. About 0.25% to 0.5% sodium amalgam is

produced in the cell. The sodium amalgam reacts with water in the decomposer and produces caustic soda and hydrogen. The caustic soda then flows out of the decomposer as 50% caustic. The unreacted brine flows out of the exit end box.

1.2.2 Diaphragm Cells

The diaphragm cell is a rectangular box with metal anode supported and metal screen as cathode. Asbestos, dispersed as a slurry, is vacuum deposited onto the cathodes, forming a diaphragm.

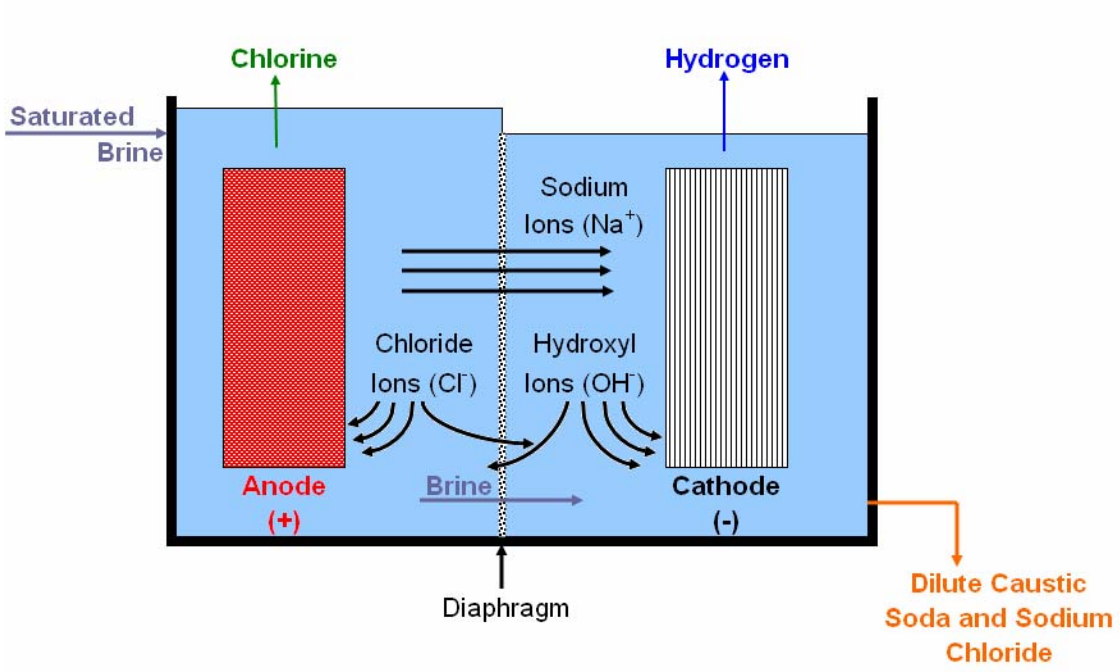

Figure 2. Diaphragm cell [3]

Saturated brine enters the anode compartment and the chlorine gas, liberated at the anode during electrolysis, exits from the anode compartment. It is partially saturated with water vapor at a partial pressure of water over the anolyte. The sodium ions are transported from the anode compartment to the cathode compartment, by the flow of the solution and by electromigration. In the cathode, the sodium ions combine with the hydroxyl ions generated during the formation of the hydrogen from the water molecules. The diaphragm resists the back migration of the hydroxyl ions, which would otherwise react with the

chlorine in the anode compartment. In the cathode compartment, the concentration of the sodium hydroxide is ~12%, and the salt concentration is ~14%. There is also some sodium chlorate formed in the anode compartment, dependent upon the pH of the anolyte.

1.2.3 Membrane Cells

In a membrane cell, an ion-exchange membrane separates the anode and cathode compartments. The separator is generally a bi-layer membrane made of perfluorocarboxylic and perfluorosulfonic acid-based films.

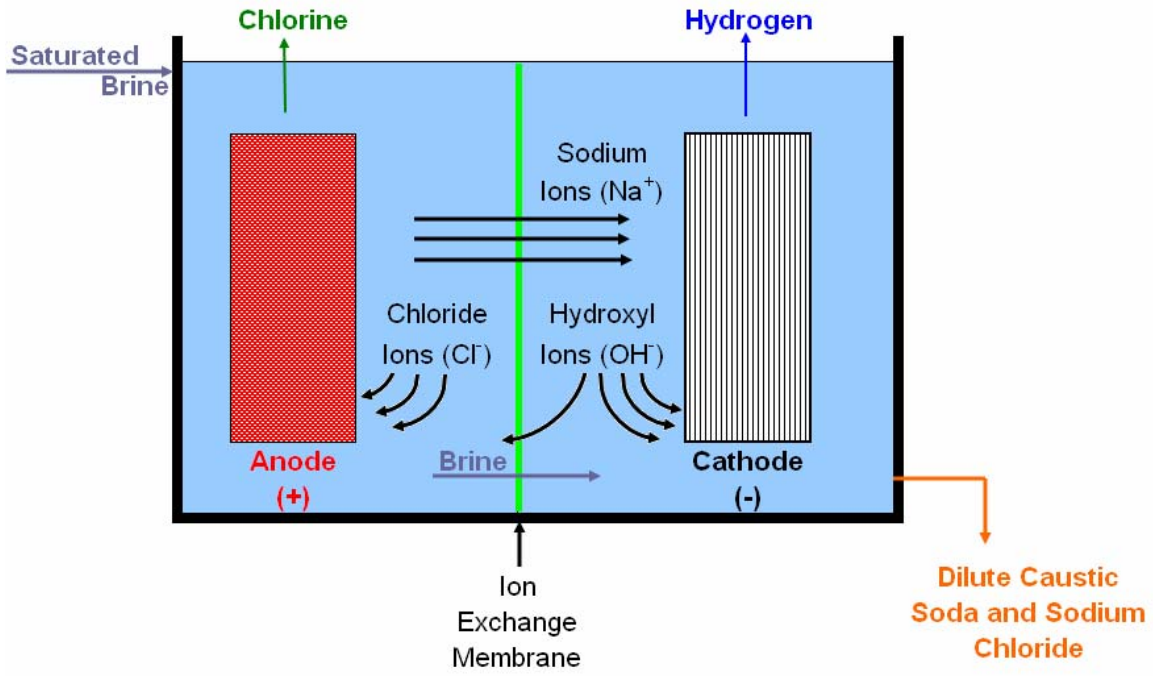

Figure 3. Membrane cell [3]

The saturated brine is fed to the anode compartment where chlorine is liberated, and the sodium ion migrates to the cathode compartment. Unlike in the diaphragm cells, only the sodium ions and some water migrate through the membrane. The unreacted sodium chloride and other inert ions remain in the anolyte. About 30-32% caustic soda is fed to the cathode compartment, where sodium ions react with hydroxyl ions produced during the hydrogen gas evolution from the water molecules. The hydrogen gas, saturated with water, exits

from the catholyte compartment. Only part of the caustic soda product is withdrawn from the cathode compartment. The remaining caustic is diluted to ~32% and returned to the cathode compartment.

1.3 Membrane Cells: Substitution of Traditional Hydrogen-Evolving with an Oxygen-Consuming Cathodes

The production of chlorine and caustic soda by electrolysis is a process that required an high-energy consumption. The total energy requirement is for instance 2% in the USA and 1% in Japan of the gross electric power generated to maintain this process by the chlor-alkali industry [4-6].

Chlor-alkali cells produce two commodity chemicals, chlorine (Cl_2) and caustic soda (NaOH), traditionally through electrolysis of water and salt:

$$2H_2O + 2NaCl \rightarrow 2NaOH + H_2 + Cl_2$$

Not only does this reaction have high energy requirements, but the hydrogen produced is of relatively low value. Technology based on this reaction is mature, and no significant energy savings can result from further membrane cell development without a change in the fundamental approach to chlor-alkali electrolysis.

The new approach to chlor-alkali electrolysis is based on the substitution of oxygen-consuming cathodes in place of conventional hydrogen-evolving cathodes. Replacing hydrogen-evolving cathodes with oxygen cathodes significantly reduces the cell voltage and leads to an energy savings of 30-40% [7-27].

The new reaction has lower energy requirements and also eliminates the hydrogen byproduct present in conventional cells.

The figure 4 explains schematically the relationship between the conventional membrane chlor-alkali electrochemical reactor (ECR) (a), and the modified chlor-alkali ECR employing an oxygen cathode, (b).

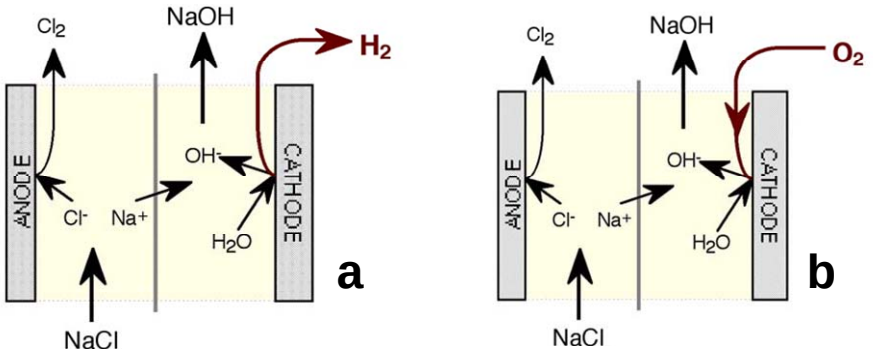

Figure 4. Conventional membrane (a) and the modified (b) chlor-alkali electrochemical reactor [28]

The oxygen electrode belongs to the family of "gas diffusion electrodes." In these electrodes, the gaseous reactant diffuses through a thin liquid film to reach the catalyst site. This process must occur with minimal transport losses. Furthermore, a thin layer of the catalyst has to be applied in a highly optimized way to ensure effective catalyst utilization and high reaction rates.

The above two requirements must be fulfilled by the initial cathode composition and structure, and must also be maintained throughout long-term cell operation. This second requirement is particularly demanding in chlor-alkali cells because the oxygen cathode is highly susceptible to the possible extremes of "flooding" (by the alkaline solution in the cathode compartment) or excessive dry-out of the catalyst layer (resulting in loss of electrocatalytic activity)

Chlorine and caustic soda, obtained by the electrolysis of an aqueous solution of sodium chloride, are products of the chlor-alkali electrochemical process. Total cell reaction proceeds through the following anodic and cathodic half-cell reactions:

Anode $2Cl^- \rightarrow Cl_2 + 2e^-$ E = 1.358 V vs. NHE (1)

In alkaline solutions,

Cathode $2H_2O + 2e^- \rightarrow 2OH^- + H_2$ E = - 0.828 V vs. NHE (2)

Therefore, the overall reaction is:

$2H_2O + 2Cl^- \rightarrow Cl_2 + 2OH^- + H_2$ E = 2.186 V (3)

The thermodynamic potential difference ΔE (decomposition voltage) of total electrode reactions is approximately 2.2 V.

The substitution of traditional hydrogen-evolving cathodes with an oxygen-consuming GDE results in the formation of caustic and chlorine without hydrogen:

Anode reaction: $2Cl^- \rightarrow Cl_2 + 2e^-$ E = + 1.358 V vs. NHE (1)

Cathode reaction: $2H_2O + O_2 + 4e^- \rightarrow 4OH^-$ E = + 0.401 V vs. NHE (4)

Overall reaction: $2H_2O + O_2 + 2Cl^- \rightarrow Cl_2 + 4OH^-$ E = 0.957 V (5)

The equilibrium potential of reactions (2) and (4) is -0.82 and +0.40 V vs. NHE, respectively. Thus, the equilibrium potential of the oxygen reduction reaction vs. NHE (4) is about 1.2 V higher than that of the hydrogen evolution reaction (2). Therefore, replacing hydrogen-evolving cathodes with oxygen cathodes significantly reduces thermodynamic cell voltage and leads to an energy savings.

1.4 Introduction to Water Electrolysis

Electrolysis of water is the dissociation of water molecules into hydrogen and oxygen gas. Water is subjected to electrical power and the result is hydrogen and oxygen.

$$2H_2O + \text{energy} \rightarrow 2H_2 + O_2 \qquad E° = 1.229\ V \qquad (6)$$

There are three principal types of water electrolyzer: alkaline (referring to the nature of its liquid electrolyte), proton-exchange membrane (referring to its solid polymeric electrolyte), and solid-oxide (referring to its solid ceramic electrolyte). The alkaline electrolyzer currently dominates global production of electrolytic hydrogen. However, electrolyzers using a solid polymer electrolyte (SPE) and electrolyzers using solid-oxide electrolyte (SOE) have recently received considerable attention because they offer the possibility of achieving higher energy efficiencies.

1.4.1 Alkaline Electrolyzer

In alkaline electrolyzers a liquid electrolyte is used, typically a 30% potassium or sodium hydroxide solution, for transferring hydroxyl ions. Alkaline

electrolyzers operate at relatively low current densities of < 0.4 A/cm^2 and conversion efficiencies range from 60-90%. Without auxiliary purification equipment, gas purities are typically 99.8% and 99.2% for H_2 and O_2 respectively. Several large alkaline electrolyzers of > 100MW have been applied (e.g. in Egypt and Congo to utilise hydropower to generate 'renewable hydrogen'). A modern alkaline electrolyser will achieve an efficiency of ~ 90% (consuming about 4kWh of electricity per m^3 of H_2 generated) and deliver gas at up to 30bar without auxiliary compression. However, a significant post-electrolysis electricity consumption is incurred for gas compression to deliver H_2 and O_2 at the pressures required by industry and for storage on-board hydrogen vehicles (350-700 bar).

The key factors favouring the alkaline electrolyzer are that it obviates the need for expensive platinum-based catalysts, in fact, this system use nickel coated with a film of platinum as the cathode catalyst and nickel or copper coated with metal oxides (Mn, Ru or W) as the anode catalyst. The electrode reactions that occur in such systems are given by equations:

Anode: $2\,OH^-\,(aq) \rightarrow 1/2O_2\,(g) + H_2O\,(l) + 2e^-$ (7)

Cathode: $2\,H_2O\,(l) + 2e^- \rightarrow H_2\,(g) + 2OH^-\,(aq)$ (8)

Overall reaction: $H_2O\,(l) \rightarrow H_2\,(g) + 1/2O_2$ (6)

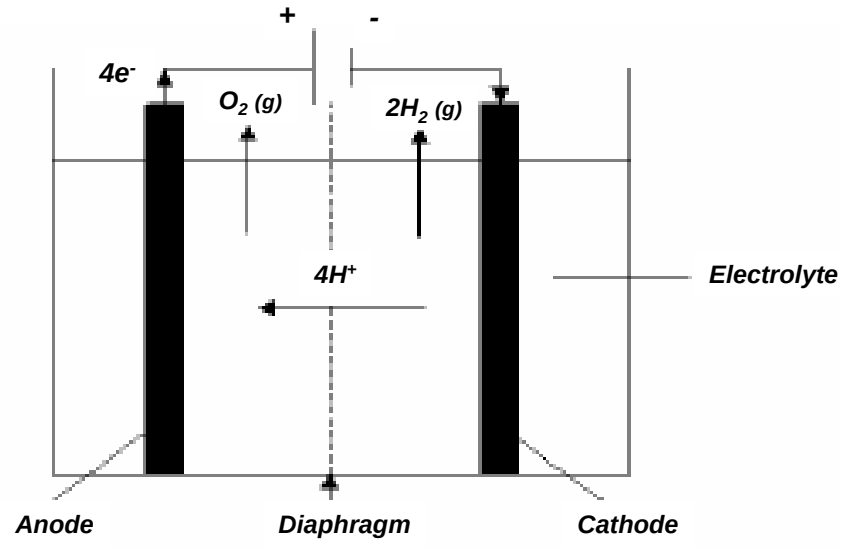

Figure 5. Alcaline Electrolyzer [29]

1.4.2 Solid Oxide Electrolyte Electrolyzer

The operation of a solid-oxide electrolyzer depends on a solid ceramic electrolyte (zirconia/ceria), which at temperatures of 800-1000°C transfers oxygen ions (O^{2-}). The solid oxide electrolyzer requires a source of high-temperature heat. By operating at elevated temperatures, the heat input meets some of the energetic requirement for electrolysis and so less electricity is required per m^3 of H_2 generated, compared with the other electrolyzer technologies. However, to date, prototype solid-oxide electrolyzer units have not achieved useful operational lives and substantial engineering problems exist with respect to thermal cycling and gas sealing.

The materials are similar to those developed for solid oxide fuel cells, namely, an yttrium stabilised zirconia (YSZ) electrolyte, a nickel containing YSZ anode, and a cathode made from lanthanum. In a SOE electrolyzer the following takes place: water is supplied to the cathode, oxygen is transported through the electrolyte and hydrogen is produced at the cathode. The electrode reactions that occur in such systems are given by equations:

Anode: $O^{2-} \rightarrow 1/2O_2\ (g) + 2e^-$ (9)

Cathode: $H_2O\ (l) + 2e^- \rightarrow H_2\ (g) + O^{2-}$ (10)

Overall reaction: $H_2O\ (l) \rightarrow H_2\ (g) + 1/2O_2\ (g)$ (6)

The efficiency of a SOE electrolyzer depends on the operating temperature. Efficiencies based on electrical input alone are reported to be between 85 and 90%.

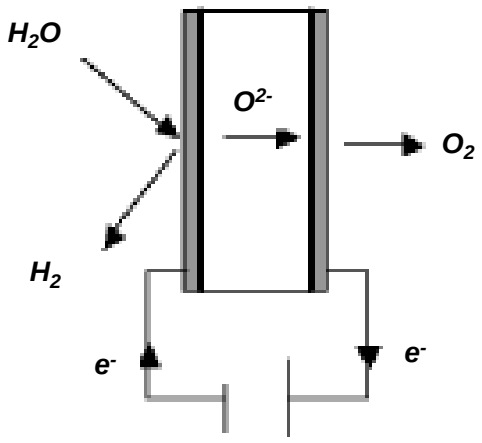

Figure 6. Solid oxide electrolyte electrolyzer [29]

1.4.3 Solid Polymer Electrolyte (SPE) Electrolyzer

Solid polymer electrolyte (SPE) electrolyzer, also known as proton exchange membrane (PEM) electrolyzers, have received considerable attention in latest years. The technology is based on recent advances in PEM fuel cell technology. In this system the electrolyte is a solid ion conducting membrane. The membrane allows the H^+ ion to transfer from the anode side of the membrane to the cathode side, where it forms hydrogen. The SPE membrane also serves to separate the hydrogen and oxygen gasses. A SPE electrolyzer requires expensive noble metals such as platinum black as cathode catalyst and iridium or ruthenium oxide as anode catalyst. SPE electrolyzer units can typically operate at high current densities (1-2 A cm^{-2}) and achieve efficiencies of 60-80%. The main chemical reactions occurring at the two electrodes are:

Anode: $H_2O\ (l) \rightarrow 1/2O_2\ (g) + 2H^+ + 2\ e^-$ (11)

Cathode: $2H^+ + 2\ e^- \rightarrow H_2\ (g)$ (12)

Global reaction: $H_2O\ (l) \rightarrow H_2\ (g) + 1/2O_2\ (g)$ (6)

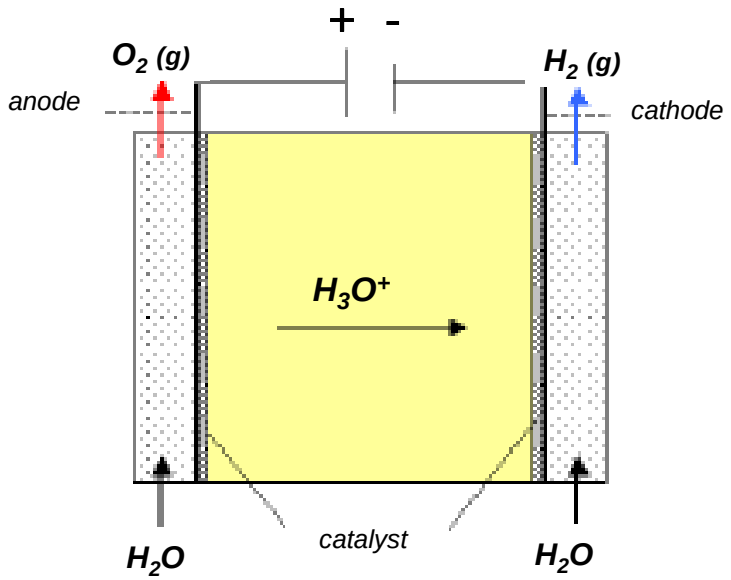

Figure 7. Solid polymer electrolyte electrolyzer [29]

1.5 Theory and Background to SPE Electrolyzer

Solid Polymer Electrolyte (SPE) water electrolysis is considered a promising technology method to produce hydrogen from renewable energy resources such as wind, photovoltaic (PV) and hydropower with a high degree of purity [30]. SPE

water electrolyzers utilize a proton exchange membrane between the cathode and the anode and an electrical potential larger than the thermoneutral potential for water splitting ($V = \Delta H/nF = 1.47$ V at 80°C) [31] is applied across the electrochemical cell to induce electrochemical reactions at both electrodes. The reaction kinetic for water splitting is mainly determined by the applied electrochemical potential, temperature, anode and cathode electrocatalyst and membrane resistance.

Water electrolysis in a proton exchange membrane device is characterized by high efficiencies and suitable current density even at low temperatures. Electrolysis systems based on PEMs have a number of advantages in comparison to the traditional alkaline electrolyzers, such as ecological cleanliness, considerably smaller mass–volume characteristics and, essentially, a high degree of gases purity [30, 32-33]. There is also the opportunity to obtain compressed gases directly from the electrolyzer at an increased level of safety [30, 32-33]. The main disadvantage of PEM electrolysis is the high cost, which is mainly due to the use of noble metal catalysts, perflurinated membranes etc. [30, 32-33].

The high anode overpotential is the limiting factor for the whole process and, together with the large reversible potential, it mainly contributes to the energy supply necessary to run the PEM electrolyzer. It is therefore important to find an optimal oxygen-evolution electro-catalyst in order to minimize the energy loss. Several investigations have shown that noble metal oxides, particularly Rutile-type oxides like RuO_2, IrO_2 are considerably better as oxygen-evolution electrodes than the corresponding metals as well as other noble-metals [34-37]. Some of these metal oxides offer high activity, appropriate long-term stability and small efficiency losses due to corrosion or poisoning [38-47]. One of the main disadvantages of elemental metals like Pt is, beside the modest specific activity for oxygen evolution, their easy electrochemical sintering at high operating potentials.

The first SPE electrolyzer was developed in 1966 by General Electric Company (USA) [48-49]. These units were initially developed to provide oxygen for aerospace and submarines but the design readily be adapted and upscaled to

large hydrogen generation plants. Such electrolyzers were created for the special purposes (spacecrafts, submarines, etc.), and also for needs of the civil industry.

Today SPE electrolyzers are used in producing high purity hydrogen for fuel cells, hydrogen welding, metallurgy of especially pure metals and alloys, manufacture of pure substances for the electronics industry, analytical chemistry [30]

1.6 Principles of SPE Electrolyzer

The SPE electrolyzer converts electrical energy into chemical energy by splitting water to its constituents, hydrogen and oxygen. The gases can then be stored in suitable containers. The stored hydrogen can be directly burned inside an internal combustion engine or used in a fuel cell to power automobiles, as well as to provide electrical energy in rural areas or during peak demands. Hydrogen produced by SPE electrolyzer is with high degree of gas purity, when the electricity needed to run the SPE electrolyzer is generated by renewable sources, such as wind, photovoltaic (PV) or hydropower. The electricity can be supplied during off-peak times when extra electricity is available.

When hydrogen is produced by water electrolysis process, half the number of moles of oxygen is produced simultaneously as a by-product of hydrogen. If large quantities of hydrogen are required to be produced from renewable resources by electrolysis process, by-product oxygen also will be produced in large scale. In such the situation, by-product oxygen should be fully utilized, because oxygen is an important industrial gas utilized in many processes such as combustion, semiconductor production, wastewater treatment, etc. The effective utilization of oxygen would improve energy efficiency of some industrial processes [50].

Water is introduced at the anode side, which is connected to a power source. A potential is applied to the anode, which splits the water into protons, electrons and oxygen. Reactions that occur at the electrodes are following reported:

Anode:

$H_2O \rightarrow 1/2O_2 + 2\,H^+ + 2\,e^-$ $\quad E°\ (25°C) = 1.229\ V$ (11)

The oxygen produced is removed and stored using a suitable method, while protons permeate through the solid polymer membrane to the cathode side. Electrons follow a path an external circuit to the cathode and recombine with the protons to form hydrogen gas, which can be removed and stored, using a suitable method. This reaction is subsequent reported:

Cathode:

$2\,H^+ + 4\,e^- \rightarrow H_2$ $\quad E°\ (25°C) = 0.00\ V$ (12)

Therefore, the overall cell reaction is:

Global reaction:

$2\,H_2O \rightarrow 2\,H_2 + O_2$ $\quad E°\ (25°C) = 1.229\ V$ (6)

1.7 Proton Exchange Membrane (PEM)

The proton exchange membrane used for SPE electrolyzers consist of a linear polymer of fluorocarbon and a small percentage of pending acid group (not more than 10 mol%). The chemical formula is:

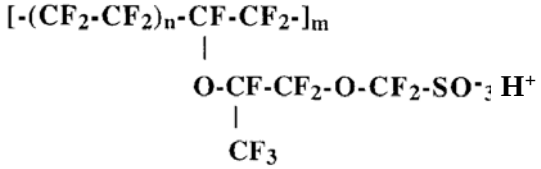

Figure 8. Chemical formula of the membrane

The acid groups are mainly sulfonic acid or carboxylic acid and in them the hydrogen ion may be partially or totally exchanged by all kinds of cations or cationic groups. The polymeric chain is chemically and thermally very stable and very suitable for very thin membranes while the acid groups are very appropriate for ion exchange [51, 52]. Dupont was the first one in 1962 to developed a perfluorosulfonic membrane which was called commercially, Nafion®. These membranes are used principally for fuel cells applications [53-58].

During the electrolysis of water the PEM serves as a solid electrolyte that conducts protons and also serves a separator of the produced gases. When the membrane is saturated with water it becomes an excellent ionic conductor. Ion conduction is brought about by the mobility of protons, which pass from one sulfonic acid group to the other.

The inherent advantage of SPE technology over the alkaline are clearly established: greater safety and reliability are expected since no caustic electrolyte is circulated in the cell stack; possibility to operate at high differential pressures, resulting in the production of pressurized gases, thus eliminating the auxiliary gas compression; the possibility of operating cells up to several A cm^{-2} with typical thicknesses of a few millimetres is afforded.

The main drawback of the Nafion membranes is the high cost. In fact, the cost of the electrodes added to the cost of the solid electrolyte seriously limits the development of SPE water electrolyzer in the industry [39].

1.8 Hydrogen Evolution Reaction (HER)

Metal and metal/C are typically used as cathodic electrocatalysts for the hydrogen evolution reaction in an SPE water electrolyzer. These noble metals is required because it yields the best catalytic activity for the HER and also because of the strong acidity of the solid electrolyte, which would cause the corrosion of non-noble metal. The standard potential of hydrogen is zero.

A volcano plot is used to compare the electrochemical activity of the hydrogen evolution reaction on various metals. In the volcano plot is reported the dependence of the exchange current density for the hydrogen evolution reaction in 1 mol dm^{-3} acid on the strength of the metal – hydrogen bond formed with the metal of the electrode. [59]

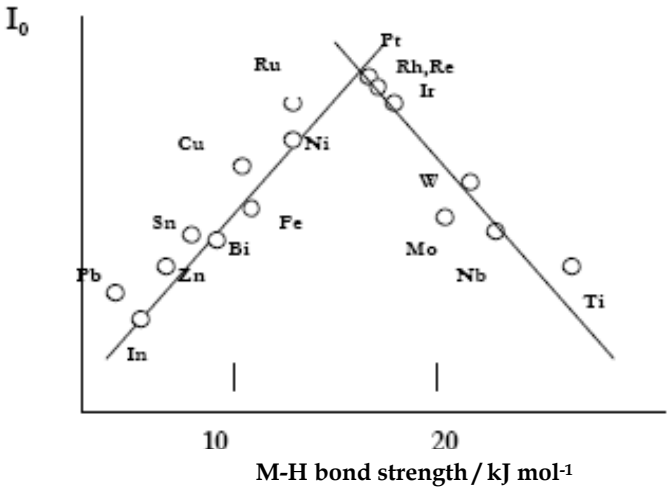

Figure 9. Volcano plot of the HER [59]

The volcano plot shows that the metal with low bond strength, the adsorption of hydrogen becomes the rate-determing step, whereas for the metal with strong bond strength, the desorption of hydrogen becomes the rate determing step. This means that, the metals with intermediate bond strengths, which are the noble metals, are the most active toward the HER. Platinum provides the best performance for the hydrogen evolution reaction and is commonly used as cathode catalyst in SPE electrolyzers [39, 41, 60-63].

1.9 Oxygen Evolution Reaction (OER)

The oxygen evolution reaction is one of the most studied electrochemical processes. Even so, this reaction and the mechanism is still not widely understood and very difficult to interpret. There have been many oxygen evolution reaction mechanism proposed, however few actually take into consideration the nature of the electrode surface, which is critical for understanding the real reaction mechanism.

Metal oxide are most frequently used as anodes in acidic media, although most transition metal oxides such as nickel, cobalt and manganese undergo corrosion under these conditions. The cations of these metals are known to poison the membrane by attaching to the sulphonic acid groups, thereby reducing the conductivity of the membrane. Platinum group metal oxides such as RuO_2 and

IrO_2 and some transition metal oxides such as PbO_2 and SnO_2, have been found to be more stable during the OER. The standard potential for OER is 1.23 V_{RHE} (RHE, reversible hydrogen electrode). This value is above of the standard potential of almost all solid materials, that explaining why only a few materials are stable under the OER.

There are many proposed reaction mechanisms for the oxygen evolution reaction [62]. In the acid medium, the reaction mechanism of O_2 evolution on the active oxide electrodes [65-66] is as follows:

$$S + H_2O \rightarrow S\text{-}OH^*_{ads} + H^+ + e- \quad (13)$$

$$S\text{-}OH^*_{ads} \rightarrow S\text{-}OH_{ads} \quad (14)$$

$$S\text{-}OH_{ads} \rightarrow S\text{-}O_{ads} + H^+ + e- \quad (15)$$

$$S\text{-}O_{ads} \rightarrow S + (1/2)O_2 \quad (16)$$

where S stands for response active sites on the coating surface, and $S\text{-}OH^*_{ads}$, $S\text{-}OH_{ads}$, $S\text{-}O_{ads}$ are three adsorption intermediates. This mechanism predicts the following Tafel slope: 125 mV dec^{-1} if step (13) is the rate determining step, rds, 60 mV dec^{-1} for step (14), 40 mV dec^{-1} for step (15) and 30 mV dec^{-1} for step (16). Which step is the rds depends on the strength of the adsorption of the intermediates, which is in turn governed by the composition of the oxide layer [64].

1.10 References

[1] Gritzner G (1977) US Patents 4 035 254 and 4 035 255

[2] Gestaut L, et al. (1983) abstracts of ECS Fall Meeting, No. 393

[3] http://electrochem.cwru.edu/encycl/art-b01-brine.htm

[4] Kiros Y, Pirjamali M, Bursell M. Oxygen reduction electrodes for electrolysis in chlor-alkali cells. Electrochimica Acta 51 (2006) 3346–3350

[5] Furuya N, Aikawa H. Comparative study of oxygen cathodes loaded with Ag and Pt catalysts in chlor-alkali membrane cells. Electrochim Acta 45(2000) 4251-4256

[6] Los Alamos National Laboratory, Chlor-Alkali Cells Technology, www.lanl.gov/fuelcells/chlor alkali.html.

[7] Okajima K, Nabekura K, Kondoh T, Sudoh M. Degradation Evaluation of Gas-Diffusion Electrodes for Oxygen-Depolarization in Chlor-Alkali Membrane Cell. *Journal of The Electrochemical Society*, 152 (8) D117-D120 (2005)

[8] Aikawa H., Poblotzki, Soda and Chlorine, 47, 85 (1994)

[9] Gestaut LJ, Clere TM, Niksa AJ, Graham CE (1983) The Electrochemical Society Extended Abstracts, Abstract 124:196, Vol. 83-2, Los Angeles, CA, May 8-13 1983

[10] Chlistunoff J. Oxygen-Depolarized Chlor-Alkali Cells. Some Consequences of Using Oxygen Diffusion Cathodes. Los Alamos National Laboratory MST-11, P.O.Box 1663, MS D429 Los Alamos, NM 87545, USA

[11] Yeager E. Soda and Chlorine. 31 (1980) 13

[12] Morimoto T, Suzuki K, Matubara T, Yoshida N. Oxygen reduction electrode in brine electrolysis. Electrochim. Acta 45 (2000) 4257-4262

[13] Yamaguchi K, Chlor-alkali technologies applied in Japan, in H.S. Burney, N. Furuya, F. Hine and K.-I. Ota (Eds), Chlor-Alkali and Chlorate Technology: R.B. MacMullin Memorial Symposium, 196th Meeting of the Electrochemical Society, Hawaii, October (1999), Electrochemical Society Proceedings, Vol. 99-21, pp. 127–144.

[14] Federico F, Martelli GN, Pinter D. Gas-diffusion Electrodes for Chlorine-related (Production) Technologies, in J. Moorhouse (Ed.), Modern Chlor-Alkali

Technology, Proceedings of the 2000 London International Chlorine Symposium Organized by SCI's
Electrochemical Technology Group, London, UK, 31st May–2nd June (2000) (Blackwell Science, 2001), pp. 114–127.
[15] Martelli GN, Reduzzi E, Caldarera A, Urgeghe C. Performance of the falling film chlor-alkali cell equipped with carbon-free oxygen depolarized cathode. Joint International Meeting. The Electrochemical Society Inc., Honolulu, Hi, USA, October 3–8 2004
[16] Chatenet M, Aurousseau M, Durand R, Andolfatto F. Silver-Platinum bimetallic catalysts for oxygen cathodes in chlor-alkali electrolysis. J. Electrochem. Soc., 150, D47 (2003).
[17] Lipp L, Gottesfeld S, Chlistunoff J. Peroxide formation in a zero-gap chlor-alkali cell with an oxygen-depolarized cathode. Journal of Applied Electrochemistry (2005) 35:1015–1024
[18] Ichinose O, Kawaguchi M, Furuya F. Effect of silver catalyst on the activity and mechanism of a gas diffusion type oxygen cathode for chlor-alkali electrolysis. J Appl Electrochem 34 (2004)55-59
[19] Sugiyama M, Saiki K, Sakata A, Aikawa H, Furuya N. Accelerated degradation testing of gas diffusion electrodes for the chlor-alkali process. J Appl Electrochem 33 (2003) 929-932.
[20] Hine F, Murakami K. J Electrochem Soc 127 (1980) 292
[21] Aikawa H. Soda and Chlorine 47 (1996) 45
[22] Aikawa H. Soda and Chlorine 47 (1996) 93
[23] Aikawa H. Soda and Chlorine 47 (1996) 192
[24] Aikawa H, Sakata A, Saiki K. Soda and Chlorine 48 (1997) 297
[25] Wang X, Koda S, Denki Kagaku 65 (1997) 1002
[26] Wang X, Koda S, Denki Kagaku 65 (1997) 1004
[27] Sudoh M, Kondoh T, Kamiya N, Ueda T, Okajima K. J Electrochem Soc 147 (2000) 3739
[28] http://www.lanl.gov/orgs/mpa/mpa11/chlor.htm
[29] http://www.itpower.co.uk/investire/pdfs/electrolyser.pdf

[30] Grigoriev SA, Porembsky VI, Fateev VN. Pure hydrogen production by PEM electrolysis for hydrogen energy. Int J Hydrogen Energy 2006;31:171–5.

[31] P. Millet , R. Ngameni, S.A. Grigoriev, N. Mbemba, F. Brisset, A. Ranjbari, C. Etie´vant. PEM water electrolyzers: From electrocatalysis to stack development. Int J of hydrogen energy 3 5 (2 0 1 0) 5 0 4 3 – 5 0 5 2

[32] Slavcheva E, Radev I, Bliznakov S, Topalov G, Andreev P, Budevski E. Sputtered iridium oxide films as electrocatalysts for water splitting via PEM electrolysis. Electrochim Acta 2007;52:3889–94.

[33] B. Borresen, G. Hagen, R. Tunold. Hydrogen evolution on RuxTi1−xO2 in 0.5 M H2SO4. Electrochim. Acta 2002;47:1819-27.

[34] Marshall A, Børresen B, Hagenm G, Tsypkin M, Tunold R. Preparation and characterisation of nanocrystalline IrxSn1-xO2 electrocatalytic powders. Mater Chem Phys 2005;94(2–3):226–32.

[35] Marshall, A.; Tsypkin, M.; Børresen, B.; Hagen, G. K; Tunold, R. Nanocrystalline IrxSn1-xO2 Electrocatalysts for Oxygen Evolution in Water Electrolysis with Polymer Electrolyte - Effect of Heat Treatment. J. New Materials Electrochem Syst. 2004;7:197-204.

[36] Trasatti S. Electrocatalysis in the anodic evolution of oxygen and chlorine. Electrochim Acta 1983; 29(11):1503-12.

[37] Trasatti S. Physical Electrochemistry of ceramic oxides. Electrochim Acta 1991; 36(2):225-41.

[38] Andolfatto F, Durand R, Michas A, Millet P, Stevens P. Solid polymer electrolyte water electrolysis: electrocatalysis and long-term stability. Int. J. Hydrogen Energy 1994;19:421-427.

[39] Millet P, Andolfatto F, Durand R. Design and performance of a solid polymer electrolyte water electrolyzer. Int. J. Hydrogen Energy 1996;21:87-93.

[40] Yamaguchi M, Ohisawa K, Nakanori T. Development of high performance solid polymer electrolyte water electrolyzer in WE-NET. Proceedings of the Intersociety Energy Conversion Engineering Conference 1997;3–4:1958-61.

[41] Ledjeff K, Mahlendorf F, Peinecke V, Heinzel. Development of electrode/membrane units for the reversible solid polymer fuel cell (RSPFC). Electrochim Acta 1995;40:315-9

[42] Rasten E, Hagen G, Tunold R Electrocatalysis in water electrolysis with solid polymer electrolyte. Electrochim Acta 2003;48:3945-52.

[43] Ma H, Lui C, Liao J, Su Y, Xue X, Xing W. Study of ruthenium oxide catalyst for electrocatalytic performance in oxygen evolution. Journal of Molecular Catalysis A: Chemical:2006;247(1-2):7-13

[44] Hu JM, Zhang JQ, Cao CN. Oxygen evolution reaction on IrO2-based DSA type electrodes: kinetics analysis of Tafel lines and EIS. Int. J. of Hydrogen Energy 2004;29:791-97.

[45] Song S, Zhang H, Ma X, Shao Z, Baker RT, Yi B. Electrochemical investigation of

electrocatalysts for the oxygen evolution reaction in PEM water electrolyzers. Int J Hydrogen Energy 2008;33:4955-61.

[46] Nanni L, Polizzi S, Benedetti A, De Battisti A. Morphology, microstructure, and electrocatalytic properties of RuO2-SnO2 thin films. J. Electrochem Soc. 1999;146(1):220-5.

[47] De Oliveira-Sousa A, da Silva MAS, Avaca LA, Lima-Neto P. Influence of the preparation method on the morphological and electrochemical properties of Ti/IrO2-coated electrodes. Electrochim. Acta 2000;45(27):4467-73.

[48] Solid polymer electrolyte water electrolysis technology developed for large scale hydrogen production. General Electric Company, DOE Report DOE/ET/26 202-1 (1981).

[49] Davenport RJ, Schubert FH. Space water electrolysis: space station through advanced missions. J Power Sources 1991;36:235–50.

[50] Kato T, Kubota M, Kobayashi N, Suzuoki Y. Effective utilization of by-product oxygen from electrolysis hydrogen production. Energy 30 (2005) 2580–2595

[51] Heitner-Wirguin C. Recent advances in perfluorinated ionomer membranes: structure, proprierties and applications. J Membrane Science 1996;120:1-33.

[52] X Fang, PK Shen, S Song, V Stergiopoulos, P Tsiakaras. Degradation of perfluorinated sulfonic acid films: An in-situ infrared spectro-electrochemical study. Polymer Degradation and Stability 94 (2009) 1707–1713

[53] Saccà, A., Carbone, A., Passalacqua, E., D'Epifanio, A., Licoccia, S., Traversa, E., Sala, E, Ornelas, R. Nafion-TiO2 hybrid membranes for medium temperature polymer electrolyte fuel cells (PEFCs). Journal of Power Sources 152 (1-2), pp. 16-21

[54] Aricò, A.S., Cretì P., Antonucci, P.L., Antonucci, V. Comparison of ethanol and methanol oxidation in a liquid-feed solid polymer electrolyte fuel cell at high temperature. Electrochemical and Solid-State Letters 1 (2), pp. 66-68

[55] R. B. Moore, C. R. Martin. Chemical and Morphological Properties of Solution-Cast Perfluorosulfonate Ionomers. Macromolecules 1988, 21, 1334-1339.

[56] K.D. Kreuer. On the development of proton conducting polymer membranes for hydrogen and methanol fuel cells. Journal of Membrane Science 185 (2001) 29–39

[57] Ram Devanathan. Recent developments in proton exchange membranes for fuel cells. Energy Environ. Sci., 2008, 1, 101–119

[58] V. Baglio, A.S. Aricò, A. Di Blasi, V. Antonucci, P.L. Antonucci, S. Licoccia, E. Traversa, F. Serraino Fiory. Nafion–TiO2 composite DMFC membranes: physico-chemical properties of the filler versus electrochemical performance. Electrochimica Acta 50 (2005) 1241–1246

[59] Trasatti S. Work function, electronegativity, and electrochemical behaviour of metals. III. Electrolytic hydrogen evolution in acid solutions J Electroanal Chem 1972; 39:163.

[60] K. Onda, T. Murakami, T. Hikosaka, M. Kobayashi, R. Notu, K. Ito. Performance analysis of polymer-electrolyte water electrolysis cell at a small-unit test cell and performance prediction of large stacked cell. J. Electrochem Soc 149 (2002) A1069.

[61] Holze R, Ahn J. Advances in the use of perfluorinated cation exchange membranes in integrated water electrolysis and hydrogen/oxygen fuel cell systems J. Membr. Sci. 73 (1992) 87.

[62] Millet P. Water electrolysis using eme technology: electric potential distribution inside a nafion membrane during electrolysis. Electrochim Acta 39 (1994) 2501.

[63] Ioroi T, Yasuda K, Siroma K, Fujimara N, Miyazaki Y. Thin film electrocatalyst layer for unitized regenerative polymer electrolyte fuel cells J. Power Sources 112 (2002) 583.

[64] Damjanovic A, Dey A, Bockris JOM, Kinetics of oxygen evolution and dissolution on platinum electrodes J Electrochim Acta 11 (1966) 791.

[65] Trasatti S, Electrodes of Conductive Metallic Oxides, Elsevier Science Publishing Company, Amsterdam, 1980.

[66] Ye Z, Meng HM, Chen D, Yu HY, Huan ZS, Wang XD, Sun DB. Structure and characteristics of Ti/IrO_2(x) + MnO_2*(1 - x)* anode for oxygen evolution. Solid State Sciences 10 (2008) 346-354

CHAPTER 2

Degradation of oxygen-depolarized Ag-based Gas Diffusion Electrodes for chlor-alkali Cells

2.1 Introduction

Chlorine and caustic soda, obtained by the electrolysis of an aqueous solution of sodium chloride, are products of the chlor-alkali electrochemical process. Total cell reaction proceeds through the following anodic and cathodic half-cell reactions:

$2Cl^- \rightarrow Cl_2 + 2e^-$ E = 1.358 V vs. NHE (1)

In alkaline solutions,

$2H_2O + 2e^- \rightarrow 2OH^- + H_2$ E = - 0.828 V vs. NHE (2)

Therefore, the overall reaction is:

$2H_2O + 2Cl^- \rightarrow Cl_2 + 2OH^- + H_2$ E = 2.186 V (3)

The thermodynamic potential difference ΔE (decomposition voltage) of total electrode reactions is approximately 2.2 V.

The main drawback of chlor-alkali electrolysis (3) is high power consumption, about 4kA m^{-2}@ 3V [1]. Therefore, in order to improve the process, it is necessary to reduce energy consumption. In the early 1980's, chlor-alkali cells utilizing air cathodes were developed at ELTECH System Co. [2,3]. The use of these Gas Diffusion Electrodes (GDEs) was introduced as a feasible technological approach for the reduction of power consumption in the chlor-alkali membrane cell process.

The substitution of traditional hydrogen-evolving cathodes with an oxygen-consuming GDE results in the formation of caustic and chlorine without hydrogen:

Anode reaction: $2Cl^- \rightarrow Cl_2 + 2e^-$ E = + 1.358 V vs. NHE (1)"

Cathode reaction: $2H_2O + O_2 + 4e^- \rightarrow 4OH^-$ E = + 0.401 V vs. NHE (4)

Overall reaction: $2H_2O + O_2 + 2Cl^- \rightarrow Cl_2 + 4OH^-$ E = 0.957 V (5)

The equilibrium potential of reactions (2) and (4) is -0.82 and +0.40 V vs. NHE, respectively. Thus, the equilibrium potential of the oxygen reduction reaction vs. NHE (4) is about 1.2 V higher than that of the hydrogen evolution reaction (2). Therefore, replacing hydrogen-evolving cathodes with oxygen cathodes significantly reduces thermodynamic cell voltage and leads to an energy savings of 30-40% [4-6].

The first GDE structures were based on silver catalyst particles supported on active carbon [7,8]. These catalysts were affected by significant deactivation phenomena:

- Electrode flooding, due to a progressive loss of hydrophobicity and the intrusion of the catholyte into electrode pores. This is favoured by the differential pressure existing between the gas and liquid sides of the electrode. Progressive corrosion of both carbonaceous components and the silver catalyst, followed by silver redistribution
- Sensitivity to uncontrolled shut-down.

All these reasons suggested attention be concentrated on a different type of electrode design based on a carbon-free catalyst.

Catalysts used in this study were based on a mixture of micronized silver particles and PTFE binder. The silver particles showed a very uniform size distribution and contained a limited amount of second metal (i.e. Hg) that was introduced to increase their stability to corrosion, as demonstrated by the RDE analysis of catalyst powder [9].

The purpose of the present study was to investigate the cathodic properties of oxygen reduction on gas-diffusion electrodes by electrochemical measurements, and surface and morphologic analyses. Attention was focused on deactivation phenomena involving this type of GDE configuration. In this study, we compared fresh gas diffusion electrodes to electrodes tested at different times in a chlor-alkali cell. Electrode stability was investigated with life-time tests. The surface of the gas diffusion electrodes was observed and analyzed for both fresh and used cathodes by scanning electron microscopy and X-ray photoelectron spectroscopy.

The bulk of gas diffusion electrodes was investigated by X-ray diffraction and thermogravimetric analysis.

2.2 Experimental

Catalysts used for the cathodic reaction were based on a mixture of silver particles containing a limited amount of Hg (comprised in the range 0.5-10% by weight) and PTFE binder. Electrodes tested in this study were composed of an Ag net loaded with a 1 kg m^{-2} catalyst. With respect to what is considered optimum in current literature [10], a large excess of metal loading was used in this study to avoid any degradation of support after prolonged operation, thus focusing attention on phenomena occurring mainly at the surface of the electrocatalyst. The electrodes were prepared by a powder roller of PTFE and a silver-mercury alloy obtained by a co-precipitation process and, subsequently, reduced electro-chemically, according to the patent of Janowitz et al. [11]. In this investigation, the following samples obtained from the same electrode roll were analysed: GDE-fresh (before electrochemical characterization), GDE-1 (after a 50-hour time-study), GDE-2 (after a 145-hour time-study), and GDE-3 (after a 526-hour time-study). A standard chlor-alkali electrolyser (300g/l NaCl; 90°C) was used. A sodium chloride solution was fed to the anode, to produce chlorine gas (1); whereas, oxygen was fed to the cathode (2). The sodium hydroxide, formed at the cathode, was maintained separate from the sodium chloride solution present in the anodic compartment by a membrane made of a perfluorinated polymer containing anionic groups (i.e. DuPont N324). A more detailed description of the electrolyser and a design of this type of cell is illustrated in the figure 1 [1].

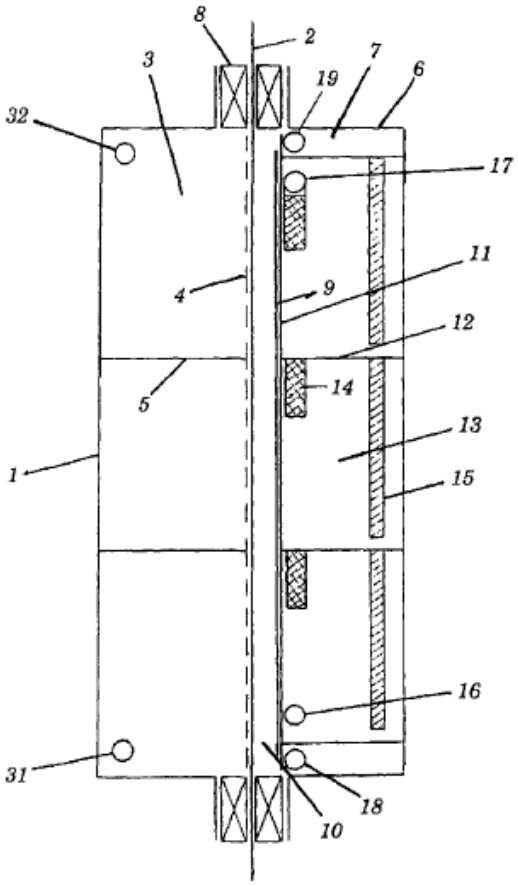

1. the anodic shell; 2. the ion exchange membrane; 3. the anodic compartment; 4. anode of a perforated sheet; 5. Conductive supports; 6. the cathodic shell; 7. the cathodic compartment; 8. the peripheral gaskets; 9. the oxygen diffusion cathode; 10. caustic soda flows; 11. the frame; 12. conductive supports; 13. chambers; 14. dynamic pressure drop device; 15. accumulating liquid; 16. nozzle for the oxygen fed; 17. nozzle for the residual oxygen discharged; 18. nozzle for the caustic soda fed; 19. nozzle for the caustic soda discharged; 31. nozzle for the sodium chloride solution; 32. nozzle for the withdrawing the produced chlorine and the diluted solution [1].

Figure 1. Membrane electrolysis cell

Electrochemical deactivation phenomena were monitored by chrono-amperometric tests at 3 and 4 kA m^{-2}. The geometrical electrode surface was 0.16 m^2. Cell resistance was determined and monitored as a function of time by using the current interruption method. Morphology was investigated by using SEM-EDX (FEI XL 30)_instruments. Structural analysis was done by X Ray Diffraction (Philips X'Pert, diffractometer, Cu Kα source) (figure 2).

Figure 2. X-ray diffractiometer

To investigate the surface chemical composition of gas-diffusion electrodes, XPS analysis was performed by using a PHI 5800-01 spectrometer with an Al Kα monochromatic source (Figure 3). An Ar^+ sputtering procedure was used in order to obtain a qualitative depth-profile of electrode composition.

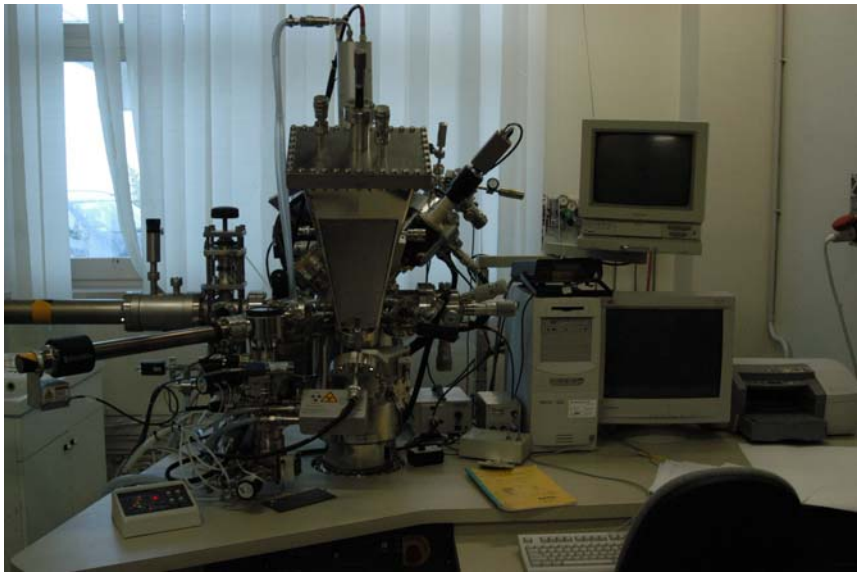

Figure 3. X-ray photoelectron spectroscope

Thermogravimetric analysis of gas diffusion electrodes was carried out by a Netzesch STA 409 Cell analyser. The thermal analysis yielded information about bulk composition with regard to PTFE and Ag content. Transmission Electron

Microscopy (FEI CM 12) was used to obtain qualitative information on the degree of hydrophobicity at the reaction pores (Figure 4).

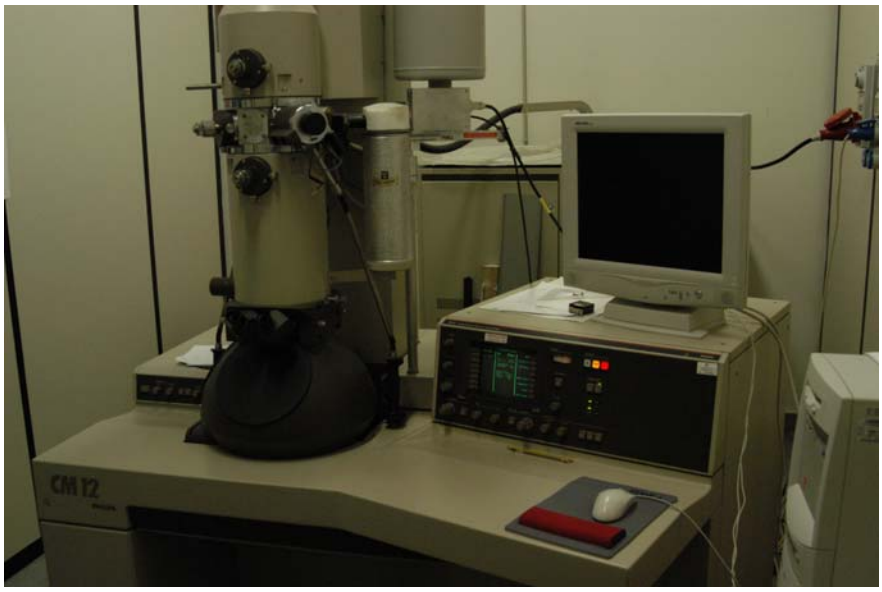

Figure 4. Transmission Electron Microscope

2.3 Results and Discussion

The variation of cell potential as a function of operational time under constant electrochemical conditions (3 and 4 kA m^{-2}, 90°C, NaOH 33 % w/w) is given below for the first 120 hours (Fig. 5). A significant variation in cell potential is observed during the first period of operation; whereas, only small changes are observed after prolonged operation. No relevant modifications in electrochemical behaviour were observed from 120 to 526 hours (not shown). Previous electrochemical studies have assigned an increase in cell potential vs. time primarily to the oxygen reduction process in gas diffusion electrodes (4), which represents the rate determining step for the overall process [14].

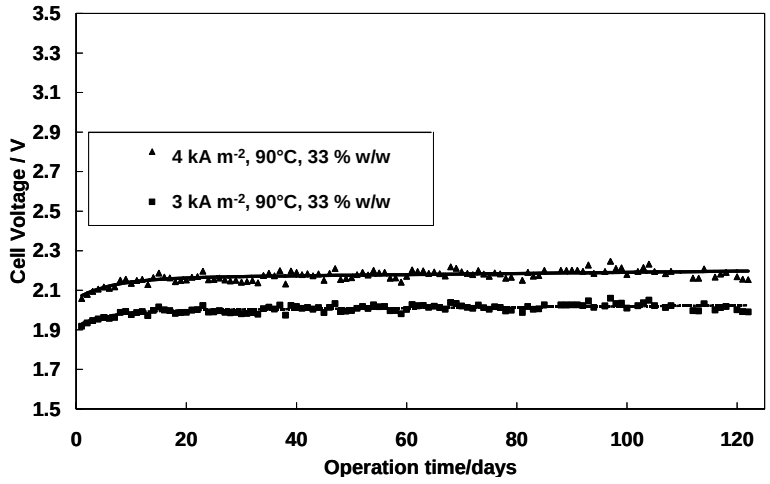

Figure 5. Cell voltage of chlor-alkali cell versus time. Lines represent curve fitting according to equation 5 (—) and 6 (- - -)

A very low overpotential at a current density of 4 kA m^{-2} was observed for the chlorine evolution (equation 1) in half-cell experiments [12,13]. Previous studies reported no change in the anodic overpotential in a time-test of more than 2 years at a current density of 4 kA m^{-2} [12].

A significant loss of potential in these electrochemical devices occurs by effect of the ohmic drop caused by the polymer membrane (about 400 mV at 4 kA m^{-2}); yet, according to cell resistance measurements (not shown), the voltage loss due to the ohmic resistance does not significantly increase with time.

The cell used in the present study demonstrated excellent stability during uncontrolled shut-down conditions (normal frequency 0.02 h^{-1}, maximum frequency 0.05 h^{-1}, during normal operation). The curve fitting shows that in the first 120 hours of operation, two main degradation phenomena occur on different time-scales. A dramatic increase in cell potential is observed at low operational times (up to 40 hours) that overlays with a smooth decay after more than 40-50 hours have passed. The curve fitting related to an increase in overpotential (η) with operation time is mathematically expressed by equations (6) and (7)

$$\eta_1 = 2.16157 - 0.10255 \times e^{-\frac{t}{6.766192}} + 0.00029 \times t \quad (6)$$

$$\eta_2 = 1.99568 - 0.07608 \times e^{-\frac{t}{5.39529}} + 0.00023 \times t \quad (7)$$

The first phenomenon suitably fits a neperian exponential term with a negative pre-exponential factor and reflects a strong deactivation process. The second process is associated with a progressive decay that is approximated by a linear function. The first phenomenon is more significant and its effect also influences long-term electrochemical behaviour even if to a lesser extent than what was initially observed.

This behaviour was quite reproducible, indicating that it is associated with physical-chemical changes in electrode properties at interface. To have a complete picture of the electrode changes, both bulk and surface analyses were carried out on electrodes discharged after specific operation times.

Figure 6 shows a comparison of different atomic ratios for the GDE-fresh, GDE-1, GDE-2, and GDE-3 samples as derived from SEM-EDX. The atomic ratio of F/Ag and C/Ag decreased with time whereas the atomic ratio of O/Ag increased. This means that hydrophobicity decreased and the amount of hydroxides increased. A drastic decrease in the Hg/Ag ratio was observed in the first 50 hours.

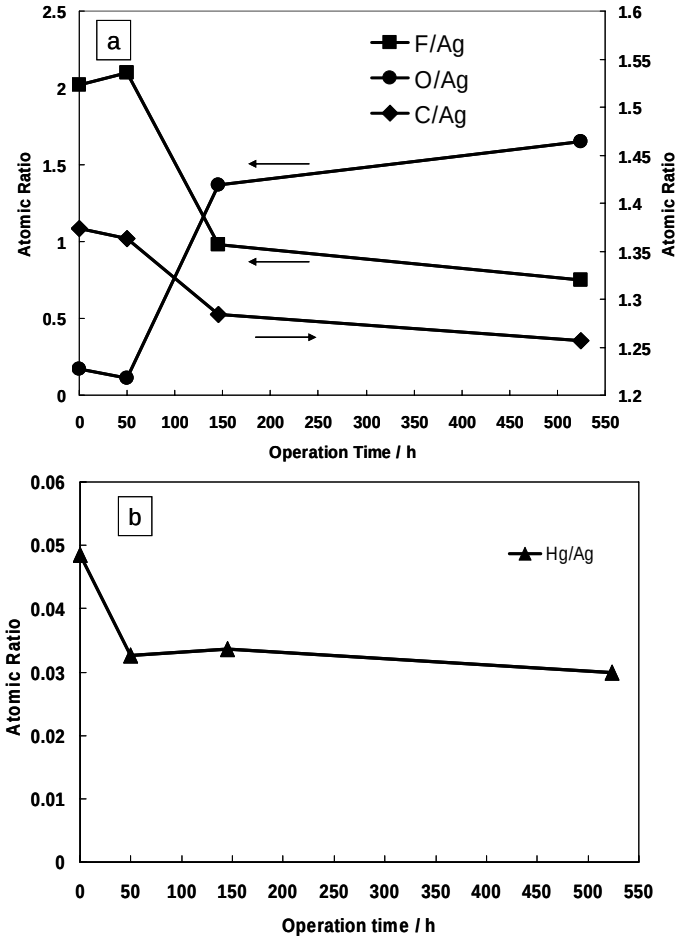

Figure 6. (a) (b) EDX analysis at GDE-fresh, GDE-1 (50 hours), GDE-2 (145 hours) and GDE-3 (526 hours). Atomic ratios of different elements

The decrease of hydrophobicity was further investigated by TEM analysis (Figures 7 a-b). It was observed that catalyst pores were properly coated with the PTFE polymer in the fresh electrode. Upon operation, this PTFE coating is partially lost due to a progressive flooding of the electrode surface.

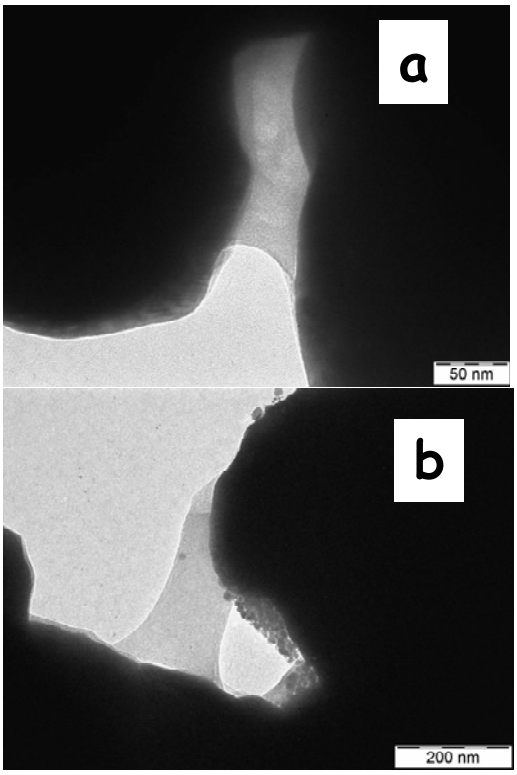

Figure 7. TEM images of GDE-fresh (a) and GDE-2 (b)

In Figures 8 a-b, XRD patterns and the values of particle size for the main Ag peaks, i.e. 111, 220, and 200, are reported. There was no significant change in the particle size of the catalysts at different intervals of operation. This indicates that the degradation of electrodes is not associated with an electrochemical sintering of the catalysts. In effect, the raw particle size of Ag is quite large, about 25 nm; whereas, electrochemical sintering phenomena involving dissolution and reprecipitation in fuel cell catalysts used in the oxygen reduction process are usually associated with small particle sizes (<10 nm) [15].

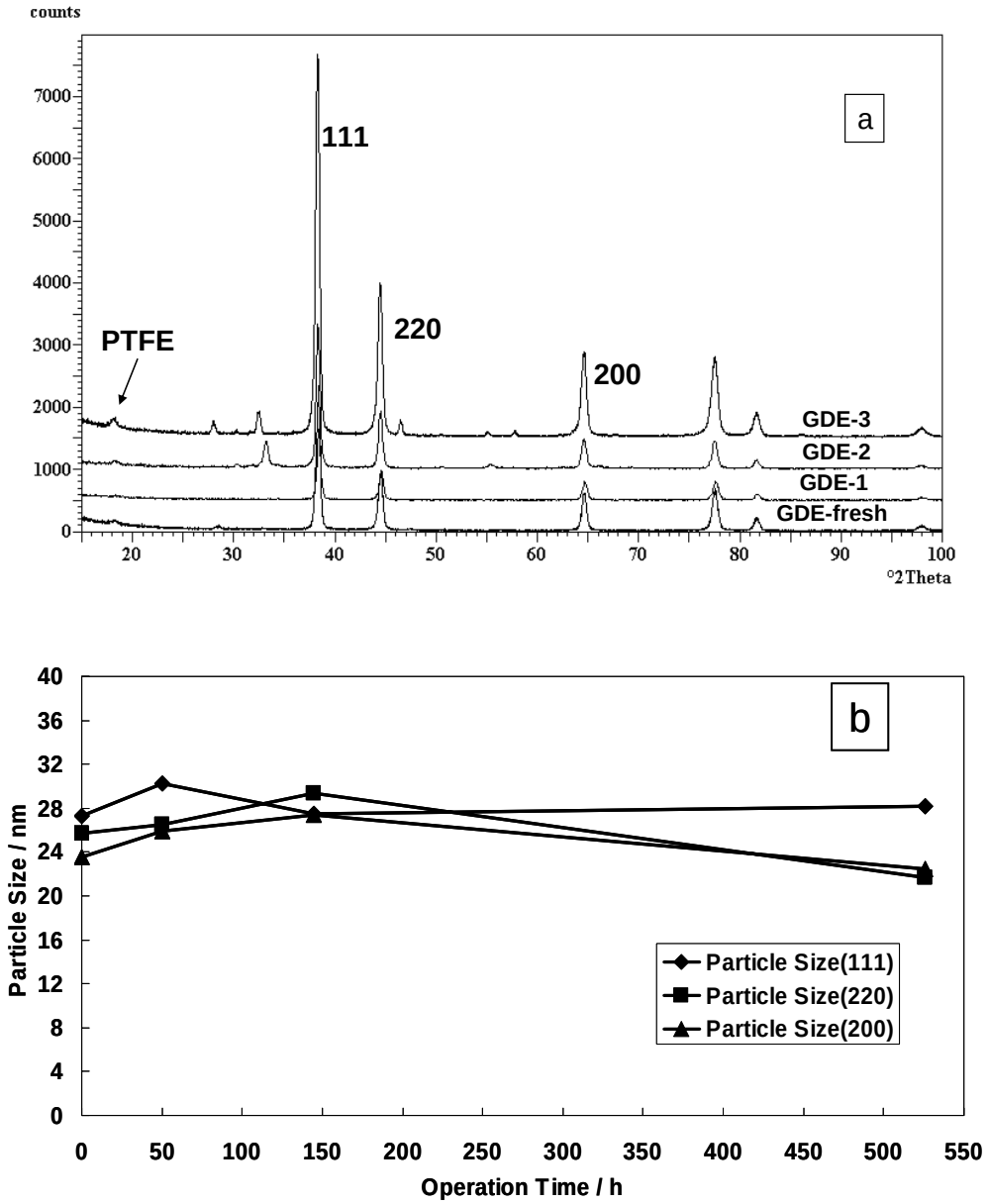

Figure 8. (a) X-ray diffraction patterns of GDE-fresh, GDE-1, GDE-2 and GDE-3 electrodes. (b) Comparison of the values of particle size of main peaks of Ag fcc crystalline structure i.e. 111, 220 and 200 reflections

Figure 9 shows Ag 3d and Hg 4f XPS spectra of GDE-fresh, before and after sputtering. After sputtering, the binding Energy (B.E.) of Ag 3d does not change; whereas, a shift at lower B.E. values is observed for Hg 4f. This reveals that Hg is partially oxidised on the surface; whereas, it is suitably alloyed in the inner layer. From the comparison of peak intensities before and after sputtering, it seems that the amount of Ag decreases from the inner to outer layers; whereas, Hg increases. If one combines information about the electronic properties of Hg and its surface enrichment caused by segregation (see below), it appears that Hg is partially lost

from the surface during the first hours of operation. This speculation is confirmed below by the XPS and EDX analyses carried out at different operation times.

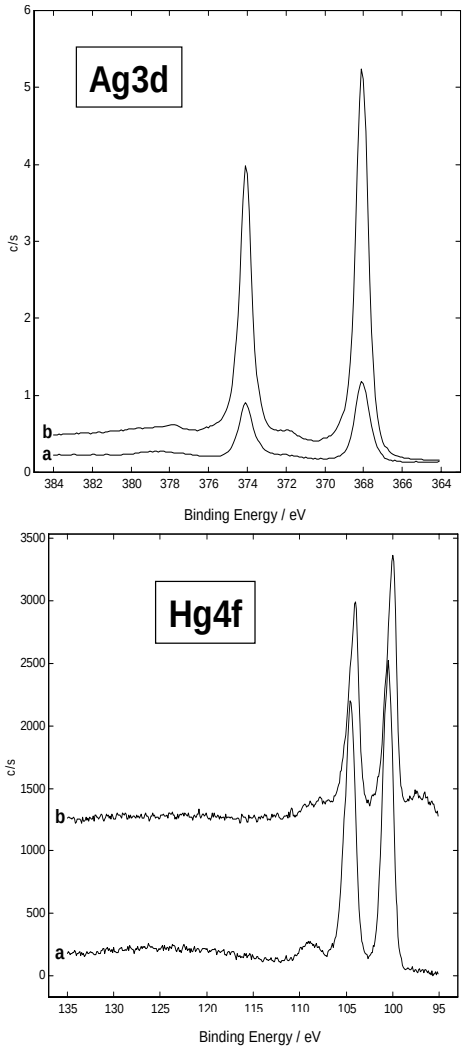

Figure 9. Ag 3d and Hg 4f XPS spectra of GDE-fresh, before (a) and after (b) sputtering

Figure 10 shows F 1s and C 1s XPS spectra of GDE-fresh, before and after sputtering. The peaks of fluorine and carbon decreased after sputtering and significantly shifted to lower B.E. values. This indicates a degradation of the PTFE binder by effect of Ar^+ ions with a consequent change of B. E. and, possibly, a loss of the insulating (charging) effect.

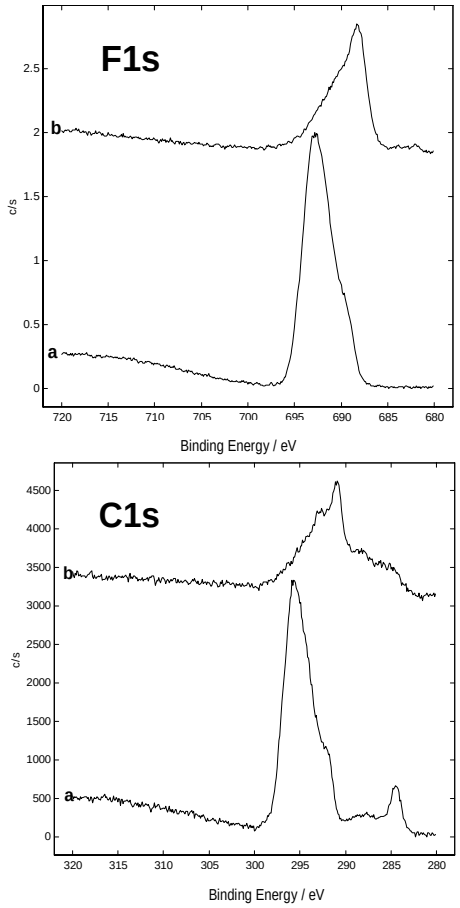

Figure 10. F 1s and C 1s XPS spectra of GDE-fresh, before (a) and after (b) sputtering

Figure 11 shows Ag 3d and Hg 4f XPS spectra of GDE-1 discharged after 50 hours of operation, before and after sputtering. After sputtering, the peak of silver increased; whereas, the Hg 4f did not change. By comparing these results to those of fresh electrodes and taking into account the EDX analysis, it appears that significant Hg loss occurs during the first 50 hours; subsequently, Hg dissolution proceeds at a lower rate than at the beginning of operation. From sputtering results, we may conclude that the Hg distribution content in the inner layers is homogeneous.

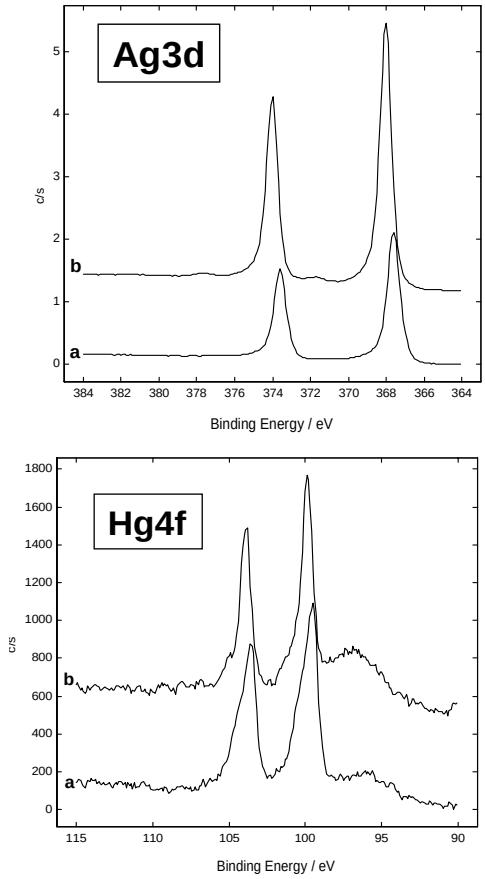

Figure 11. Ag 3d and Hg 4f XPS spectra of GDE-1 (50 hours), before (a) and after (b) sputtering

Figure 12 shows C1s and F1s XPS spectra of GDE-1 (50 hours), before and after sputtering. After sputtering, the C1s signal at high B.E. values associated with PTFE (292 eV) and the F1s signal shifted toward lower binding energies as observed above. A comparison of fresh electrodes to GDE-1 showed the amount of adventitious carbon (284.6 eV) was significant due to an increased uptake of carbon compounds from the environment.

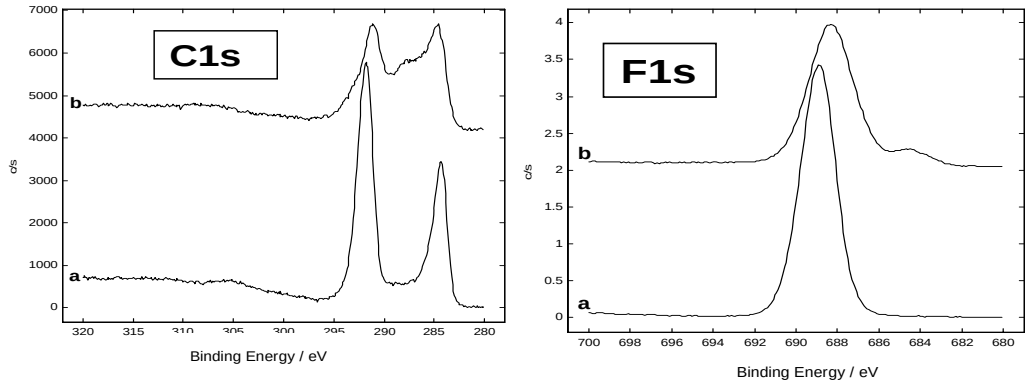

Fig. 12. C 1s and F 1s XPS spectra of GDE-1 (50 hours), before (a) and after (b) sputtering

Figure 13 shows Cl 2p and Na 1s XPS spectra of GDE-1, before and after sputtering,. A low Cl 2p signal indicates that there is no significant precipitation of AgCl after 50 hours; the Na 1s signal does not change significantly in intensity after sputtering. The shift is attributed to a charging effect. It is concluded that sodium hydroxides solidify in the catalyst pores during the electrochemical process.

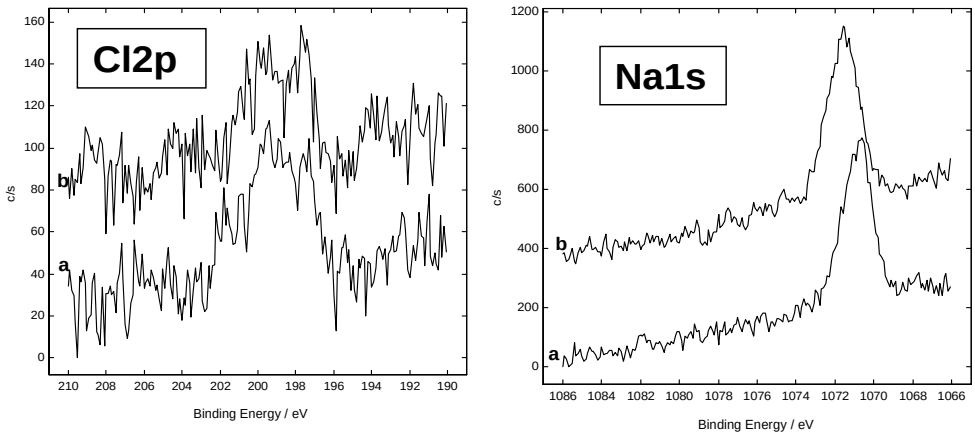

Figure 13. Cl 2p and Na 1s XPS spectra of GDE-1, before (a) and after (b) sputtering

XPS analysis was also carried out on electrodes discharged after 145 and 526 hours of operation. The results of Ag 3d and Hg 4f were qualitatively similar to those observed after 50 hours of operation. The C1s and F1s profiles were somewhat different from that in electrodes tested for 50 hours. Figure 14 shows the C 1s and F 1s XPS spectra of GDE-2 (145 hours), before and after sputtering. After sputtering, carbon and fluorine signals associated with PTFE decreased due to degradation.

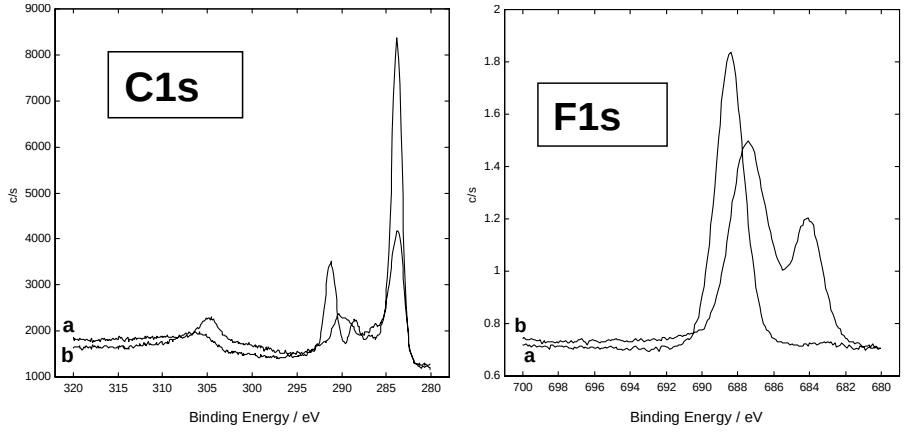

Figure 14. C 1s and F 1s XPS spectra of GDE-2, before (a) and after (b) sputtering

In this sample, it was observed that adventitious carbon peak (284.6 eV) prevailed with respect to the C1s signal associated with PTFE (292 eV). This is due to a large uptake of contaminants from the environment after prolonged electrochemical operation. Figure 15 shows Cl 2p and Na 1s XPS spectra of GDE-2 (145 hours), before and after sputtering. After sputtering, Cl 2p decreased whereas Na 1s increased. Both AgCl and sodium hydroxide species precipitated in the pores. It seems that sodium hydroxide precipitation in the inner layers is more significant than that of AgCl.

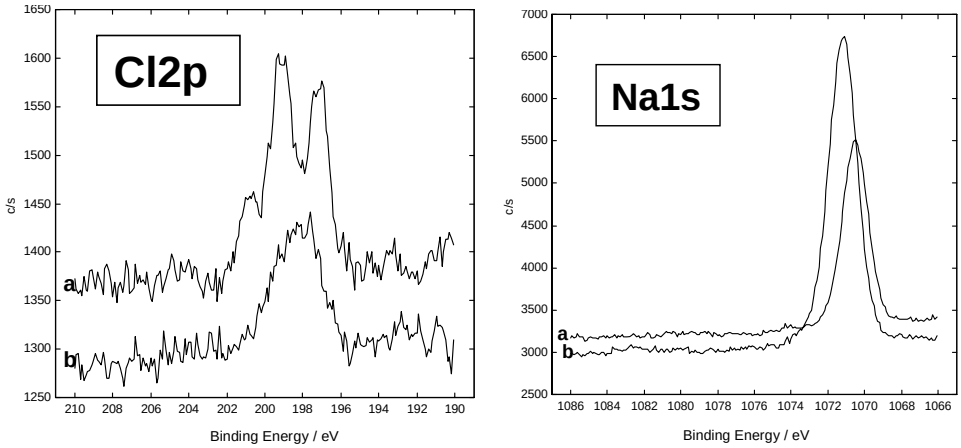

Figure 15. Cl 2p and Na 1s XPS spectra of GDE-2, before (a) and after (b) sputtering

The surface characteristics of GDE-3 (526 hours) were similar to those of GDE-2 (145 hours). This is in agreement with the absence of any significant variation in electrochemical properties after 120-150 hours (not shown).

A quantitative determination of the various elements was made from XPS spectra. Relative concentrations were normalised to the silver content and reported as a function of operation time in a chlor-alkali cell.

Figure 16 shows the variation of relative XPS concentrations for the various elements versus operation time.

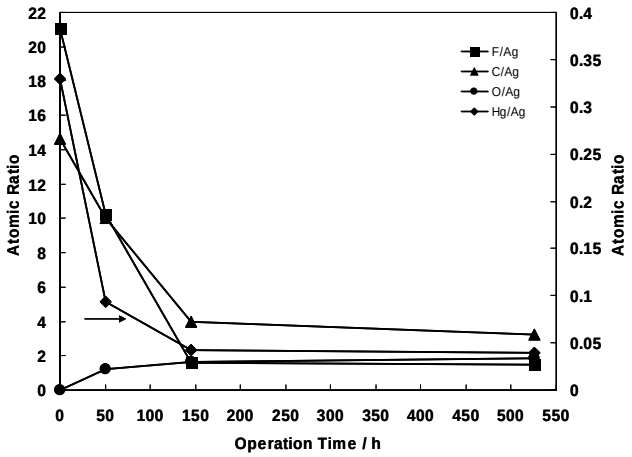

Figure 16. Comparison of relative concentrations for GDE-fresh, GDE-1, GDE-2 and GDE-3 electrodes derived from XPS before sputtering

The atomic ratio of F/Ag and C/Ag decreased with time while O/Ag increased. This means that hydrophobicity decreased and the amount of hydroxides increased. The most significant variation in surface properties occured in the first period of operation. A drastic decrease is observed in Hg in the first 50 hours according to the EDX analysis. The precipitation of sodium hydroxide and AgCl is also confirmed by the plot of Na and Cl concentrations normalized to Hg versus time (Fig. 17). As observed above, it seems that the formation of hydroxides prevails with respect to AgCl.

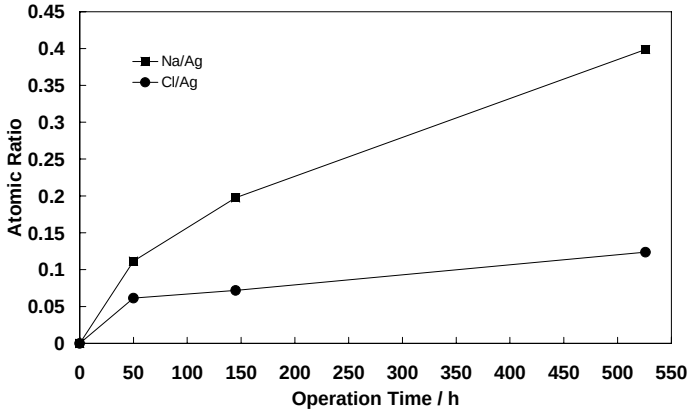

Figure 17. Variation of Na/Ag and Cl/Ag ratios vs. operation time as derived from XPS

Interestingly, the decrease of Hg content from the inner layers (Fig. 18a), as determined by XPS analysis of the sputtered electrodes, is not as drastic as that observed in the outer layers by both XPS and EDX.

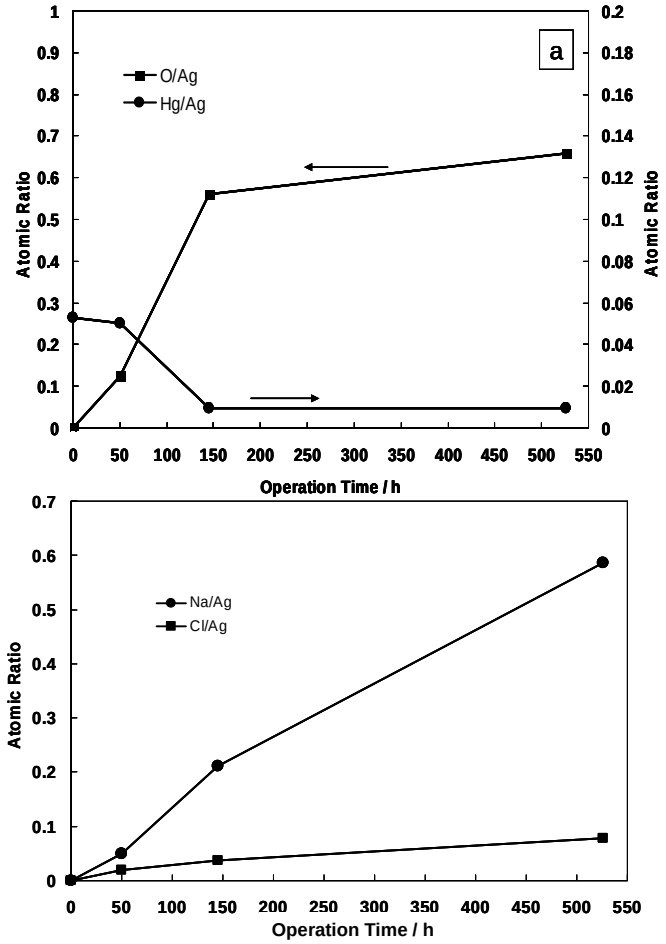

Figure 18. Qualitative comparison among GDE-fresh, GDE-1, GDE-2 and GDE-3 versus atomic ratio of different elements using XPS after sputtering:
(a) O/Ag and Hg/Ag; (b) Na/Ag and Cl/Ag

This indicates that there is a progressive migration of Hg from the bulk to the surface, followed by dissolution into the electrolyte. The precipitation of sodium hydroxide and AgCl is observed in the XPS data on sputtered electrodes (Fig. 18 b).

Careful observation of electrodes by SEM and by using EDX allowed the identification of a local formation of sodium hydroxide, AgCl, and Hg particles on the surface resulting from precipitation and Hg segregation, respectively. This is a qualitative confirmation of what is derived from EDX and XPS analyses (Fig. 19).

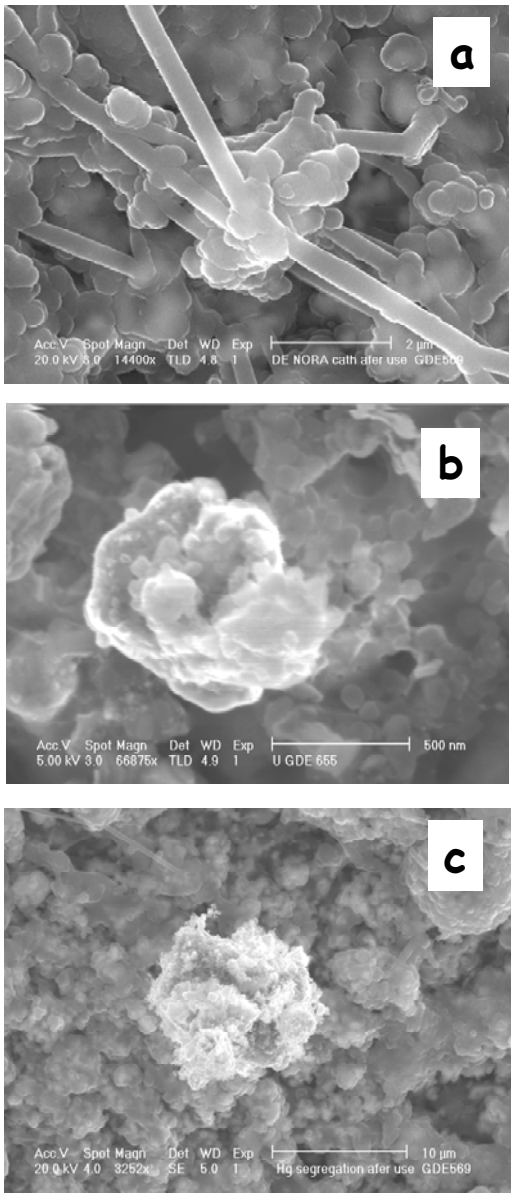

Figure 19. SEM pictures of the electrode surface: a) panoramic view of the electrode surface evidencing PTFE fibres; b) evidence of sodium hydroxide particle; c) Evidence of Hg particles segregated in the surface

Figure 20a shows a comparison of mass change versus temperature in GDE-fresh, GDE-1, and GDE-2. The result of thermal analysis carried out on the electrodes discharged after 526 hours were similar to those of the electrodes discharged after 145 hours.

The TG-DSC analysis of the various electrodes allowed the identification of three main mass-change regions associated with a loss of volatile compounds (up to 150°C), PTFE degradation (up to 320°C), and an Hg loss in bulk (Fig. 20 a). The Hg loss in the thermal analysis experiments decreased progressively as a function of operation time, indicating a reduction of Hg content in electrodes as the length

of time of operation in a chlor-alkali cell increases (Fig. 20 b). This is a further confirmation that Hg diffuses from the bulk to the interface, segregating on the surface as observed by SEM; subsequently, it dissolves into the solution.

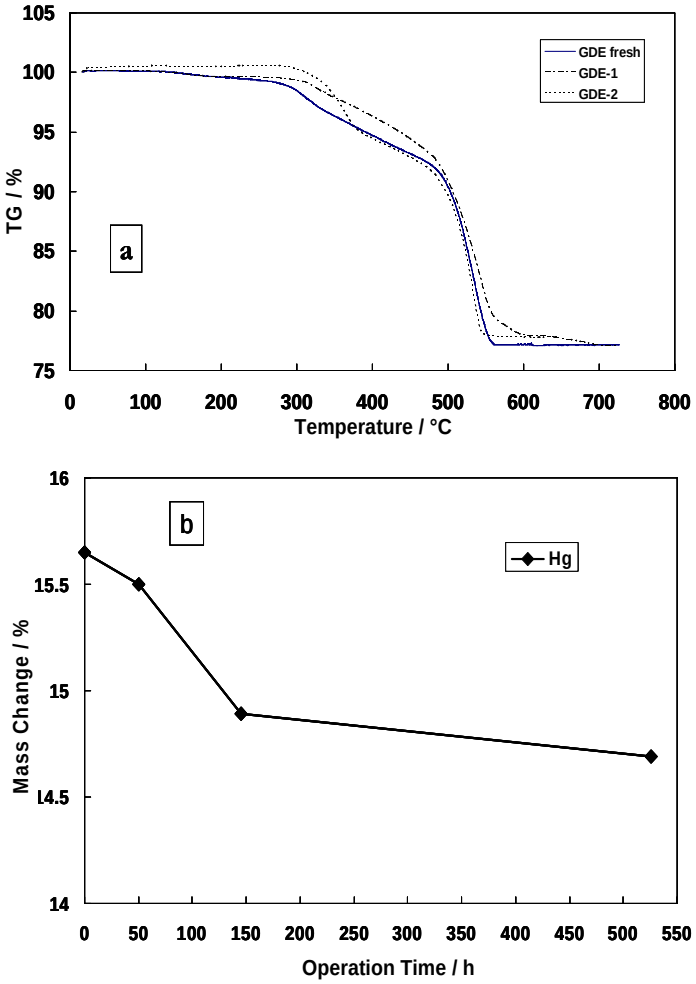

Figure 20. (a) TG-analysis of GDE-fresh, GDE-1 and GDE-2. (b) Hg mass change in the bulk vs. operation times

Previous studies concerning the use of oxygen cathodes in chlor-alkali cells have shown there is a high potential of reducing the power requirements of these devices [10]. Life-time operation of more than 1200 days has been demonstrated for carbon black supported Ag electrodes. Cell voltages between 2.2 and 2.4 V @ 3 kA m^{-2} were observed for Ag loading as small as 2.6 mg cm^{-2} [10]. The role of Ag in the ORR in a 32% NaOH electrolyte at 80°C was attributed to the promotion of the four-electron oxygen reduction to OH^- while avoiding H_2O_2 as reaction intermediate [8].

In our experiments, we recorded cell voltages of 2 V @ 3 kA m^{-2} but only in the presence of a large excess of Ag catalyst. This catalyst layer differs from the carbon supported Ag catalysts previously reported in the literature on large Ag loading and Hg addition. Large Ag loading allows the proper protection of a current collector and ensures long-term stability. This reaction occurs at the interface with the electrolyte; thus, only a small fraction of the total amount of Ag is involved in the electrochemical process. Despite higher costs, this approach reduces the risks of process interruption over several years of operation. From previous reports on fuel cells [16], we preferred to avoid a carbon support since it is oxidized into CO_2 by the oxygen feed over long periods of operation. This usually causes irreversible degradation of the catalyst. Hg is reported to stabilize Ag against corrosion [12]. However, the present analysis shows that this protection is less effective during the first period of operation, in which Hg migrates towards the surface causing a small segregation. This phenomenon, is possibly responsible for a rapid increase in overpotential at the beginning of electrochemical testing. Yet, it does not continue as significantly over time as revealed by our physico-chemical analyses. After the first 40 hours, cell voltage shows only a small, steady decay over time. The present physico-chemical analysis shows a small loss in hydrophobicity with time. This improves the wetting properties of the catalyst surface but causes constraints on oxygen mass transport at interface.

Electrodes prepared in accordance with this approach show the capacity to operate for two decades in chlor-alkali cells; however, it is imperative to reduce the initial decay that affects overall performance. The identification of the constraints that determine cell voltage increase vs. time is the first step towards this goal.

2.4 Conclusions

The purpose of the present study was to investigate the cathodic properties for the oxygen reduction at gas-diffusion electrodes (GDEs) for electrolysis in chlor-alkali cells at 90°C.

Gas diffusion electrodes were analysed before and after different operation times in a chlor-alkali cell [17]. Electrode stability was investigated by life-time tests. The surface of gas diffusion electrodes was analyzed for both fresh and used cathodes by scanning electron microscopy (SEM-EDX) and X-ray photoelectron spectroscopy (XPS). The bulk of gas diffusion electrodes was studied by X-ray diffraction (XRD) and thermogravimetric analyses (TG-DSC). Two main degradation processes occurring on different time-scales have been identified and attributed to a segregation and loss of Hg at the interface and a decrease in hydrophobic properties with time. The Hg loss at the interface was identified in both EDX and XPS analyses and qualitatively observed by SEM. This process is quite significant in the first 50 hours of operation. The dramatic (logarithmic) increase in overpotential is most likely associated with Hg segregation on the surface and dissolution at interface. Subsequent to the first 50 hours, this process proceeds less rapidly with time, involving a slow migration from the bulk (TG analysis). The decrease of hydrophobic properties occurs progressively during all periods of operation as evidenced by EDX and XPS analyses and qualitatively corroborated by TEM. This latter process, together with progressive Hg loss from the bulk, could be associated with the linear decay on a large time-scale. Furthermore, an increase in the precipitation of products from the reaction process also contributes to a decrease in performance resulting from the occlusion of reaction pores. Such an effect should influence, primarily, mass transport properties at high current densities. The effects of this phenomenon are not clearly envisaged from the electrochemical experiments carried out at practical current densities. These phenomena may cause electrode blocking after prolonged operation. There is no significant change in the particle size of the catalysts at different intervals of operation; this indicates that the degradation of electrodes is not associated with any electrochemical sintering of the catalysts.

2.5 References

[1] Faita G, Federico F (2002) European Patent 1362133

[2] Gritzner G (1977) US Patents 4 035 254 and 4 035 255

[3] Gestaut L, et al. (1983) abstracts of ECS Fall Meeting, No. 393

[4] Aikawa H, Poblotzki J (1996) Soda and Chlorine 47**:**93

[5] Gestaut LJ, Clere TM, Niksa AJ, Graham CE (1983) The Electrochemical Society Extended Abstracts, Abstract 124:196, Vol. 83-2, Los Angeles, CA, May 8-13 1983

[6] Chatenet M, Aurousseau M, Durand R, Andolfatto F, (2003) J Electrochem Soc 150:D47

[7] Uchimura A, Ichinose O, Furuya N (1997) Denki Kagaku 65:1032

[8] Ichinose O, Kawaguchi M, Furuya F (2004) J Appl Electrochem 34:55

[9] Aikawa H Poblotzki J (1994) Sodium Hydroxide to Enso 45:85

[10] Furuya N, Aikawa H (2000) Electrochim Acta 45:4251

[11] Janowitz K, Dresel T, Woltering P (2004) US Patent 2004/0152588 A1

[12] Nidola A in "Electrodes of Conductive Metallic Oxides", Part B, Trasatti S Ed., Elsevier Scientific Publishing Company - Chapter 11 - Technological Impact of Metallic Oxides as Anodes – p. 646

[13] Martelli GN, Ornelas R, Faita G (1994) Electrochim Acta 39(11/12):1551

[14] Martelli GN, Reduzzi E, Caldarera A, Urgeghe C (2004) Joint International Meeting, The Electrochemical Society Inc., Honolulu, Hi, USA, October 3-8 2004

[15] Staiti P, Aricò AS, Antonucci V, Hocevar S (1998) J. Power Sources 70:91

[16] Ball SC, Hudson SL, Thompsett D, Theobald B (2007) J. Power Sources 171(1):1

[17] S. Siracusano, T. Denaro, V. Antonucci, A. S. Arico`, C. Urgeghe, F. Federico. Degradation of oxygen-depolarized Ag-based gas diffusion electrodes for chlor-alkali cells. J Appl Electrochem (2008) 38:1637–1646

CHAPTER 3

Preparation and characterization of RuO_2 catalysts for oxygen evolution in a solid polymer electrolyte electrolyzer

3.1 Introduction

Water electrolysis is traditionally carried out in alkaline media with several commercial electrolyzers available on the market. Water electrolyzers using a solid polymer electrolyte (SPE) are less common and generally utilize expensive materials such as noble metal electrocatalysts and sulphonated polymers with perfluorocarbon chains as proton exchange membranes (Nafion®)[1]. The first electrolyzers using a polymer membrane as electrolyte were developed by General Electric Co. in 1996 for space applications [2].

The oxygen evolution reaction (OER) occurs at a suitable reaction rate on noble metal electrodes (e.g., Pt, Au, Ir, Rh, Ru, and Ag); however, metal oxides are generally more active electrocatalysts for this reaction than metal electrodes [3-5]. The most active oxides for the OER are RuO_2 and IrO_2 [6-14]. IrO_2 exhibits high corrosion– resistance properties, but slightly lower activity than RuO_2 [15]. From the point of view of electro-catalysis, it is important to consider the crystal-field stabilization energy, the dispersion, the crystallinity, and the crystallite size of these oxides. RuO_x is generally prepared by thermal decomposition of $RuCl_3$ [16], which is applied as thin coating on a metallic substrate, usually titanium. The properties of the oxide layer depend on several factors: technique of applying the salt solution, concentration of solution, temperature of calcination, time of heating, etc.

Various methods were developed for the synthesis of noble metals based oxides [17, 18], i.e. the Adams fusion method [19], sol-gel methods [20-24], polyol methods [9, 25]. The different methodologies can affect the properties of the obtained oxide materials. Furthermore, various steps are necessary to complete the oxide powder synthesis. In the present study, a simple, fast and low cost method of preparation of a RuO_2 electro-catalyst, compared to the literature [26-28], was used. A similar procedure was developed by Zheng et al. [29] for electrochemical

capacitor applications; yet, in that case, the particle size was about 20 nm. This synthesis allowed us to obtain a crystalline phase with a suitable particle size (about 10 nm) at low temperatures with a yield of 95%. As reported by H. Ma et al. [28], particle sizes and heat treatment of the material influence the catalytic performance of RuO_2 for OER and the stability. Calcined RuO_2 with large particle sizes showed higher corrosion resistance than uncalcined and low-temperature treated materials [28]. For this reason, in the present study, the synthesized RuO_2 was subjected to different calcination temperatures and investigated in half-cell and single-cell experiments.

3.2 Experimental

3.2.1 Preparation of RuO_2 electrocatalysts

0.01 mol of $RuCl_3 \cdot 3H_2O$ (Aldrich) was dissolved in 100 mL of deionized water. The aqueous solution was then heated (100°C) under air atmosphere and magnetically stirred for 10 min. 1 ml of sodium hydroxide (1 M) was added to the solution in order to obtain the precursor Ru-hydroxide. The reaction mixture was maintained under stirring and heat (100°C) for 45 min. Afterwards, the solution was centrifuged for 10 minutes and filtered. The precipitate was washed several times with deionized water to remove the remaining chlorides. The Ru-hydroxide was dried for 5 h at 80°C. The dry paste was calcined in air at three different temperatures: 200, 300 and 350 °C for 1 h, using a heating ramp of 5 °C/min. Another sample was treated at 300°C for 3h.

3.2.2 Physico-chemical characterization

XRD was performed on the dry electrocatalytic powders using a Philips X-Pert diffractometer that used as radiation source the Kα line of the copper (CuKα). The diffractometer was operated at 40 kV and 20 mA, a step time of 0.5 $2\theta\,min^{-1}$, and an angular resolution of 0.005° 2θ. The diffraction patterns were fitted to the JCPDS (Joint Committee on Powder Diffraction Standards) and the crystalline size distribution was calculated using LBA (line broadening analysis). The TG/DSC analysis was carried out in an STA 409C of NETZSCH - Gerätebau GmbH

Thermal Analysis. The sample was heated from room temperature up to 550 °C at a heating rate of 5 °C/min under air atmosphere.

The morphology of catalysts was investigated by transmission electron microscopy (TEM) using a Philips CM12 instrument. Specimens were prepared by ultrasonic dispersion of the catalysts in isopropyl alcohol depositing a drop of suspension on a carbon-coated grid.

3.2.3 Preparation of working electrode for half-cell measurements

An aqueous solution (100 µl) of catalyst (5 mg) was prepared and mixed in an ultrasonic bath. 2 µl of aqueous solution of catalyst was deposited on a glassy carbon substrate; afterwards, the electrode was coated with 1 µl of Nafion® solution (5% Aldrich). The behaviour of the various catalysts for oxygen evolution reaction was investigated by linear voltammetry (LV).

3.2.4 Half-cell electrochemical characterization

The electrochemical analyses were carried out at room temperature in a conventional three-electrode cell consisting of the ruthenium oxide electrode (working electrode), a reference electrode ($Hg/HgSO_4$ sat.) and a platinum grid (counter electrode) (0.07 cm^2 geometrical area). The electrolyte solution was 0.1 M H_2SO_4. A inert gas was fed to the solution for 30 min before the test. The cell was connected to an AUTOLAB PGSTAT 302 Metrohm potentiostat/galvanostat. To evaluate catalysts activity for OER, a linear voltammetry in a potential range from 1.20 V to 1.65 V vs. RHE was carried out.

3.2.5 Preparation of membrane and electrode assembly (MEA)

A Nafion 115 (Ion Power) membrane was used as solid polymer electrolyte. The oxygen evolution catalysts were directly deposited onto one side of the Nafion 115 by spray technique at 80°C. Catalytic inks were composed of aqueous dispersions of catalyst, deionised water, Nafion® solution (5% Aldrich) and anhydrous Ethylic alcohol (Carlo Erba); the anode catalyst loading was about 3 mg/cm^2. A Ti/Pt (95:5) grid was used as backing layer. A commercial 30%

Pt/Vulcan XC-72 (E-TEK, PEMEAS, Boston, USA) was used as catalyst for the H_2 evolution. The cathode electrode was prepared by directly mixing in an ultrasonic bath a suspension of Nafion ionomer in water with the catalyst powder. The obtained paste was spread at room temperature on carbon cloth backings (GDL ELAT from E-TEK) with a Pt loading of 0.6 mg cm^{-2}. The ionomer content in both electrodes was 33 wt.% in the catalytic layer after drying. MEAs (5 cm^2 geometrical area) were directly prepared in the cell housing by tightening at 9 N·m (70 $Kgcm^{-2}$) using a dynamometric wrench.

3.2.6 Electrochemical characterization of MEA

The SPE electrolyzer performance was evaluated at 80°C. Heated deionised water, which was circulated by a pump at a flow rate of 2 ml/min, was supplied to the anode compartment. The water temperature was maintained at the same cell temperature. Measurements of cell potential as a function of current density, electrochemical impedance spectroscopy (EIS) and chrono-amperometry were carried out by using an Autolab PGSTAT 302 Potentiostat/Galvanostat equipped with a 20 A booster (Metrohm).

3.3 Results and Discussion

XRD analyses were carried out on the anode catalysts. Figure 1 shows XRD patterns of the precursor powder before and after calcination at 200, 300 and 350°C. The XRD peaks were assigned to RuO_2 in a tetragonal crystallographic structure. No presence of Ru in a metallic form was found. The mean crystallite size was estimated from the broadening of main peaks by the Debye-Scherrer equation. The crystallite size found was in an interval from 8 to 12 nm and it was similar for the powders calcined at the different temperatures. In order to investigate the precursor calcination process, a thermal analysis was carried out. The results of TGA and DSC measurements are shown in Figure 2.

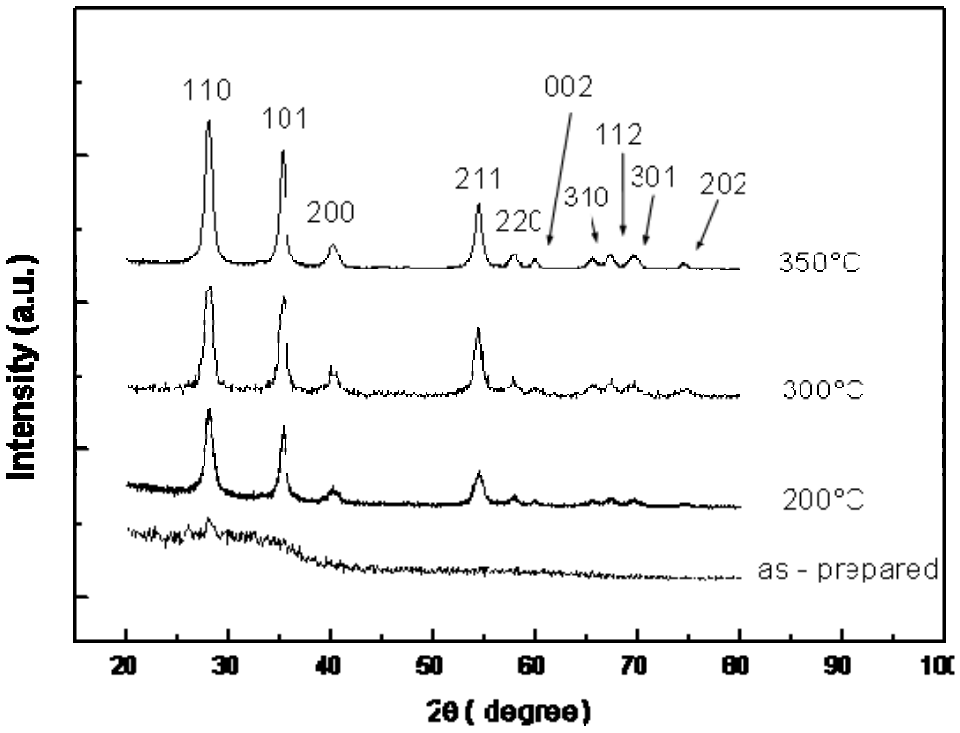

Figure 1. X-Ray diffraction patterns of RuO_2 as-prepared and calcined powders at various temperatures

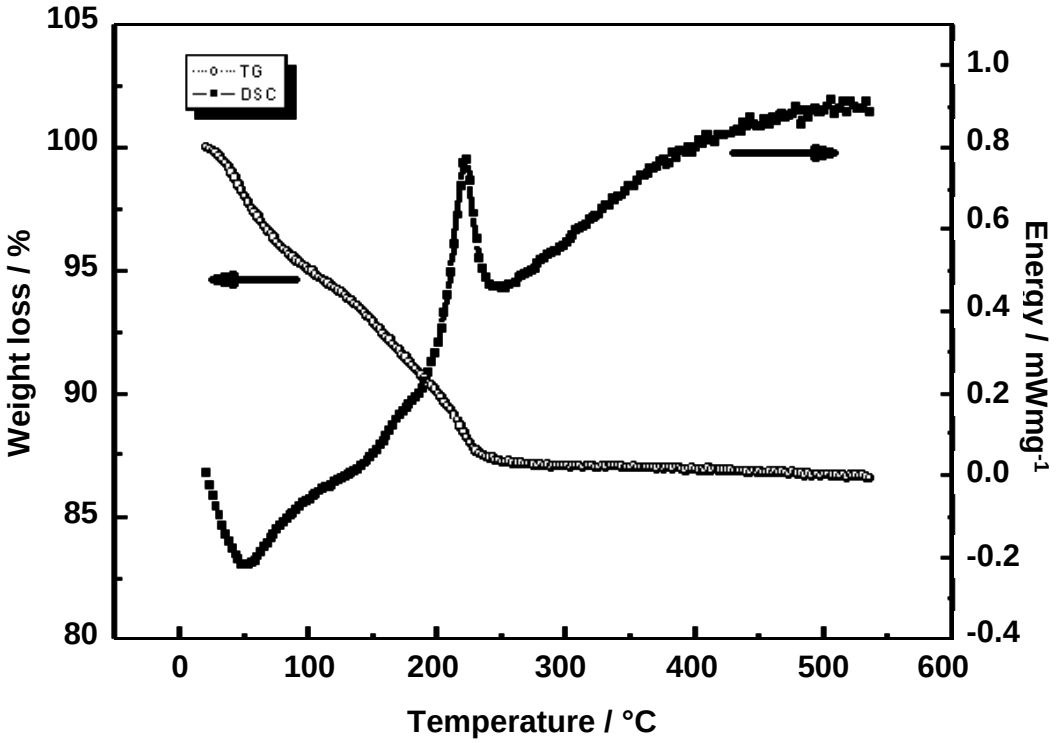

Figure 2. TGA and DSC curves of RuO_x as-prepared powder

The first weight loss was assigned to physical dehydration (below 120°C); whereas, the second one was attributed to chemical dehydration (in the range 120-210°C). An endothermic peak was observed in the range 180-260°C due to an amorphous to crystalline structure phase transition of RuO_2 as confirmed by XRD. Above 260°C a slight oxygen loss was recorded. Total weight losses of 14 wt.% were observed after treatment at 550°C.

Figure 3 shows the half-cell I-V curves for uncalcined and calcined samples. The best performance for the oxygen evolution reaction at ambient temperature was obtained for the RuO_2 powder calcinated at 300°C. The maximum current density was 180 mA cm^{-2} at 1.65 V. This catalyst was selected for the further investigations in an SPE electrolyzer. In order to evaluate the effect of duration of the thermal treatment, a RuO_2 calcined at 300°C for 3 h was also prepared for comparison.

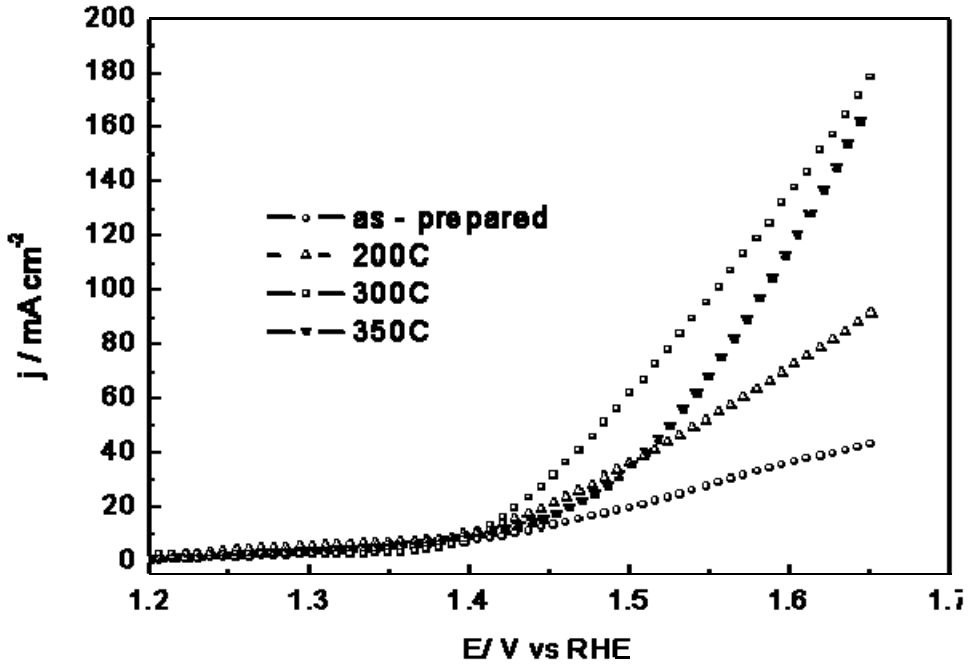

Figure 3. Linear Voltammetry of RuO_2 powder-based electrodes, synthesized and calcined at various temperatures, in 0.5 M H_2SO_4 half – cell at 25°C

In order to determine the morphology of the powders, TEM analysis was carried out on the amorphous precursor and on the most promising catalyst (sample calcinated at 300°C). Images are shown in Figures 4-5.

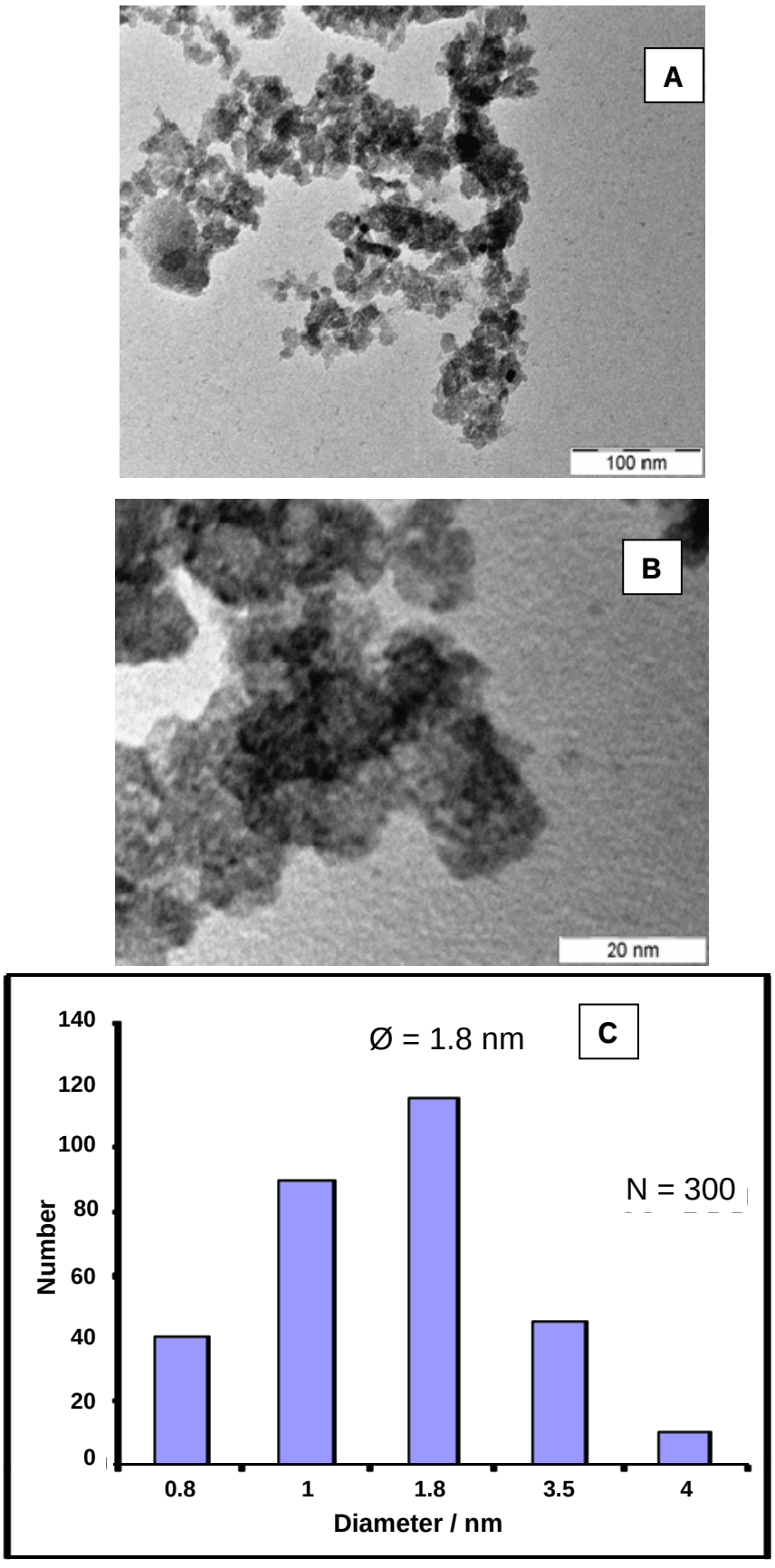

Figure 4. TEM micrographs of RuO_x synthesized: (A) and (B) at different magnifications (C) Particle size distribution analysis

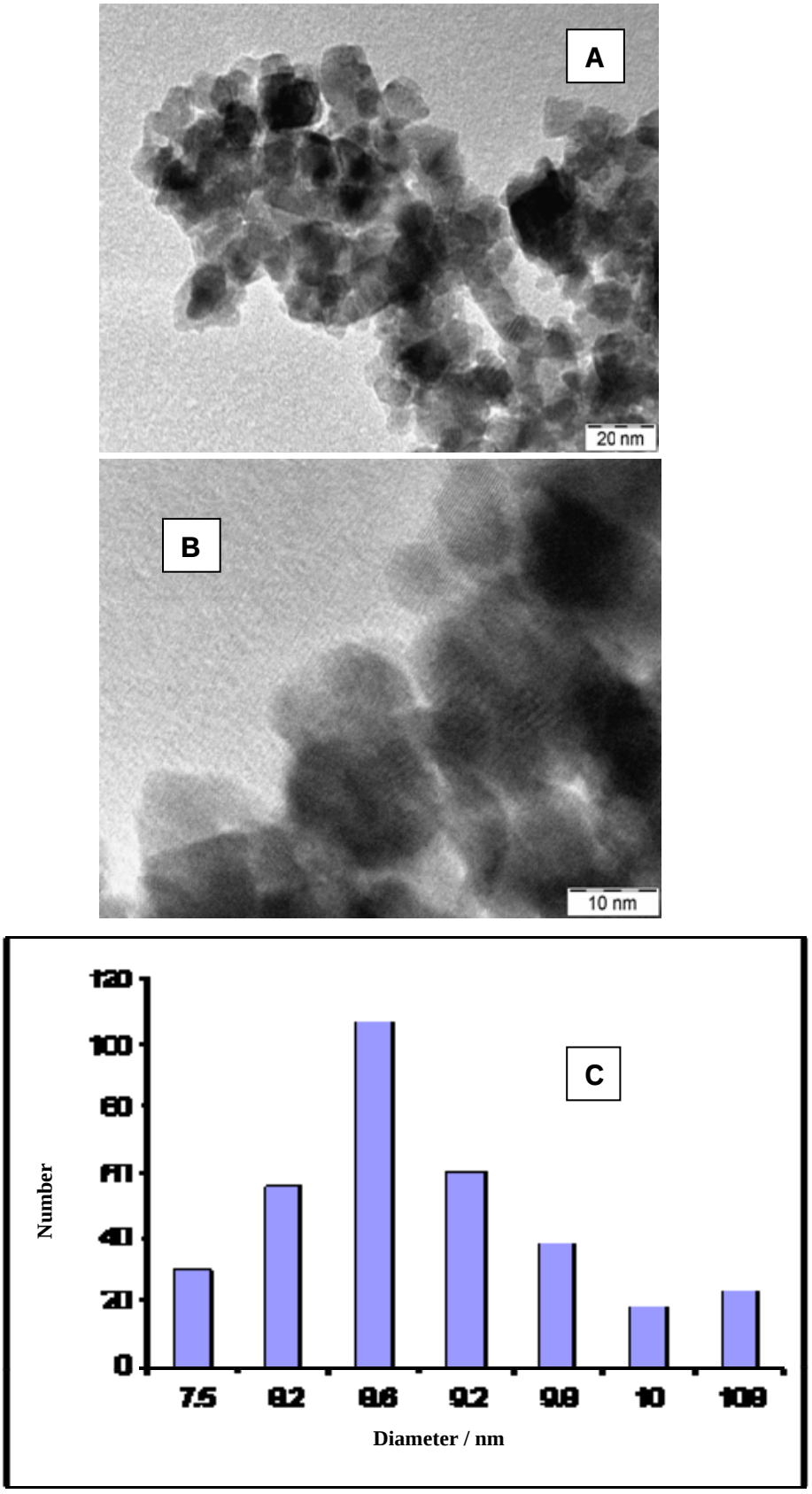

Figure 5. TEM micrographs of RuO_2 calcined at 300 °C/1 h: (A) and (B) at different magnifications (C) Particle size distribution analysis

From this analysis, agglomerates of small size appear to be present mainly in amorphous powder with a particle size of 1.8 nm; whereas, for the 300°C 1 h calcined powder, a crystalline structure with a particle size of about 9 nm was clearly observed. Processing of this TEM image by Fourier transformations and using Carine crystallography software allowed to confirm the tetragonal crystal phase of RuO_2; a scheme representation of the crystal structure is presented in figure 6. The powder calcined for 3 h showed a similar morphology of the sample calcined for 1 h (not shown).

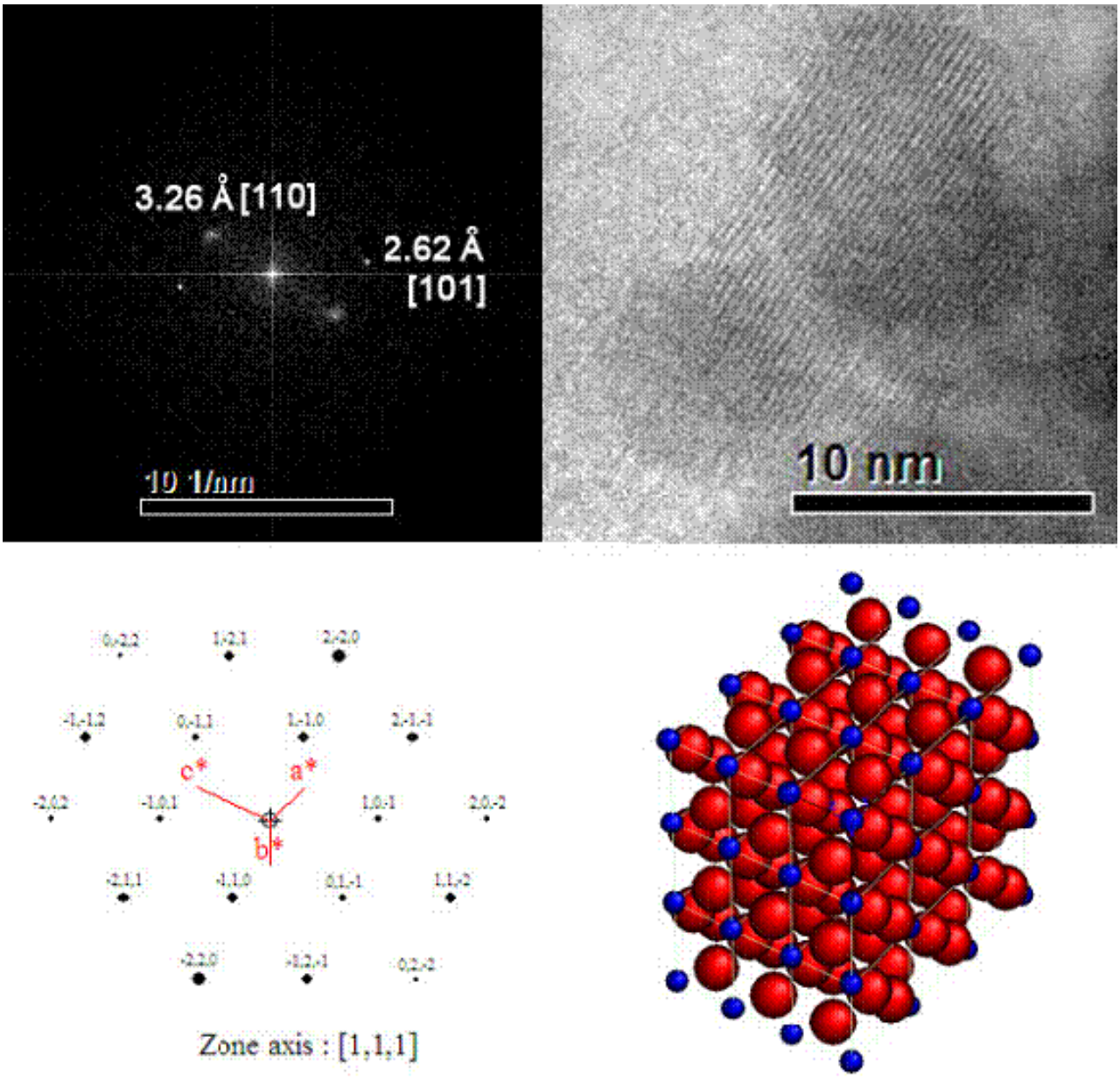

Figure 6. TEM image of RuO_2 calcined at 300 °C/1 h: Scheme representation of tetragonal RuO_2 crystal structure by Carine Crystallography Software

The three samples were analyzed in a SPE single cell electrolyzer (Figure 7).

Figure 7. SPE single cell electrolyzer (5 cm^2 active area)

Series and charge transfer resistances were evaluated by means of EIS at 1.5 V. Figure 8 shows the EIS spectra of electrolyzers with the above mentioned catalysts at 80°C under atmospheric pressure.

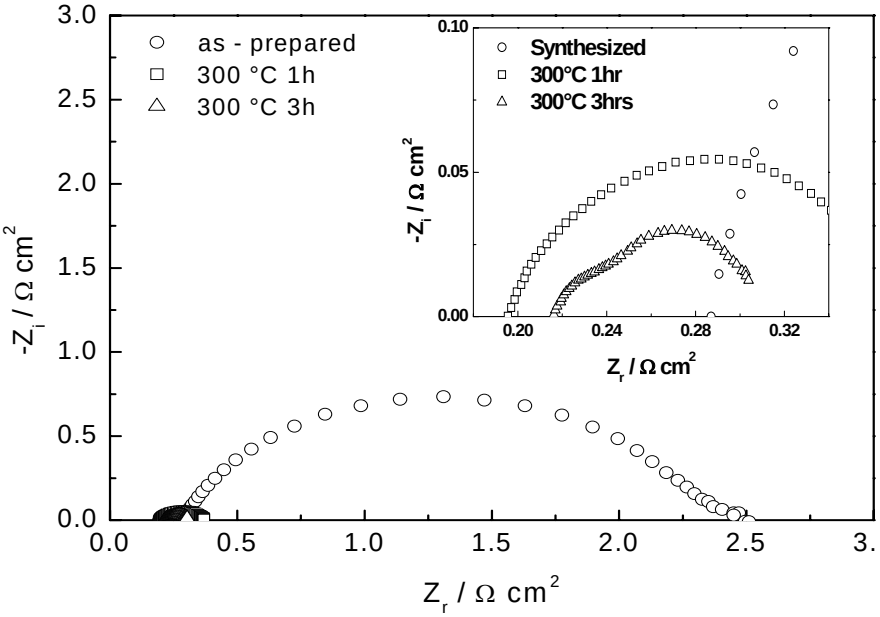

Figure 8. Impedance Spectroscopy of the SPE electrolyzer based on RuO_2 electrocatalysts, as-prepared and calcined at 300°C for 1 h and 3 h at 80°C and 1.5 V

The impedance plots (Nyquist) reveal a larger series and charge transfer resistance for the amorphous RuO_2 than the calcined ones. The minimum in the series resistance was observed for the electrolyzer with the powder calcined at 300°C for 1h with a value of 0.19 ohm·cm^2; whereas, the lowest charge transfer resistance was obtained for the sample calcined for 3 h, i.e. 0.085 ohm·cm^2.

Figure 9 shows the I-V curves at 80°C under atmospheric pressure for the amorphous sample and for the powder after calcination at 300 °C for 1 h and 3 h.

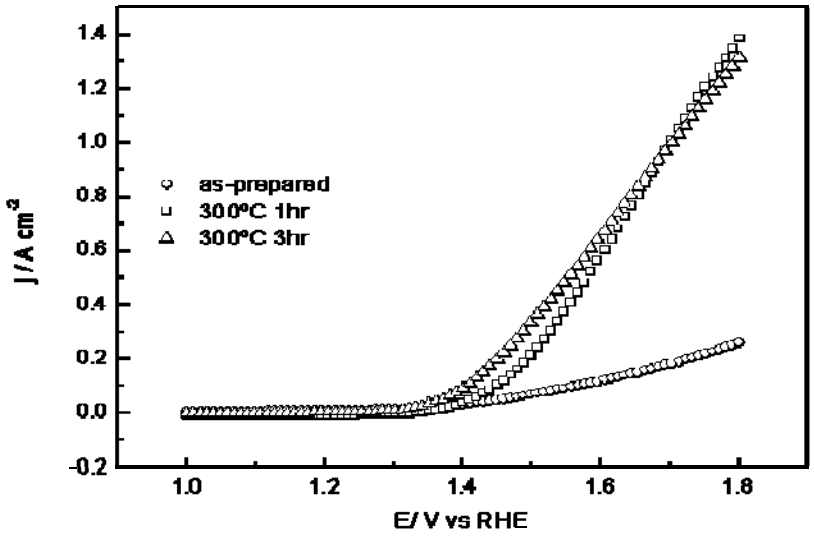

Figure 9. Linear Voltammetry of the SPE electrolyzer based on RuO_2 powders, as-prepared and calcined at 300°C for 1 h and 3 h at 80°C

The electrocatalyst performance in the single cell is significantly larger than in half cell primarily due to the higher noble metal loading in the MEA electrodes. A contribution of sulfate anions adsorption in determining a poorer performance on half cell experiments is not discarded. The cell equipped with RuO_2 calcined at 300°C for 3 h showed an onset for the OER more shifted towards lower potentials according to the lower charge transfer resistance obtained by the EIS analysis. This indicates a better catalytic activity of this catalyst probably due to a suitable crystalline structure. The cell based on RuO_2 calcined at 300°C for 1 h showed a higher onset potential for OER than the previous one, but a better behavior in terms of ohmic characteristics, according to a lower series resistance recorded by EIS analysis for this cell. Thus, the maximum current density at high potential (1.8 V) was obtained using RuO_2 calcined at 300°C for 1 h; it was about 1.4 A cm^{-2}.

This performance appears to be comparable to the state of art [30-34] in this field and it appears promising if one considers that a simple catalyst preparation method, which can be subjected to further improvement, was used.

The ohmic-drop-corrected Tafel plots for oxygen evolution reaction at the RuO_2 electrocatalysts calcined at 300°C for 1 h and 3 h are shown in Figure 10. Two Tafel slopes have been identified for the oxygen evolution process at 80°C in the PEM electrolyser. At low current densities, the Tafel slope is 65-75 mV·dec^{-1}, whereas at large current densities it is 132-133 mV·dec^{-1}. These values are similar to those already observed in the literature at room temperature for the oxygen evolution process with oxide based electrodes [15, 35-38]; i. e., 60 mV·dec^{-1} and 120 mV·dec^{-1} in the low and high current density range respectively.

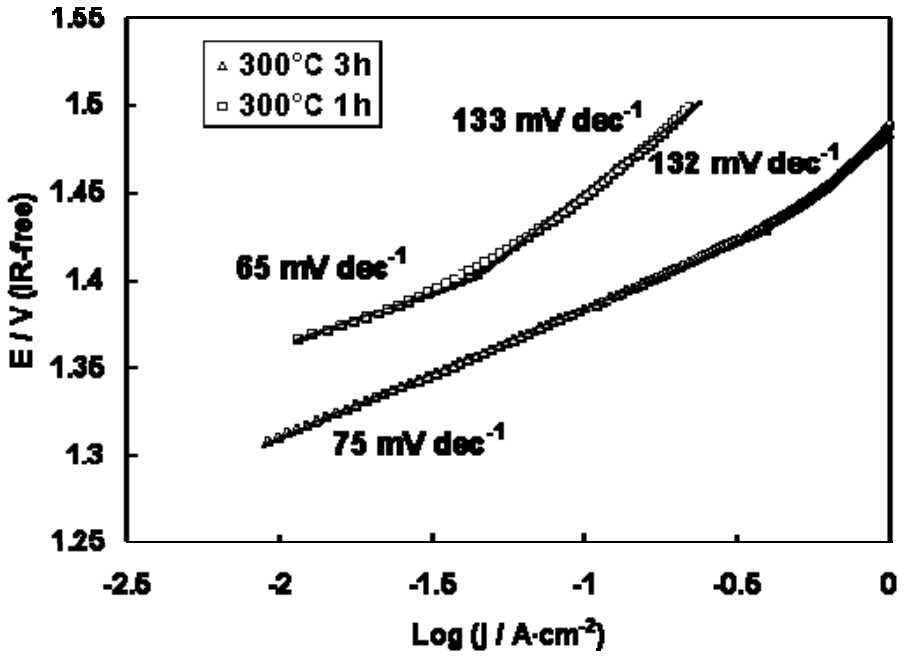

Figure 10. Tafel plot for oxygen evolution reaction in a SPE electrolyser for the RuO_2 powder calcined at 300°C for 1 h and 3 h at 80°C

A Tafel slope of 120 mV·dec^{-1} is generally attributed to the dissociative water adsorption with release of a proton and electron according to the following mechanism:

$$S + H_2O \rightarrow S - OH + H^+ + e^- \quad (1)$$

The low Tafel slope can be attributed to the presence of adsorption intermediates involving OH species on the electrode surface with different energy states [15, 35]. It is not discarded a possible contribution to the rate determining

step of the electrochemical desorption of a proton from the adsorbed OH species as reaction intermediates at low current densities.

Figure 11 shows the chronoamperometric measurements carried out at 80°C and atmospheric pressure for the RuO_2 electrocatalysts calcined at 300°C for 1 h and 3 h. These experiments were performed at a potential of 1.6 V for 20 hours. The cell equipped with RuO_2 calcined at 300°C for 3 h showed a higher current density compared to the cell equipped with RuO_2 calcined at 300°C for 1 h. This evidence was in agreement with the I-E curves (Fig. 9). It was observed that the current density slightly decreased during the time for both measurements. This could be due to the presence of small particles in the catalysts that can be more subjected to corrosion, on the contrary of large RuO_2 particles which appear to be sufficiently stable [28]. However, our evidences confirm the low stability of RuO_2 that was discussed in several papers in the literature [12, 13]. The largest loss was showed with RuO_2 calcined at 300°C for 1 h. This could be due to the higher stability of RuO_2 particles calcined for 3 h compared to RuO_2 particles calcined for 1 h. However, an increase of the RuO_2 particle size causes a decrease of catalytic activity for oxygen evolution for the sample calcined at 350°C. Further studies are in due course to assess the stability of larger RuO_2 nanoparticles. Another strategy to improve the stability of the RuO_2 electrocatalyst relies on the use of IrO_2-RuO_2 solid solutions. The aim is to reach a good compromise between stability and performance.

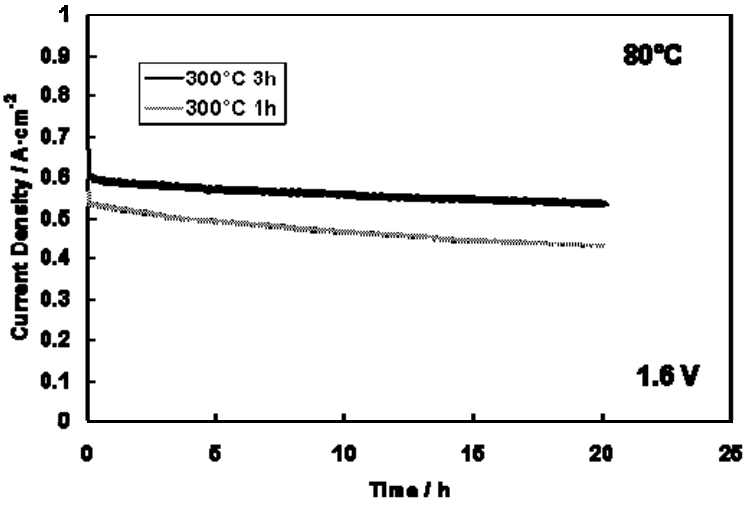

Figure 11. Chronoamperometric measurement of the SPE electrolyser based on RuO_2 calcined at 300°C for 1 h and 3 h at 80°C

3.4 Conclusions

A simple, fast and low temperature colloidal method for the obtainment of RuO_2 nano-particles was developed [39]. Catalysts were prepared by colloidal deposition at a temperature near to 100°C and, successively, calcined at different temperatures from 200 to 350°C. The physico-chemical characterization was carried out by XRD, TG-DSC and TEM analyses. The electrochemical activity of these catalysts as anodes in an SPE electrolyzer was investigated. The maximum current density at high potential (1.8 V) was obtained using RuO_2 calcined at 300°C for 1 h; it was about 1.4 A cm^{-2}. Yet, the best results were obtained for the RuO_2 calcined at 300°C for 3 h in the chronoamperometric measurements with a higher current density at 1.6 V for 20 hours compared to the RuO_2 calcined at 300°C for 1 h. However, chronoamperometric measurements showed a slightly decrease of performances with time. A further optimization of the physico-chemical proprieties of these materials is necessary in order to increase the stability and performance for application in a PEM electrolyzer.

3.5 References

[1] R. Oberlin, M. Fischer, Brown Boveri Review, 73, 445 (1986).

[2] W. Kreuter, H. Hofmann, Hydrogen Energy Progress XI, 1, 537 (1996).

[3] V. Baglio, A. Di Blasi, T. Denaro, V. Antonucci, A.S. Aricò, R. Ornelas, F. Matteucci, G. Alonso, L. Morales, G. Orozco, L.G. Arriaga, J. New Materials for Electrochem. Systems, 11, 105 (2008).

[4] L.G. Arriaga, W.M. Martínez, U. Cano, H. Blud, Int. J. Hydrogen Energy, 32, 2247 (2007).

[5] Marshall A, Børresen B, Hagen G, Tsypkin M, R. Tunold, Materials Chemistry and Physics, 94, 226 (2005).

[6] L.M. Da Silva, J.F.C. Boodts, L.A. De Faria, Electrochim. Acta, 46, 1369 (2001).

[7] H. Tamura, C. Iwakura, Int. J. Hydrogen Energy, 7, 857 (1982).

[8] S. Trasatti, G. Lodi, in: S. Trasatti (Ed.), Electrodes of Conductive Metallic Oxides : Part B. Elsevier, Amsterdam, 1980 .

[9] E. Rasten, G. Hagen, R. Tunold, Electrochim. Acta, 48, 3945 (2003).

[10] A. de Oliveira-Sousa, M.A.S. da Silva, S.S. Machado, L.A. Avaca, P. de Lima-Neto, Electrochim. Acta 45, 4467 (2000).

[11] T. Ioroi, N. Kitazawa, K. Yasuda, Y. Yamamoto, H. Takenaka, J. Electrochem. Soc., 147, 2018 (2000).

[12] R. Kotz, H.J. Lewerenz, S. Stucki, J. Electrochem. Soc., 130, 825 (1983).

[13] R. Kotz, S. Stucki, Electrochim. Acta, 31, 1311 (1986).

[14] Y. Matsumoto, E. Sato, Materials Chemistry and Physics, 14, 397 (1986).

[15] J. M. Hu, J. Q. Zhang, C. N. Cao. Int. J. Hydrogen Energy, 29, 791 (2004).

[16] Y. Zhang, C. Wang, N. Wan, Z. Mao, Int. J. Hydrogen Energy, 32 (2007) 400.

[17] J. R. Osman, J. A. Crayston, A. Pratt, D. T. Richens, Materials Chemistry and Physics, 110, 256 (2008).

[18] Q.L. Fang, D.A. Evans, S.L. Roberson, J.P. Zheng, J. Electrochem. Soc., 148, A833 (2001).

[19] R. Adams, R. Shriner, J. Am. Chem. Soc., 45, 2171 (1923).

[20] Y. Murakami, H. Ohkawauchi, M. Ito, K. Yahikozawa, Y. Takasu, Electrochim. Acta, 39, 2551 (1994).

[21] Y. Murakami, S. Tsuchiya, K. Yahikozawa, Y. Takasu, Electrochim. Acta, 39, 651 (1994).

[22] M. Ito, Y. Murakami, H. Kaji, H. Ohawauchi, K. Yahikozawa, Y. Takasu, J. Electrochem. Soc., 141, 1243 (1994).

[23] K. Kameyama, S. Shohji, S. Onoue, K. Nishimura, K. Yahikozawa, Y. Takasu, J. Electrochem. Soc., 140 (1993) 1034.

[24] T. Lassali, J. Boodts, L. Bulhoes, J. Non-Cryst. Solids, 273, 129 (2000).

[26] M. Lopez, A. Schleunung, P. Biberbach, Patent n° WO2005049199.

[27] C. Urgeghe, PhD thesis on "Oxygen Evolution and Oxygen Reduction in Electrochemical Energy", University of Ferrara, Italy,2005.

[28] H. Ma, C. Liu, J. Liao, Y. Su, X. Xue, W. Xing, Journal of Molecular Catalysis A: Chemical, 247, 7 (2006).

[29] P. Zheng, P. J. Cygan, and T. R. Jow, J. Electrochem. Soc., 142, 2699 (1995).

[30] S. Song, H. Zhang, X. Ma, Z. Shao, R.T. Baker, B. Yi, Int. J. Hydrogen Energy, 33, 4955 (2008).

[31] L. Krusin-Elbaum, M. Wittmer, J. Electrochem. Soc., 135, 2610 (1988).

[32] L. Nanni, S. Polizzi, A. Benedetti, A. De Battisti, J. Electrochem. Soc., 146, 220 (1999).

[33] M. Ito, Y. Muratami, H. Kaju, K. Yahikozawa, Y. Takasu, J. Electrochem. Soc., 143, 32 (1996).

[34] A.S. Aricò, V. Antonucci, V. Alderucci, E. Modica, N. Giordano, J. Appl. Electrochem., 23 (1993) 1107.

[35] Z. G. Ye, H. M. Meng, D. Chen, H. Y. Yu, Z. S. Huan, X. D. Wang, D. B. Sun, Solid State Sciences, 10, 346 (2008).

[36] A. Damjanovic, A. Dey, J. O. M. Bockris, J. Electrochim. Acta, 11, 791 (1966).

[37] R. Mraz, J. Krysa, J. Appl. Electrochem. 24, 1262 (1994).

[38] S. X. Jin, S. Y. Ye, Electrochim. Acta 41, 827 (1996).

[39] J. C. Cruz, V. Baglio, S. Siracusano, V. Antonucci, A. S. Aricò, R. Ornelas, G. Osorio-Monreal, L. Ortiz-Frade, L.G. Arriaga. Preparation and characterization of

RuO_2 catalysts for oxygen evolution in a solid polymer electrolyte electrolyzer. Int J Hydrogen Energy. Submitted

CHAPTER 4

Nanosized IrO_2 electrocatalysts for oxygen evolution reaction in an SPE electrolyser

4.1 Introduction

Water electrolysis is one of the few processes where hydrogen can be produced from renewable energy sources such as the photovoltaic or wind energy without evolution of CO_2. In particular, an SPE electrolyser is considered as a promising methodology for producing hydrogen as an alternative to the conventional alkaline water electrolysis. A PEM electrolyser possesses certain advantages compared with the classical alkaline process in terms of simplicity, high energy efficiency and specific production capacity. This system utilizes the well know technology of fuel cells based on proton conducting solid electrolytes. Unfortunately, electrochemical water splitting is associated with substantial energy loss, mainly due to the high over-potentials at the oxygen-evolving anode. It is therefore important to find the optimal oxygen-evolving electro-catalyst in order to minimize the energy loss.

Typically, platinum is used at the cathode for the hydrogen evolution reaction (HER) and iridium or ruthenium oxides are used at the anode for the oxygen evolution reaction (OER) [1-2]. These metal oxides are required, compared to the metallic platinum, because they offer a high activity, a better long-term stability and less efficiency losses due to corrosion or poisoning [3-12].

A high surface area is required for the anode electrocatalyst to increase the number of catalytic sites involved in the reaction. Accordingly, most preparation methods aim at obtaining nanosized primary particles. Moreover, being the oxygen evolution process a structure sensitive reaction, it is important to tailor the structural properties which determine the turnover frequency of the catalytic process. This work is mainly addressed to the synthesis and characterization of nanosized IrO_2 catalysts. Various methods are reported in the literature for the synthesis of noble metal based oxides. The Adams fusion method [13] has been

widely used to produce fine noble metal oxide powders [10, 14-17]; it is based on the oxidation of metal precursors in a molten nitrate melt. Sol–gel methods have also proved useful in producing noble metal based oxides [18-22]. A very interesting approach was proposed by Marshall et al. [23-24]; it was based on a modified polyol method in which a glycol-precursor solution was heated under nitrogen atmosphere to the refluxing temperature in order to obtain a colloid. Also Song et al. [10] used this approach to synthesize IrO_2 catalysts with a specific surface area of 203 $m^2\ g^{-1}$. In our work, nanosized IrO_2 catalysts were prepared from $H_2IrCl_6 \cdot nH_2O$ using a similar colloidal process; yet, in order to make it economically competitive and easily applicable, water was used as the solvent instead of ethylene glycol [23-24] and the process was simply carried out under air atmosphere at 100 °C. The resulting hydroxides were then calcined at various temperatures to tailor the structural properties. By using this approach nanosized crystalline particles in the range of 7–9 nm were obtained, allowing the attainment of a good compromise between catalytic activity and stability [25]. We focused our attention on the effect of thermal treatments on the crystallographic structure and particle size of IrO_2 catalysts and how these properties may influence the performance of oxygen evolution electrode. Electrochemical characterizations were carried out by polarization curves, impedance spectroscopy and chrono-amperometric measurements.

4.2 Experimental

4.2.1 Preparation of IrO_2 electrocatalysts

An $H_2IrCl_6 \cdot nH_2O$ (STREM Chemicals, Inc.) powder was first dissolved in deionised water. The aqueous solution was then heated (100°C) under air atmosphere and magnetically stirred for 45 minutes. A sodium hydroxide solution (1 M) was added in order to favour the formation of an Ir-hydroxide. Afterwards, the solution was placed in a centrifuge for 10 minutes and filtered. The precipitate was washed with deionised water to remove the chlorides. The Ir-hydroxide was dried for 5 hrs at 80°C. The dry powder was subjected to a thermal analysis, in order to investigate the processes occurring for the as-prepared catalyst as a

function of the temperature. Afterwards, it was calcined in air at different temperatures, 200, 300, 400 and 500°C for 1 hr, using a heating ramp of 5°C/min. The resulting powders were characterized by X-ray diffraction (XRD) to determine the crystallographic structure and particle size. Catalyst morphology and porosity were investigated by Transmission Electron Microscopy (TEM) and BET measurements, respectively.

4.2.2 Physico-chemical characterization

XRD was performed on the dry electrocatalytic powders using a Philips X-Pert diffractometer that used as radiation source the Kα line of copper (CuKα). This diffractometer operated at 40 kV and 20 mA, step time of 0.5 2θ min^{-1}, angular resolution of 0.005° 2θ. The diffraction patterns were fitted to JCPDS (Joint Committee on Powder Diffraction Standards) and crystalline size distribution was calculated using LBA (line broadening analysis). The TG/DSC analysis was carried out in an STA 409C of NETZSCH - Gerätebau GmbH Thermal Analysis. The sample was heated from room temperature up to 550 °C at a heating rate of 5 °C/min under air atmosphere.

The morphology of the in-house prepared catalyst was investigated by transmission electron microscopy (TEM) using a Philips CM12 instrument and compared to a commercial catalyst (IrO_2 from SPECTRUM). Specimens were prepared by ultrasonic dispersion of the catalysts in isopropyl alcohol and depositing a drop of suspension on a carbon-coated grid.

BET surface area, pore size distribution and pore volume characteristics for the in-house prepared catalyst were measured by a Thermoquest 1990 series Sorptomatic. The Barrett–Joiner–Halenda (BJH) method (C = 0.8) was used for the determination of cumulative area and pore size. Since the aim of this work was to obtain a nanosized catalyst characterized by high surface area, these properties were compared to those of a commercial catalyst to assess the progress beyond the state of art.

4.2.3 Preparation of membrane-electrode assembly (MEA)

A Nafion 115 (Ion Power) membrane was used as the solid polymer electrolyte. The IrO_2 catalysts were directly deposited onto one side of the Nafion 115 by a spray technique. Inks were composed of aqueous dispersions of catalyst, deionised water, Nafion® solution (5% Aldrich) and Ethanol (Carlo Erba); the anode catalyst loading was 3 mg/cm^2. A Ti/Pt (95:5) grid was used as backing layer. A commercial 30% Pt/Vulcan XC-72 (E-TEK, PEMEAS, Boston, USA) was used as the catalyst for the H_2 evolution. The cathode electrode was prepared by directly mixing in an ultrasonic bath a suspension of Nafion ionomer in water with the catalyst powder. The obtained paste was spread on carbon cloth backings (GDL ELAT from E-TEK) with a Pt loading of 0.6 mg/cm^2. The ionomer content in both electrodes was 33 wt.% in the catalytic layer after drying.

MEAs (5 cm^2 geometrical area) were directly prepared in the cell housing by tightening at 9 N·m (70 Kgcm^{-2}) using a dynamometric wrench.

4.2.4 Electrochemical characterization of MEA

The SPE electrolyser performance was evaluated at 80 °C under atmospheric pressure. Heated deionised water, which was circulated by a pump at a flow rate of 2 ml/min, was supplied to the anode compartment. The water temperature was maintained at the same cell temperature. Measurements of cell potential as a function of current density, electrochemical impedance spectroscopy (EIS) and stability test were carried out by an Autolab PGSTAT 302 Potentiostat/Galvanostat equipped with a 20 A booster (Metrohm). The series resistance was determined from the high frequency intercept on the real axis in the Nyquist plot. The charge transfer resistance was taken as the difference between the extrapolated low frequency intercept and the high frequency intercept on the real axis.

4.3 Results and Discussion

In order to investigate the influence of temperature on the precursor modifications, a thermal analysis was carried out. The results of TGA and DSC measurements are shown in Figure 1.

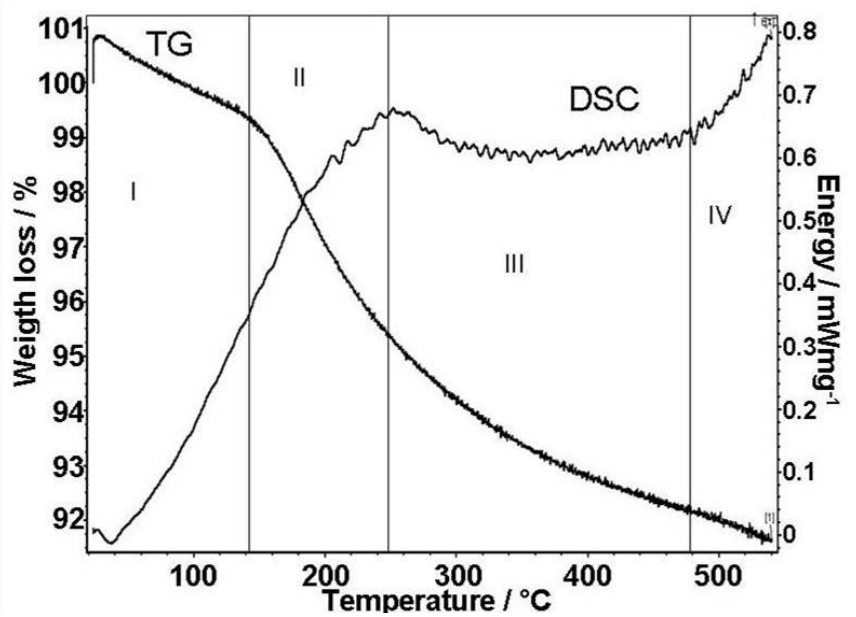

Figure 1. TGA and DSC curves of the as-synthesized IrO_x precursor

The first weight loss (I) was assigned to physical dehydration (below 140°C); whereas, the second one (II) was attributed to chemical dehydration (in the range 140-240°C). A phase transition of IrO_2 from amorphous to crystalline structure (III) was observed in the range 240 - 480°C as confirmed by XRD. This was also accompanied by a slight weight loss due to the decomposition of hydrophilic groups of the amorphous material. Above 480°C (IV) a slight oxygen loss was recorded, possibly forming a substoichiometric oxide. Total weight losses of 8 wt.% were observed after the treatment at 550°C.

Figure 2 shows XRD patterns of the precursor powder before and after calcination at 200°, 300°, 400° and 500°C.

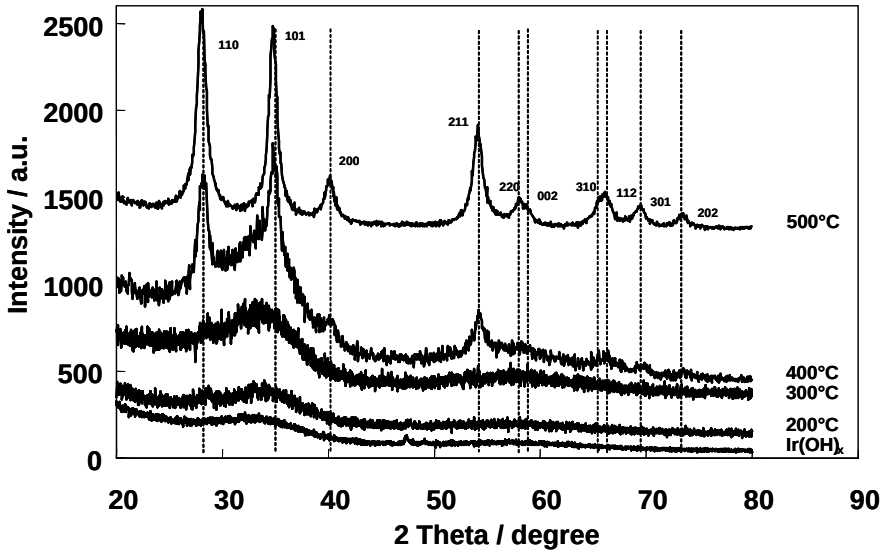

Figure 2. X-Ray diffraction patterns of IrO_2 powders, as-synthesized and calcined at various temperatures

The precursor and samples calcined at 200° and 300°C were characterized by an amorphous phase whereas those calcined at 400° and 500°C showed a crystalline phase with a tetragonal structure. The mean crystallite size for the powder calcined at 400° and 500°C was estimated from the broadening of main peaks by the Debye-Scherrer equation; it was 7 and 9 nm, respectively. No presence of metallic Ir was found in all samples.

All calcined samples were investigated electrochemically for the oxygen evolution reaction in an SPE electrolyzer. A commercial IrO_2 (SPECTRUM) catalyst was also studied for comparison. This catalyst is mainly characterized by an amorphous structure with the presence of a small amount of metallic Ir, as reported elsewhere [26-27]. Being the hydrogen evolution at the Pt/C electrode quite faster than the oxygen evolution at the IrO_2 catalyst [28], the latter represents the rate determining step of the overall electrochemical process. Furthermore, the same Pt/C cathode was used in all experiments.

Figure 3 shows I-V curves for the in-house prepared and commercial anode catalysts. The best performance at high current densities for the oxygen evolution reaction at 80°C was obtained for IrO_2 powder calcined at 400°C. The cell based on the commercial Iridium oxide showed a performance similar to the best catalyst up to 1.6 V.

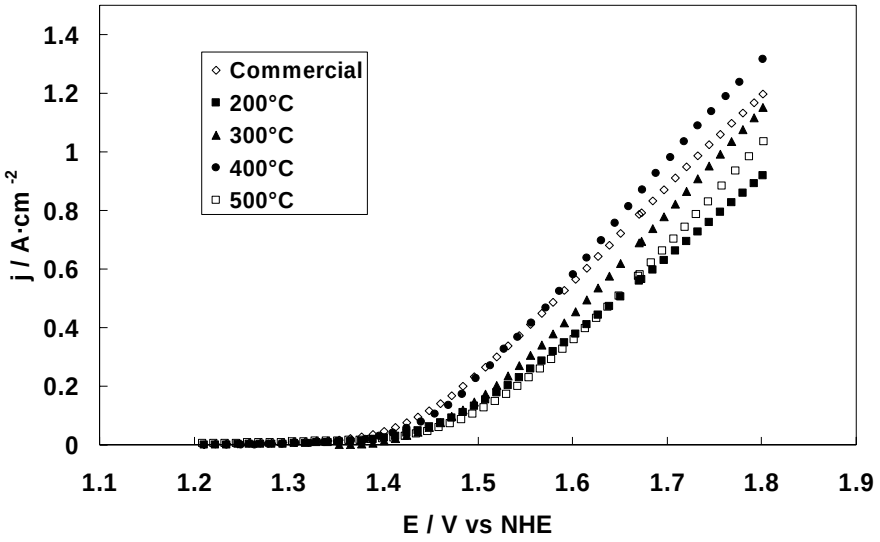

Figure 3. Linear Voltammetry at 80°C of the SPE electrolyzer based on IrO_2 powders, commercial and calcined at different temperatures

The maximum current density reached at 1.8 V with the sample calcined at 400°C was 1.32 A cm^{-2}. The high performance obtained with this catalyst calcined at 400°C was probably due to the simultaneous presence of an amorphous and crystalline structure as an optimal compromise between surface area and specific activity (see Figure 2). A different behaviour in terms of the slope of the I-V curves was also observed for the various samples. To investigate more in depth the electrochemical properties of these materials, impedance spectroscopy measurements were carried out on the different cells at 1.5 V (Figure 4).

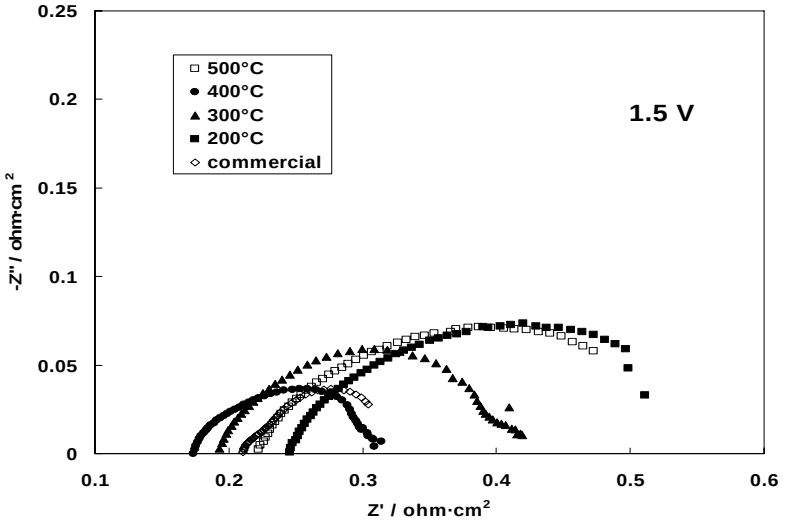

Figure 4. Impedance Spectroscopy at 80°C and 1.5 V of the SPE electrolyser based on IrO_2 electrocatalysts, commercial and calcined at different temperatures

From this analysis, it appears that the sample calcined at 400°C showed both low series (Rs) and charge transfer (Rct) resistance compared to the other samples; this justify the best performance of the cell based on this catalyst.

The cells based on the other in-house prepared catalysts showed a high Rct, indicating a low electro-catalytic activity for the oxygen evolution process. As discussed above, this was interpreted in terms of poor intrinsic activity or low active surface area as related to the structure and particle size. The cell based on the commercial catalyst showed lower charge transfer resistance compared to the sample calcined at 400°C, but larger series resistance possibly due to the amorphous structure similar to the samples treated at 200° and 300°C. Notably, an increase of series resistance is observed for the samples with crystalline structure treated at 500°C. The thermal analysis indicated for this sample an additional loss of oxygen and the onset of an exothermic peak above 450°C indicating the occurrence of structural changes at high temperatures.

As observed from the I-V curves, the onset potential in terms of oxygen evolution for the commercial catalyst is slightly lower than that obtained for the best in-house catalyst. Yet, the latter showed lower series resistance than commercial catalyst. This explains the best performance of the in-house catalyst, in particular at high current densities. In fact, the slope of the I-V curves at high currents for the two catalysts reflects the differences in ohmic drop (Rs). Moreover, from the polarization curves of Figure 3, higher diffusion constraints were observed for the commercial catalyst. This could be due to the different morphology of the two catalysts.

A TEM analysis was carried out on these samples (Figure 5).

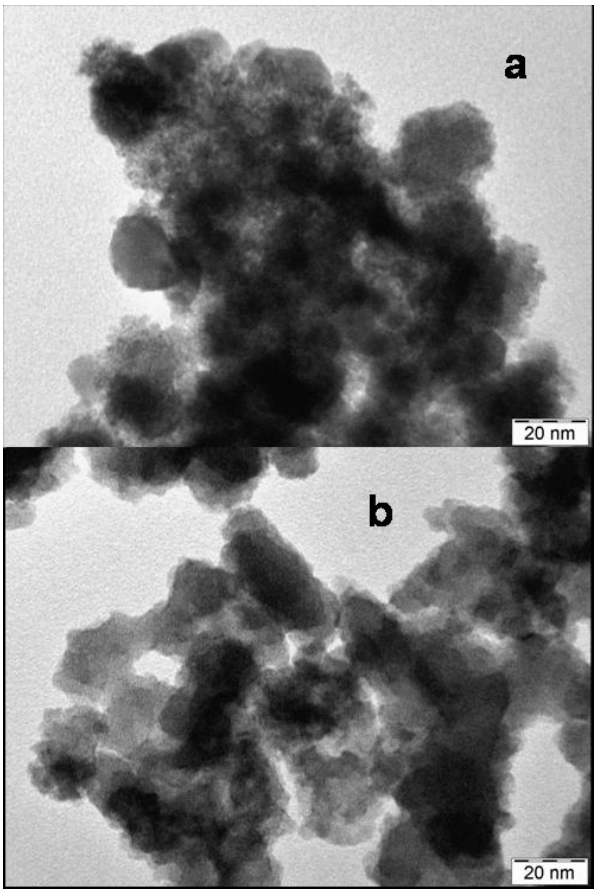

Figure 5. TEM images of a) IrO_2 calcined at 400°C and b) commercial IrO_2

The commercial catalyst (Figure 5a) showed the presence of agglomerates composed of fine particles attributed to the amorphous IrO_2 and some big particles probably due to the presence of metallic Ir. The BET surface area for this catalyst was about 23 $m^2 g^{-1}$. This catalyst appears characterized by the occurrence of micro-pores as confirmed by the porosity measurements reported in Figure 6a. On the contrary of the commercial catalyst, the in-house prepared catalyst calcined at 400°C (Figure 5b) showed larger particles and the prevailing occurrence of meso- and macro-pores (Figure 6b).

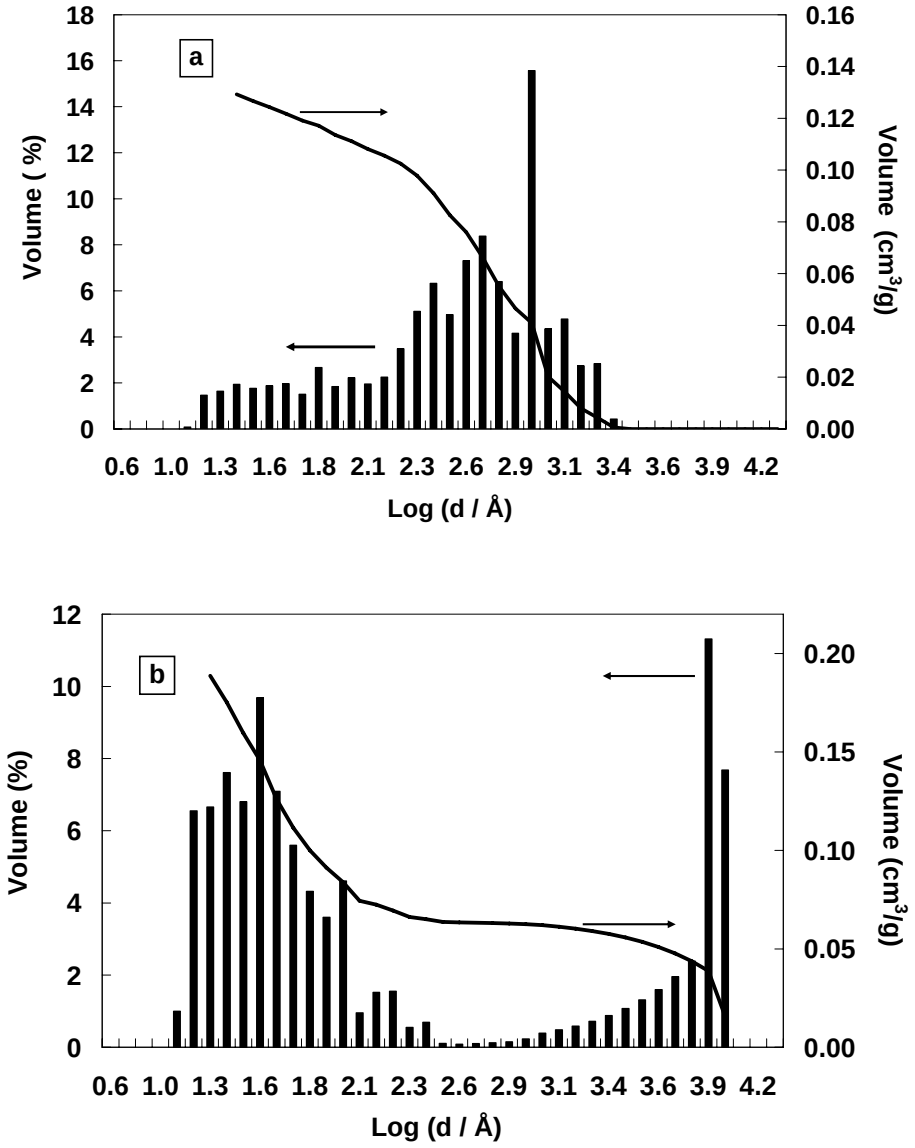

Figure 6. Pore size distribution and cumulative pore volume of a) commercial IrO_2 and b) IrO_2 calcined at 400°C

This may explain the lower mass transfer polarization of the cell based on this catalyst. The BET surface area for this in-house prepared catalyst was about 100 $m^2\ g^{-1}$, This was significantly larger than that measured for the commercial one (23 $m^2\ g^{-1}$), although it was lower than that reported by Song et al. [10] concerning their IrO_2 catalyst obtained by a colloidal method. As well known, the specific surface area is determined by both particle size and dispersion. The occurrence of very fine IrO_2 particles as well as accessible pores for the OER is indicative of a large number of catalytic sites in this sample. This confirms the paramount

influence of the nanostructure and morphology of the anode catalyst in determining the performance of SPE electrolyzers.

The Tafel plots related to the oxygen evolution reaction at the IrO_2 catalyst calcined at 400°C and commercial catalyst are shown in Figure 7.

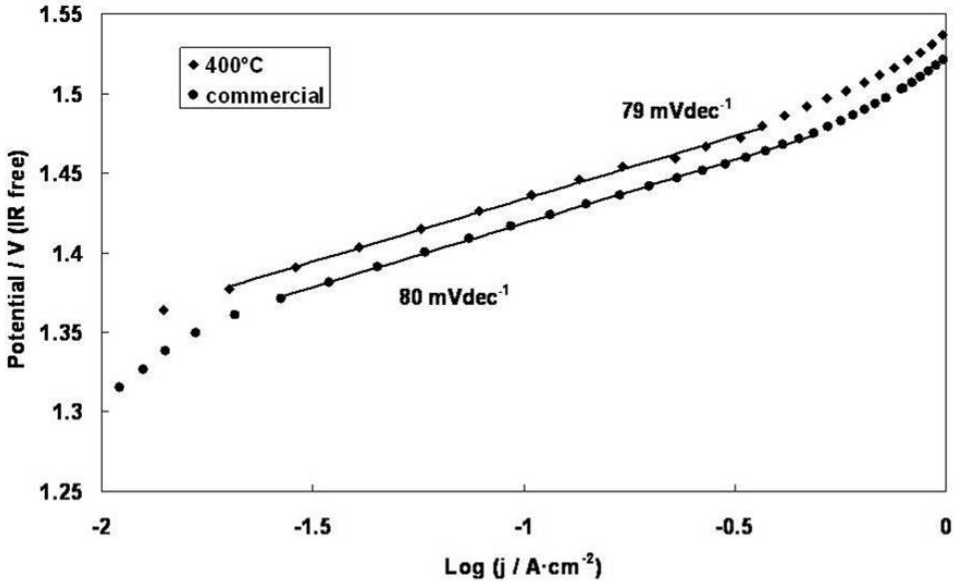

Figure 7. Tafel plots for oxygen evolution reaction in an SPE electrolyser at 80°C for the IrO_2 powder calcined at 400°C (1hr) and the commercial one

These curves were corrected for the ohmic drop (iR) to extract electro-kinetic parameters. The same Tafel slopes were identified for the two catalysts. The value was about 80 mV·dec^{-1}, which reflects a Temkin adsorption condition [29].

As envisaged from the ac-impedance results, the ohmic resistance at low overpotentials (1.5 V) contributes to more than 50% to the overall process for the best performing in-house catalyst. This aspect is more significant at high currents. On such basis, appropriate increase in performance at practical current densities can be achieved by using thinner or better proton conducting membranes than conventional ones.

Figure 8 is related to the chrono-amperometric measurement carried out at 80°C and atmospheric pressure for the IrO_2 catalyst calcined at 400°C.

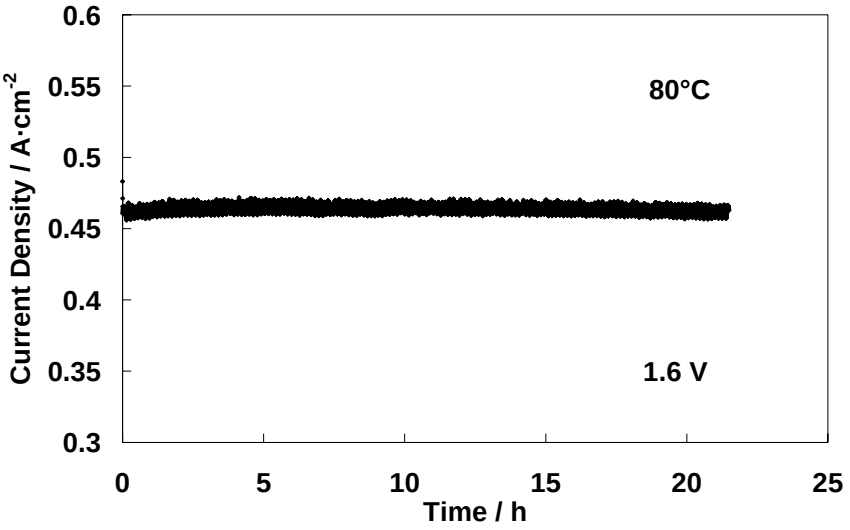

Figure 8. Chrono-amperometric measurement of the SPE electrolyser based on IrO_2 calcined at 400°C/1h

The test was performed at a potential of 1.6 V for a period of 20 h. The current density remained constant throughout the test, at 460 mA/cm^2, indicating a stable behaviour of the in-house prepared IrO_2 electrocatalyst.

4.4 Conclusions

A cheap, simple and fast low temperature colloidal method was used for obtaining nanosized IrO_2 catalysts characterized by a good compromise between catalytic activity and electrochemical stability [30]. These properties were achieved by a proper combination of nanostructure and morphology. A mean crystallite size of 7 nm, a suitable morphology and a BET surface area of 100 m^2 g^{-1} were obtained for the best electrocatalyst. The preparation method consisted in a colloidal process carried out in aqueous solution at ~100 °C and subsequent calcination at temperatures varying from 200 to 500 °C. The largest current density in an SPE electrolyzer at practical voltages (above 1.6 V) was obtained for the IrO_2 calcined at 400 °C for 1 h. In terms of electrochemical activity, the best anode catalyst achieved 1.32 A cm^{-2} at 1.8 V in an SPE electrolyzer. Chrono-amperometric measurements demonstrated a suitable stability of the in-house prepared Iridium oxide catalyst for the OER.

4.5 References

[1] Ardizzone S, Fregonara G, Trasatti S (1990) ‘‘Inner’’ and ‘‘outer’’ active surface of RuO2 electrodes. Electrochim Acta 35:263–267

[2] Da Silva LA, Alves VA, Da Silva MAP, Trasatti S, Boodts JFC (1997) Oxygen evolution in acid solution on IrO2?TiO2 ceramic films. A study by impedance, voltammetry and SEM. Electrochim Acta 42:271–281

[3] Andolfatto F, Durand R, Michas A, Millet P, Stevens P (1994) Solid polymer electrolyte water electrolysis: electrocatalysis and long-term stability. Int J Hydrogen Energy 19:421-427.

[4] Millet P, Andolfatto F, Durand R (1996) Design and performance of a solid polymer electrolyte water electrolyzer. Int J Hydrogen Energy 21:87-93.

[5] Yamaguchi M, Ohisawa K, Nakanori T (1997) Solid polymer electrolyte water electrolysis: electrocatalysis and long-term stability. Proceedings of the Intersociety Energy Conversion Engineering Conference 3–4:1958-1961.

[6] Ledjeff K, Mahlendorf F, Peinecke V, Heinzel A (1995) Solid polymer electrolyte water electrolysis: electrocatalysis and long-term stability. Electrochim Acta 40:315-319.

[7] Rasten E, Hagen G, Tunold R (2003) Solid polymer electrolyte water electrolysis: electrocatalysis and long-term stability. Electrochim Acta 48:3945-3952.

[8] Slavcheva E, Radev I, Bliznakov S, Topalov G, Andreev P, Budevski E (2007) Solid polymer electrolyte water electrolysis: electrocatalysis and long-term stability. Electrochim Acta 52:3889-3894.

[9] Hu J-M, Zhang J-Q, Cao CN (2004) Oxygen evolution reaction on IrO2-based DSA® type electrodes: kinetics analysis of Tafel lines and EIS. Int J Hydrogen Energy 29:791-797.

[10] Song S, Zhang H, Ma X, Shao Z, Baker RT, Yi B (2008) Electrochemical investigation of electrocatalysts for the oxygen evolution reaction in PEM water electrolyzers. Int J Hydrogen Energy 33:4955-4961.

[11] Nanni L, Polizzi S, Benedetti A, De Battisti A (1999) Morphology, microstructure, and electrocatalytic properties of RuO_2-SnO_2 thin films. J Electrochem Soc 146:220-225.

[12] de Oliveira-Sousa A, da Silva MAS, Avaca LA, Lima-Neto P (2000) Influence of the preparation method on the morphological and electrochemical properties of Ti/IrO_2-coated electrodes. Electrochim Acta 45:4467-4473.

[13] Adams R, Shriner RL (1923) Platinum oxide as a catalyst in the reduction of organic compounds. III. Preparation and properties of the oxide of platinum obtained by the fusion of chloroplatinic acid with sodium nitrate. J Am Chem Soc 45:2171-2179.

[14] Rasten E (2001) Electrocatalysis in Water Electrolysis with Solid Polymer Electrolyte, Ph.D. thesis, NTNU, Trondheim, Norway.

[15] Rasten E, Hagen G, Tunold R (1991) Proceedings Energy and Electrochemical Processes for a Cleaner Environment, Electrochemical Society, Pennington, 151.

[16] Marshall A, Børresen B, Hagen G, Tsypkin M, Tunold R (2003) First European Hydrogen Energy Conference 2–5 September 2003, Grenoble, France, CO1/71.

[17] Hutchings R, Muller K, Stucki S (1984) A structural investigation of stabilized oxygen evolution catalysts. J Mater Sci 19:3987-3994.

[18] Murakami Y, Ohkawauchi H, Ito M, Yahikozawa K, Takasu Y (1994) Preparation of ultrafine IrO_2-SnO_2 binary oxide particles by a sol-gel process. Electrochim Acta 39:2551-2554.

[19] Murakami Y, Tsuchiya S, Yahikozawa K, Takasu Y (1994) Preparation of ultrafine $IrO_2Ta_2O_5$ binary oxide particles by a sol-gel process. Electrochim Acta 39:651-654.

[20] Ito M, Murakami Y, Kaji H, Ohawauchi H, Yahikozawa K, Takasu Y (1994) Preparation of ultrafine RuO_2-SnO_2 binary oxide particles by a sol-gel process. J Electrochem Soc 141:1242-1245.

[21] Kameyama K, Shohji S, Onoue S, Nishimura K, Yahikozawa K, Takasu Y (1993) Preparation of ultrafine RuO_2-TiO_2 binary oxide particles by a sol-gel process. J Electrochem Soc 140:1036-1037.

[22] Lassali T, Boodts J, Bulhoes L (2000) Effect of Sn-precursor on the morphology and composition of $Ir_{0.3}Sn_{0.7}O_2$ oxide films prepared by sol-gel process. J Non-Cryst Solids 273:129-134.

[23] Marshall A, Børresen B, Hagen G, Tsypkin M, Tunold R (2005) Preparation and characterization of nanocrystalline IrxSn1–xO2 electrocatalytic powders. Mater Chem Phys 94:226–232

[24] Marshall A, Børresen B, Hagen G, Tsypkin M, Tunold R (2006) Electrochemical characterisation of IrxSn1–xO2

[25] Ma H, Liu C, Liao J, Su Y, Xue X, Xing W (2006) Study of ruthenium oxide catalyst for electrocatalytic performance in oxygen evolution. J Mol Catal A 247:7–13

[26] Di Blasi A, D'Urso C, Baglio V, Antonucci V, Aricò AS, Ornelas R, Matteucci F, Orozco G, Beltran D, Meas Y, Arriaga LG (2009) Preparation and evaluation of RuO_2-IrO_2, IrO_2-Pt and IrO_2-Ta_2O_5 catalysts for the oxygen evolution reaction in an SPE electrolyzer. J Appl Electrochem 39:191-196.

[27] D'Urso C, Morales L, Di Blasi A, Baglio V, Ornelas R, Orozco G, Arriaga LG, Antonucci V, Aricò AS (2007) Preparation and application of Pt-IrO_2 electrocatalysts for regenerative fuel cells. ECS Transactions 11:191-196.

[28] Antonucci V, Di Blasi A, Baglio V, Ornelas R, Matteucci F, Ledesma-Garcia J, Arriaga LG, Aricò AS (2008) High temperature operation of a composite membrane-based solid polymer electrolyte water electrolyser. Electrochim Acta 53:7350-7356.

[29] Aricò AS, Antonucci V, Alderucci V, Modica E, Giordano N (1993) A.c.-impedance spectroscopy study of oxygen reduction at Nafion® coated gas-diffusion electrodes in sulphuric acid: Teflon loading and methanol cross-over effects. J Appl Electrochem 23:1107-1116.

[30] J. C. Cruz, V. Baglio, S. Siracusano, R. Ornelas, L. Ortiz-Frade, L. G. Arriaga, V. Antonucci, A. S. Arico. Nanosized IrO2 electrocatalysts for oxygen evolution reaction in an SPE electrolyzer. J Nanopart Res. DOI 10.1007/s11051-010-9917-2.

CHAPTER 5

Preparation and Characterization of Titanium Suboxides as Conductive Supports of IrO_2 Electrocatalysts for Application in SPE Electrolyzers

5.1 Introduction

Ebonex® (Atraverda Ltd., UK), is the commercial trade of an electrically conductive ceramic material consisting of several suboxides of titanium, mainly Ti_4O_7 and Ti_5O_9, which are the most conductive compounds in the homologous series of crystallographic shear structures with the general formula Ti_nO_{2n-1} ($4 \leq n \leq 10$), collectively known as Magneli phase [1,2]. Ebonex® is an attractive material for the fabrication of electrodes in various technological applications that require an electrical conductor with excellent resilience to electrochemical corrosion and high oxidation resistance [3,4], such as chloro-alkali systems, sodium hypochlorite production, lead-acid batteries and cathodic current protection systems [5–8]. Sub-stoichiometric oxides of titanium are important candidates for oxygen electrodes in water electrolysers and unitized regenerative fuel cells (URFCs) [9]. The electrode materials used for the oxygen evolution by water electrolysis are mostly based on noble metals oxides [10–21]; consequently, it is important to reduce the amount of electrocatalyst loaded in the electrodes. This may be achieved by supporting the noble metal-based electrocatalyst on a high surface area conducting support. The support provides a physical surface for the dispersion of small particles of the active phase, which is necessary for achieving high surface area and to provide good electronic conductivity. In fuel cells, a common support for the oxygen reduction electrodes is carbon black [22, 23]. The carbon material has good electronic conductivity and provides a suitable porous structure with high accessible surface area. However, this material is not stable at the anodic potentials where the oxygen evolution reaction occurs in the electrolysis process. This means that suitable support materials alternative to the common carbonaceous materials are necessary for electrolysers and URFCs. In the literature, supporting materials for electrocatalysts like boron carbide, tantalum

boride, titanium carbide and perovskyte type compounds were investigated [24, 25]. Recently, conductive suboxides of titanium, such as Ebonex®, were studied for electrochemical applications [26–28]. The aim of this work concerns the development of a suitable process for preparing Ti-suboxides. The relevant characteristics of the materials were evaluated under operating conditions, in a solid polymer electrolyte (SPE) electrolyser, and compared to those of the commercial Ebonex®. The same IrO_2 active phase was used in both systems as electrocatalyst.

5.2 Activity

5.2.1 Preparation of Ti_nO_{2n-1} powder and electronic conductivity measurements

Ti_nO_{2n-1} ceramic powders were prepared from a commercial titanium (IV) chloride solution ($TiCl_4$, Aldrich). $TiCl_4$ was dissolved in water; a chelating agent, EDTA (Aldrich), was added. The reaction mixture was maintained at a pH ~ 5 at 80 °C for 1 h. The Ti complex with EDTA was decomposed into a colloidal TiO_x dispersion by adding hydrogen peroxide. After precipitation and subsequent filtering, an amorphous Ti oxide phase was obtained. A temperature-programmed reduction (TPR, CHEMBET-3000 apparatus) was carried out to analyse the thermal reduction profile of the amorphous material. TPR measurements were carried out on the amorphous TiO_x at atmospheric pressure in a quartz microreactor placed in a ceramic tube furnace; it was heated from the room temperature up to 1050 °C at a heating rate of 5 °C/min under a controlled atmosphere of hydrogen (10%) in argon. The temperature of the catalyst bed was monitored with a thermocouple inserted into the reactor cuvette. Gases were fed with properly calibrated mass flow controllers. The total inlet flow was fixed at 20 cc/min. The Ti-suboxide with Magneli phase was prepared by reduction of the amorphous TiO_x (5 g) at 1050 °C for 2 h, in a tubular quartz reactor fed with a 10% H_2/Ar gas stream. A commercial Ti-suboxide (Ebonex®) was purchased from Atraverda (UK). Both Ti-suboxide powders were ground in a planetary ball mill for 2 h.

Electrical conductivity measurements were carried out on Ti suboxide pellets. The powders were first pressed uniaxially in a cylindrical shape to form the pellets. Two gold foils were used as electrical contacts. The through-plane electronic conductivity of the pre-formed pellets (thickness 3 mm) was measured by using a four-probe method with an applied pressure of 7MPa that was corresponding to the tightening compression of the single cell electrolyser used in this work. The resistance of the gold foils was measured in a separate experiment under the same applied pressure and subtracted from the total resistance measured for the pellets. An Autolab (Metrohm) electrochemical apparatus equipped with an FRA was used for the four-probe ac-impedance spectroscopy measurement in the frequency range 100 kHz to 1 Hz. Surface area measurements of the commercial Ebonex® and Ti-suboxide support prepared in-house were made by a Thermoquest 1990 series Sorptomatic. The Barrett–Joiner–Halenda (BJH) method was used for the determination of cumulative area and pore size.

5.2.2 Preparation of the oxygen evolution electrocatalysts

A 30% IrO_2/Ti_nO_{2n-1} powder was used as oxygen evolution electrocatalyst. To prepare the catalyst, an incipient wetness procedure was employed. It consisted of the impregnation of a commercial amorphous IrO2 (Spectrum Chemical USA, 99.9%) in deionised water onto the commercial Ebonex® (Atraverda) support or the in house made Ti_nO_{2n-1} at 80 °C. The nominal concentration of IrO_2 in both catalysts was 30 wt.% corresponding to an Ir/Ti atomic ratio of 0.14. The catalysts were dried at 120 °C before use.

5.2.3 Structural characterization

X-ray diffraction (XRD) analysis was performed on amorphous IrO_2, Ebonex® powder (ball milled), Ti-suboxide powders (reduced at 1050 °C) and IrO_2/Ti_nO_{2n-1} electrocatalysts. A Philips X-Pert X ray diffractometer was used with Cu Kα radiation source. The diffractometer operated at 40 kV and 20 mA. The diffraction patterns were fitted to the Joint Committee on Powder Diffraction Standards (JCPDS).

5.2.4 Chemical, surface and morphological characterizations

X-ray fluorescence (XRF) analysis of the 30% IrO_2/Ti_nO_{2n-1} catalysts was carried out by a Bruker AXS S4 Explorer spectrometer operating at a power of 1 kW and equipped with a Rh X-ray source, a LiF crystal analyzer and a 0.12° divergence collimator. Transmission electron microscopy (TEM) was carried out on both Ti-suboxides used as supports and on the complete catalysts by using a Philips CM 12 instrument. TEM analysis was made by first dispersing the powders in isopropyl alcohol. A few drops of these solutions were deposited on carbon film-coated Cu grids and analysed with microscope. The surface chemical composition of 30% IrO_2/Ti_nO_{2n-1} electrocatalysts was investigated by X-ray photoelectron spectroscopy (XPS). The measurements were performed by using a Physical Electronics (PHI) 5800-01 spectrometer. A monochromatic Al/Kα X-ray source was used at a power of 350W. Spectra were obtained with pass energies of 58.7 eV for elemental analysis (composition) and 11.75 eV for the determination of the chemical species. The pressure in the analysis chamber of the spectrometer was 1×10^{-9} Torr during the measurements. Spectra were collected at a photoelectron take-off angle of 45° with respect to the sample surface. The quantitative evaluation of each peak was obtained by dividing the integrated peak area, after Shirley background subtraction, by atomic sensitivity factors, which were calculated from the ionization cross-sections, the mean free electron escape depth and the measured transmission functions of the spectrometer by using the PHI Multipak 6.1 software.

5.2.5 Preparation of membrane and electrode assembly (MEA)

A Nafion 115 (Ion Power) membrane was used as solid polymer electrolyte. The oxygen evolution catalyst was directly deposited onto one side of a Nafion 115 by a spray technique. The powder suspension contained 67wt.% IrO_2/Ti_nO_{2n-1} and 33 wt.% Nafion ionomer in alcoholic solution. The IrO_2 loading in both anodes equipped with Ebonex® or support prepared in-house was $1mgcm^{-2}$. A titanium grid was used as diffusion layer and current collector at the anode to avoid corrosion phenomena. In order to favour the gas evolution, the titanium grid was

immersed in a water/FEP (1:1) (Dyneon FEP 6300 RG) solution for 1 min and then it was dried in an oven; subsequently, it was treated at 350 ◦C for 30 min. A commercial 30% Pt/Vulcan XC-72 (E-TEK, USA) catalyst was used for the H_2 evolution. The cathode electrode was prepared by directly mixing in an ultrasonic bath a suspension of Nafion ionomer in water with the catalyst powder (catalyst/dry ionomer = 2/1 wt.%); the obtained paste was spread onto a carbon cloth backing (GDL ELAT from E-TEK) up to reach a loading of 1mgPt cm^{-2}. MEAs were assembled directly in the cell housing by tightening at 70 $Kgcm^{-2}$ using a dynamometric wrench.

5.2.6 Electrochemical studies

The electrochemical behaviour of the SPE electrolysers was evaluated in a temperature range from 30 °C to 80°C at atmospheric pressure. Deionised water, heated at the same temperature of the cell, was supplied to the anode compartment by a peristaltic pump at a flow rate of 4mlmin^{-1}. Linear sweep voltammetry and electrochemical impedance spectroscopy (EIS) were carried out by an Autolab PGSTAT 302 Potentiostat/Galvanostat equipped with a 20 A booster (Metrohm) and an FRA. In situ cyclic voltammetry (CV) was carried out at room temperature with a sweep rate of 20mVs^{-1} by using the Autolab apparatus. In these CV experiments, humidified diluted hydrogen (10% in Argon) was fed to the Pt/C electrode and de-aerated water to the IrO_2-based electrode; the hydrogen electrode was used as both counter and reference electrode [29].

5.3 Results

5.3.1 Physico-chemical properties of catalysts and Ti-suboxide supports

Fig. 1 shows a TPR analysis of the amorphous titanium oxide precursor up to 1050 ◦C. Five main processes were recorded during this experiment. These have been interpreted as follows: (i) loss of physically adsorbed water below 100 °C; (ii) loss of water from surface hydroxylic species (about 200 °C); (iii) TiO_2 (Anatase) crystalline phase formation at about 300 °C; (iv) TiO_2 (Rutile) crystalline phase formation at about 850°C; (v) chemical reduction of the TiO_2 phase with formation

of a mixture of sub-stoichiometric Ti-oxides at 1050 °C. The occurrence of most of these processes was confirmed by XRD analysis or thermogravimetric analysis of the sample treated at specific temperatures (not shown). The sample was weighted after TPR analysis. A weight loss of about 30 wt.% was observed.

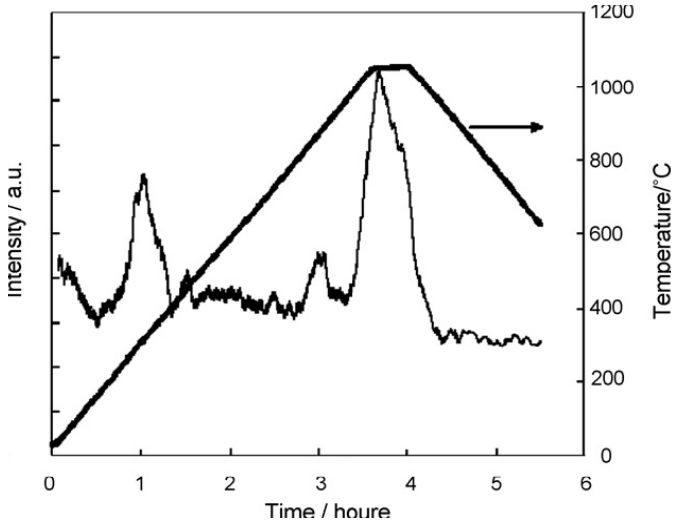

Figure 1. TPR analysis of the as-prepared amorphous titanium oxide

The diffraction pattern of the commercial Ebonex® in Fig. 2 was slightly different from that reported in the literature for the same material [30]. However, it was shown in the literature that the grinding procedure can cause slight structural modifications [30]. The main peaks of Ti_4O_7 (JCPDS: 18-1402), Ti_5O_9 (JCPDS: 11-193) and Ti_6O_{11} (JCPDS: 18-1401) phases are indicated in Fig. 2. The Ti_4O_7 structure was less evident in the present Ebonex® sample as compared to the literature [30]. For the Ebonex® powder ground in a ball mill, the prevailing crystallographic structure was Ti_5O_9 but also Ti_4O_7 and Ti_6O_{11} were present. The XRD patterns of the support prepared in-house (Fig. 2) showed a prevailing occurrence at 24–24.5° of the Ti_9O_{17} (JCPDS: 18-1405) structure. The Ti_6O_{11} phase was also occurring in this sample. According to the XRD patterns, the degree of sub-stoichiometry in the bulk was larger in the commercial sample than in the support prepared in-house. No peaks related to Anatase or Rutile was observed in the XRD patterns of both samples. All the assigned reflections belong to the Magneli phase.

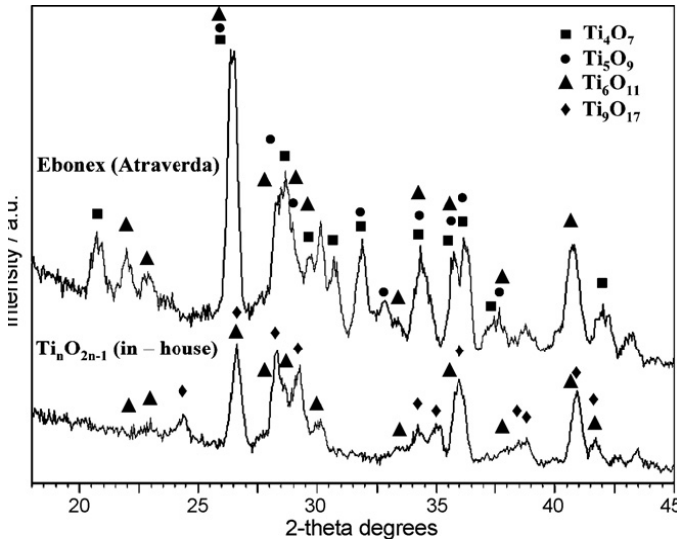

Figire 2. X-ray diffraction patterns of Ebonex® (Atraverda) and Ti_nO_{2n-1} (in-house)

The X-ray diffraction patterns of commercial IrO_2, Ti_nO_{2n-1} prepared in-house and corresponding 30% IrO_2/Ti_nO_{2n-1} catalyst are reported in Fig. 3. The 30% IrO_2/Ti_nO_{2n-1} showed an amorphous halo related to IrO_2 and the typical peaks of Ti_nO2_{n-1} (Magneli phase). The peaks at 41° and 48° 2 theta were attributed to the 111 and 200 reflections of crystallographic structure of metallic Ir (JCPDS: 6-598).

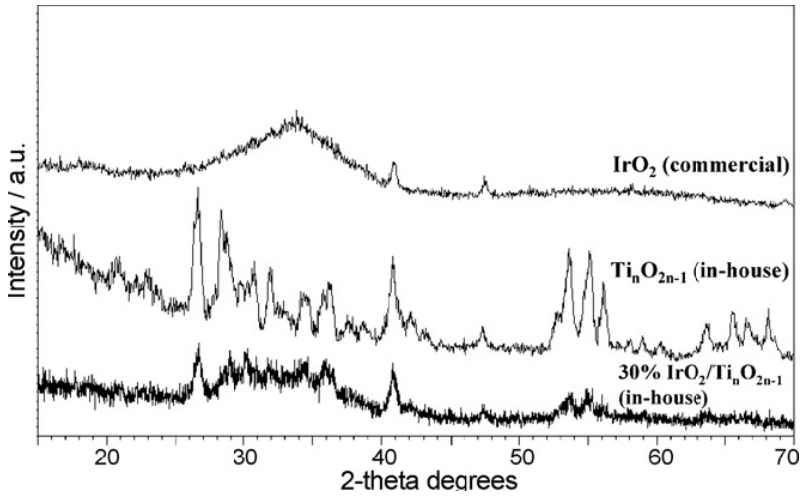

Figure 3. X-ray diffraction patterns of commercial IrO_2, Ti_nO_{2n-1} (in-house) and 30% IrO_2/Ti_nO_{2n-1} (in-house)

Fig. 4 shows the X-ray diffraction patterns of commercial IrO_2, Ebonex® and 30% IrO_2/Ebonex®. Also in this case the catalyst showed the amorphous IrO_2, a small evidence of metallic Ir and the typical peaks of Ebonex®.

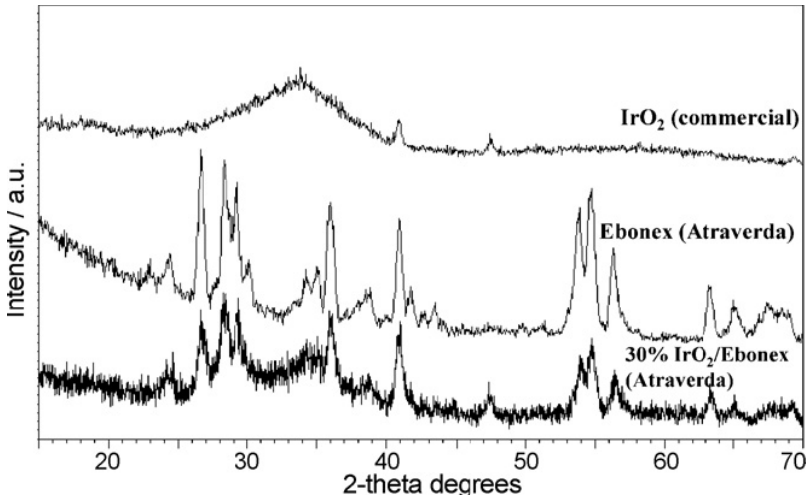

Figure 4. X-ray diffraction patterns of commercial IrO2, Ebonex® and 30% IrO_2/Ebonex®

The electrical conductivity was investigated for the two Ti suboxide samples in the pellet form by ac-impedance. An inductive response in the overall range of frequencies (not shown) was obtained for both pellets indicating the absence of significant contact resistances between the pellet and gold foils. The low frequency (1 Hz) intercept on the real axis of the Nyquist plot was used to determine the conductivity of these powders. Resistivity values of 0.0223 Ωcm for the in-house Ti_nO_{2n-1} pellet and 0.0230 Ωcm for the Ebonex® pellet were recorded. The commercial Ebonex® and Ti-suboxide supports prepared in house were analysed by BET. The cumulative area and pore volume, calculated by using the BJH method (c = 0.8), were 26.6m^2/g and 0.26cm^3/g for the in-house prepared support, whereas, they were 1.17m^2/g and 0.01 cm^3/g for the Ebonex®. The observed cumulative area for the commercial support was lower than the BET surface area of 1.6m^2/g reported in the literature [30]. The analysis of the pore size distribution (N_2 desorption branch) indicated essentially the presence of macropores for the commercial sample whereas both macro- and meso-pores were observed for the Ti_nO_{2n-1} support prepared in-house (not shown). The morphology of the ceramic supports was also investigated by TEM analysis (Fig. 5a–d). Both materials showed the presence of large particle agglomerates (500 nm). The surface roughness appeared larger for the support prepared in-house. At high magnification, the average crystallite dimension on the surface of these

agglomerates was about 50nm in the case of the Ebonex® and 25nm in the case of the Ti_nO_{2n-1} prepared in-house.

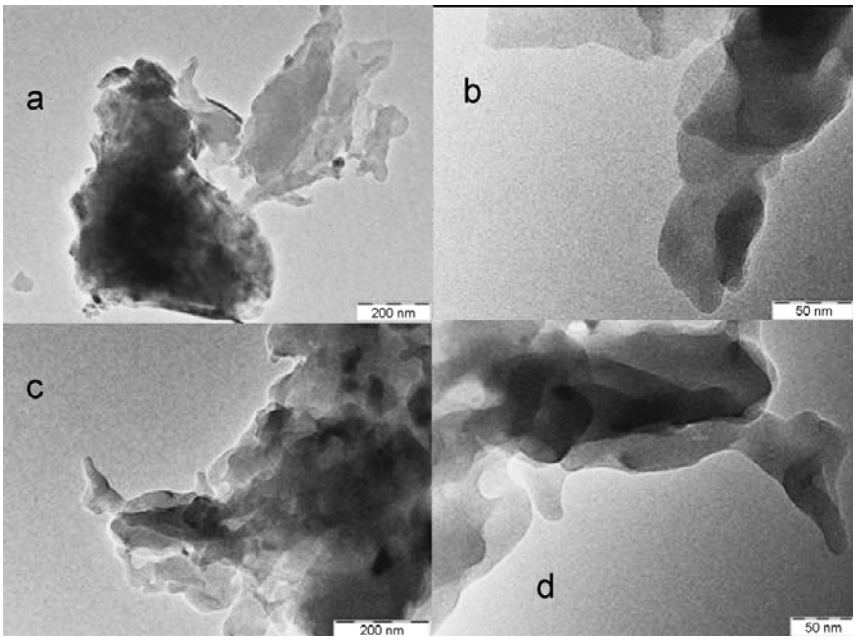

Figure 5. TEM micrographs at different magnifications: (a) and (b) Ebonex®; (c) and (d) Ti_nO_{2n-1} (prepared in-house)

The XRF analysis revealed only the presence of Ir and Ti for both electrocatalysts. Light elements are not detected by this technique. The Ir/Ti atomic ratio was 0.17 in the IrO_2/Ti_nO_{2n-1} commercial catalyst; whereas, it was 0.14 in the catalyst based on the support prepared in-house. This slight difference in composition was attributed to the washing treatment of the catalyst. However, the measured composition did not deviate significantly from the nominal composition (atomic Ir/Ti ~ 0.14).

5.3.2 Electrochemical studies

The performance of the MEAs based on the different oxygen evolution electrocatalysts, i.e. IrO_2/Ebonex® and IrO_2/Ti_nO_{2n-1} (in-house) was evaluated at different temperatures for water electrolysis in an SPE electrolyser. The polarization curves of the cell equipped with the 30% IrO_2/Ti_nO_{2n-1} in-house prepared anode catalyst and 30% Pt/C (E-TEK) cathode catalyst are reported in Fig. 6.

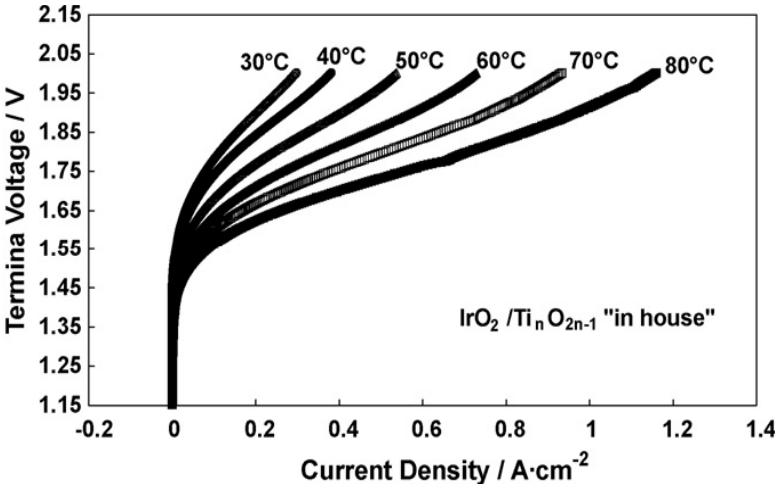

Figure 6. Terminal voltage versus current density curves of the cells equipped with IrO_2/Ti_nO_{2n-1} (in-house) and Nafion 115 membrane at different temperatures (from 30 °C to 80°C) and 1 bar abs pressure

The electrolysis performance increased as a function of the temperature. The overpotential was mainly due to the oxygen evolution, this being the rate determining step of the overall electrolysis process [31]. The best performance was recorded at 80 °C; at a cell voltage of 1.8 V, the current density was 700mAcm^{-2}, with a corresponding mass activity for the anode catalyst better than 700Ag^{-1}. This could be further ameliorated if a proper crystalline IrO_2 phase is used instead of the amorphous compound [10,16–18,21,29]. Fig. 7 shows the terminal voltage versus current density curves at different cell temperatures for the cell equipped with the 30% IrO_2 supported on the commercial Ti_nO_{2n-1} (Atraverda) as anode catalyst and 30% Pt/C (E-TEK) as cathode catalyst.

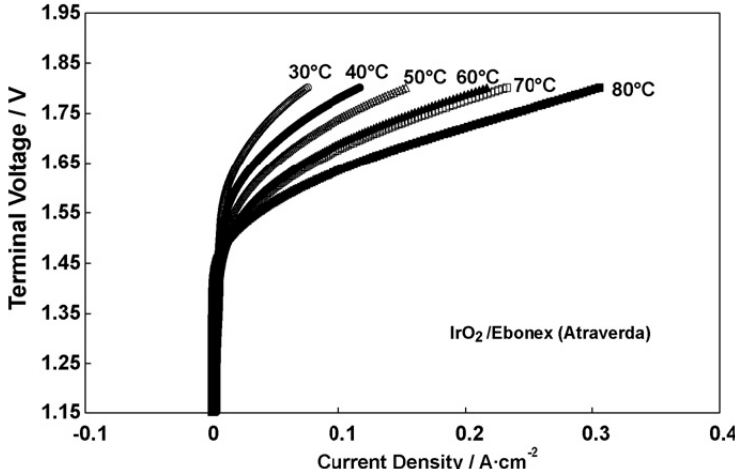

Figure 7. Terminal voltage versus current density curves of the cells equipped with IrO_2/Ebonex® and Nafion 115 membrane at different temperatures (from 30 °C to 80 °C) and 1 bar abs pressure

The achieved performance for the electrolysis process was significantly lower for the commercial support compared to the in-house made support. The current density for the electrolyser equipped with the catalyst containing the commercial support was 300mAcm^{-2} at 1.8V and 80 °C. In Fig. 8, a comparison between the polarization curves of the two MEAs, equipped with IrO_2/Ti_nO_{2n-1} prepared in-house and IrO_2/Ebonex®, at 80°C is reported.

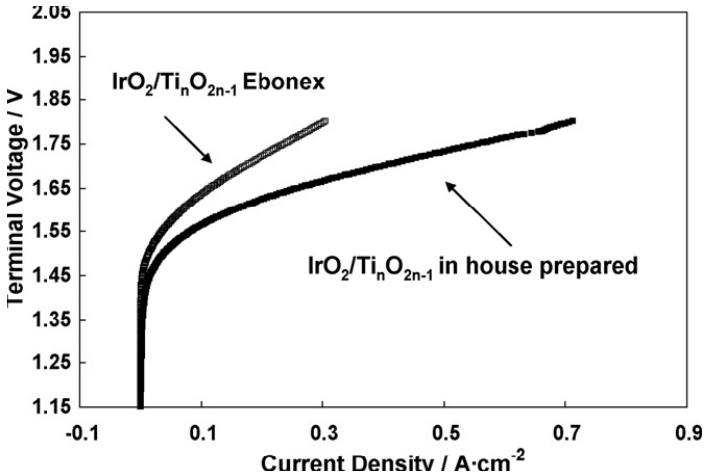

Figure 8. Comparison of terminal voltage versus current density curves of IrO_2/Ti_nO_{2n-1} (in-house) and IrO_2/Ebonex® at 1 bar abs and 80 °C

The terminal voltage of the electrolysis cell was lower for the catalyst based on the support prepared in-house than that containing Ebonex® in the overall current density range. This difference increased remarkably above 1.45 V. Both electrocatalysts showed proper stability during several days of testing. Long-term duration experiments are currently underway. The impedance behaviour for both electrolysers was evaluated at 1.5V and 80°C (Fig. 9).

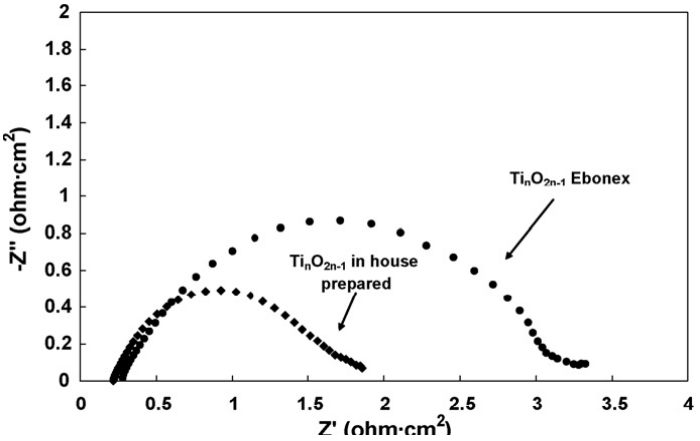

Figure 9. Impedance spectra of the IrO_2/Ti_nO_{2n-1} (in-house) and IrO_2/Ebonex® based cells at 1.5V and 80 °C

The series resistance (Rs)was determined from the intercept on the real axis of the Nyquist plot in the high frequency range. The Rs values were in the range 0.25–0.31Ωcm^2. The series resistance for the electrolyser based on the commercial support was 0.06Ωcm^2 larger than that of the catalyst based on the support prepared in-house. Accordingly, the difference in terms of ohmic drop between the two MEAs at 0.3Acm^{-2} can be quantified in about 20 mV. Instead, the actual difference between the two terminal voltages was 150 mV. The impedance data were fitted by using an equivalent circuit Rs (Rct Qdl) (R1 Q1) [17]. Qdl is a constant phase element that includes both double layer capacitance and pseudo-capacitance, Rct is the charge transfer resistance; the (R1Q1) circuit has been attributed to diffusion phenomena [17]. The capacitance values derived from Qdl were about 17$mFcm^{-2}$ mg^{-1} and 8$mFcm^{-2}mg^{-1}$ IrO_2 for the IrO_2/Ti_nO_{2n-1} prepared in-house and IrO_2/Ebonex®, respectively. A significantly larger charge transfer resistance was observed for the electrolyser based on the commercial support compared to the support prepared in-house. This indicated an increase of the overpotential for the oxygen evolution process at the electrode–electrolyte interface in the presence of the commercial support. The charge transfer resistance was obtained from the large semicircles by the difference between low and high frequency intercept on the real axis of the Nyquist plot. The Rct was about 1.4Ωcm^2 at 1.5V and 80 ◦C for the catalyst based on the support prepared in house; whereas, it was 2.75 Ωcm^2 under same conditions for the commercial support.

The voltammetric surface charge was determined from the cyclic voltammetry at a sweep rate of 20mVs^{-1} [17]. The voltammetric surface charge is generally considered an indication of the electrochemical real surface area even if a conversion of the charge into surface area is difficult because the nature of the surface reactions is not known precisely [32]. Fig. 10 shows a comparison of the CV profiles for the two electrocatalysts.

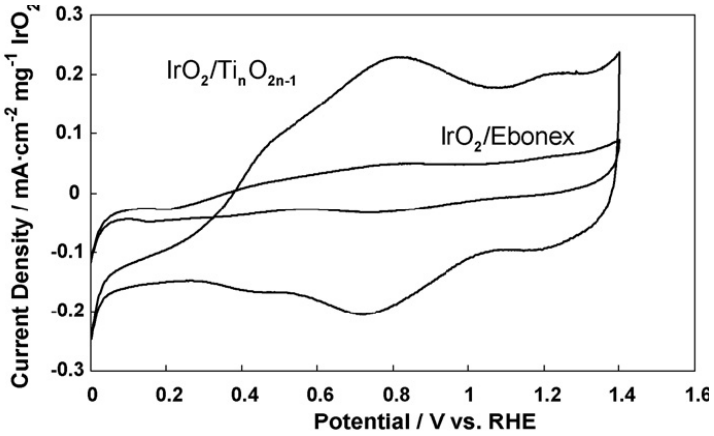

Figure 10. Cyclic voltammetry of the IrO_2/Ti_nO_{2n-1} (in-house) and IrO_2/Ebonex®-based electrodes at a sweep rate of 20mVs^{-1} and room temperature

These profiles were similar to those reported in the literature for annealed samples [17] even if the maximum temperature at which the present catalysts were treated was 120 °C. The voltammetric surface charge values were about 8.9mCcm^{-2} mg^{-1} and 2.4mCcm^{-2} mg^{-1} IrO_2 for the IrO_2/Ti_nO_{2n-1} prepared in-house and IrO_2/Ebonex®, respectively. The ohmic drop corrected Tafel plots obtained at 80 ◦C are reported in Fig. 11.

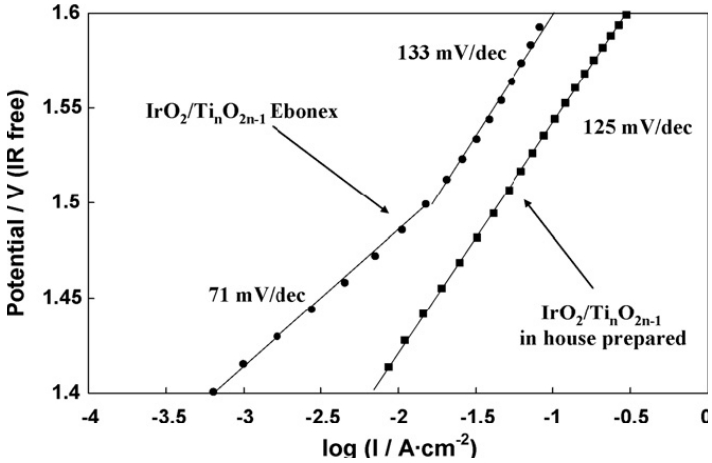

Figure 11. Tafel plots of the IrO_2/Ti_nO_{2n-1} (in-house) and IrO_2/Ebonex®

It is assumed that the hydrogen electrode does not contribute significantly to the polarization behaviour, i.e. it may be considered as both counter and reference electrode in the single cell polarization experiments [31]. Furthermore, being the hydrogen electrode the same in both experiments, it does not play any role in determining the observed differences. Two Tafel regimes were observed for

the IrO_2/Ebonex® electrocatalyst at low and high current density. These were characterized by a Tafel slope of about 71 and 133mV/dec. It is suggested that the charge transfer process occurring at low current densities is essentially governed by a Temkin adsorption isotherm, whereas Langmuir adsorption isotherm behaviour is prevailing at high current densities. This often occurs also for the oxygen reduction process in the presence of Nafion electrolyte [33]. The Temkin adsorption isotherm is characterized by a strong mutual interaction among the absorbed oxygen species that is prevailing in the potential region close to the reversible potential [33]. Such effect determines a low Tafel slope of 71 mV/dec at 80 ◦C which accounts for a two-electron transfer rate determing step. At high current densities, an increase of Tafel slope (133 mV/dec) for the IrO_2/Ebonex® was observed. A one-electron transfer rate determining step appears prevailing in the high current range for this catalyst. The IrO_2/Ti_nO_{2n-1} (in-house) catalyst showed a Tafel slope of 125mV/dec in almost the overall range of current densities (Fig. 11) excluding the region of the reversible potential where a deviation from the Tafel regime was observed for both catalysts. It is not discarded that a Temkin adsorption regime could also occur for this catalyst at low overpotentials. Although a larger slope in the low current density range was recorded for the catalyst based on the in house prepared support as compared to the other catalyst, the lower overpotential determined a better performance for the in-house support based electrode. This aspect may be related to the larger number of catalytic sites available for the reaction in the in-house catalyst compared to the catalyst based on the commercial support as determined from the voltammetric charge measurements [32]. Being the active IrO_2 phase essentially the same for the two catalysts, the different behaviour could be related to the interaction between the active phase and the support. To investigate in detail these aspects, transmission electron microscopy and X-ray photoelectron spectroscopy analyses were carried out on the two catalysts.

5.3.3 Surface and morphology characterization

The TEM micrographs for the two catalysts are shown in Fig. 12.

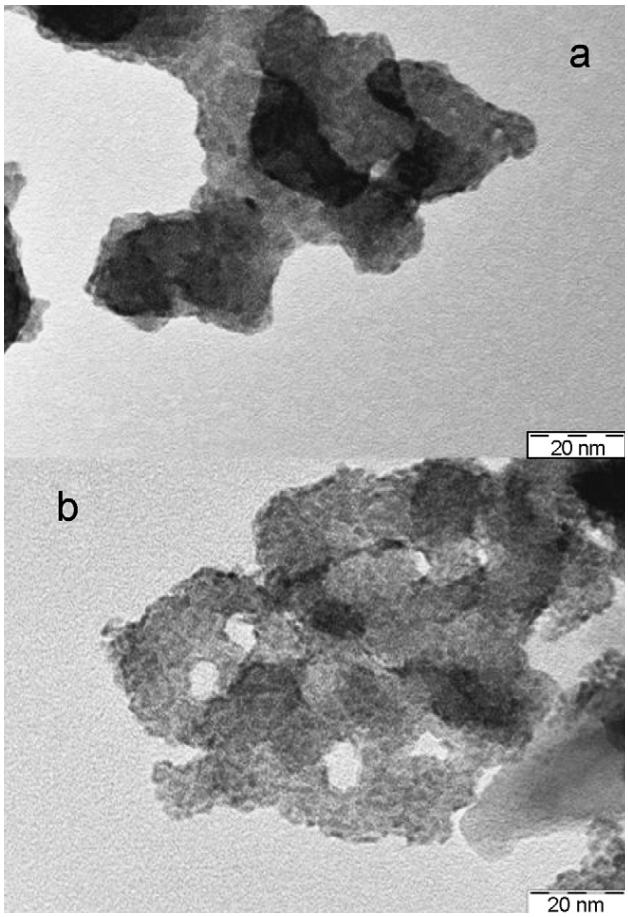

Figure 12. TEM micrographs: (a) IrO_2/Ebonex®; (b) IrO_2/Ti_nO_{2n-1} (in-house)

The fine particles were related to the amorphous IrO_2 phase. No relevant differences were envisaged in terms of particle size for this phase in the two samples. The IrO_2 dispersion was better in the case of the catalyst based on the in-house prepared Ti_nO_{2n-1} possibly indicating a strong effect of support roughness. Furthermore, most of the IrO_2 particles were allocated on the outer surface in the case of the in-house support. The surface analysis was carried out by XPS. A comparison of the survey spectra for the two catalysts is shown in Fig. 13.

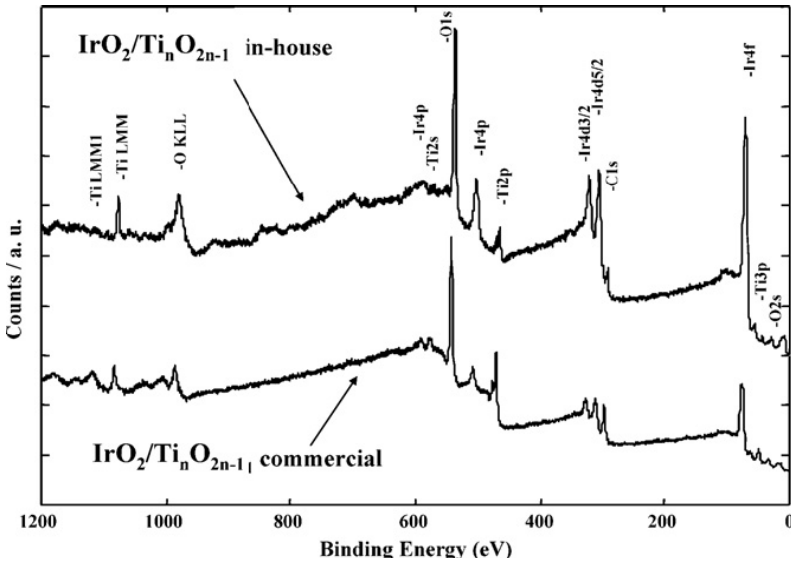

Figure 13. XPS survey spectra of IrO_2/Ti_nO_{2n-1} (in-house) and IrO_2/Ebonex®

By comparing the Ir4f and Ti2p photoelectron lines in the two samples, it clearly appeared that there was a significant enrichment of the IrO_2 phase on the surface for the catalyst based on the in-house prepared support. The surface atomic Ir/Ti ratios were 0.45 for the commercial support based catalyst and 1.93 in the catalyst based on the in-house support, whereas, the atomic ratios in the bulk were close to the nominal composition (see XRF analysis). This could be explained in terms of distribution of the IrO_2 phase on the outer surface for the in-house support and insertion of IrO_2 in the inner pores in the case of Ebonex® as envisaged by TEM. The presence of smaller pores in the Ti_nO_{2n-1} did not favour the penetration of the large amorphous IrO_2 agglomerates into the support. Thus, the morphology was less packed with respect to the catalyst based on Ebonex® (Fig. 12). Of course, this aspect was mainly determined by the preparation procedure and morphological characteristics of the supports. However, there were also differences in terms of chemical properties which are of relevant interest. Fig. 14 shows the high-resolution spectra for the two catalysts. The insets in Fig. 14 show the XRF spectra for the two formulations.

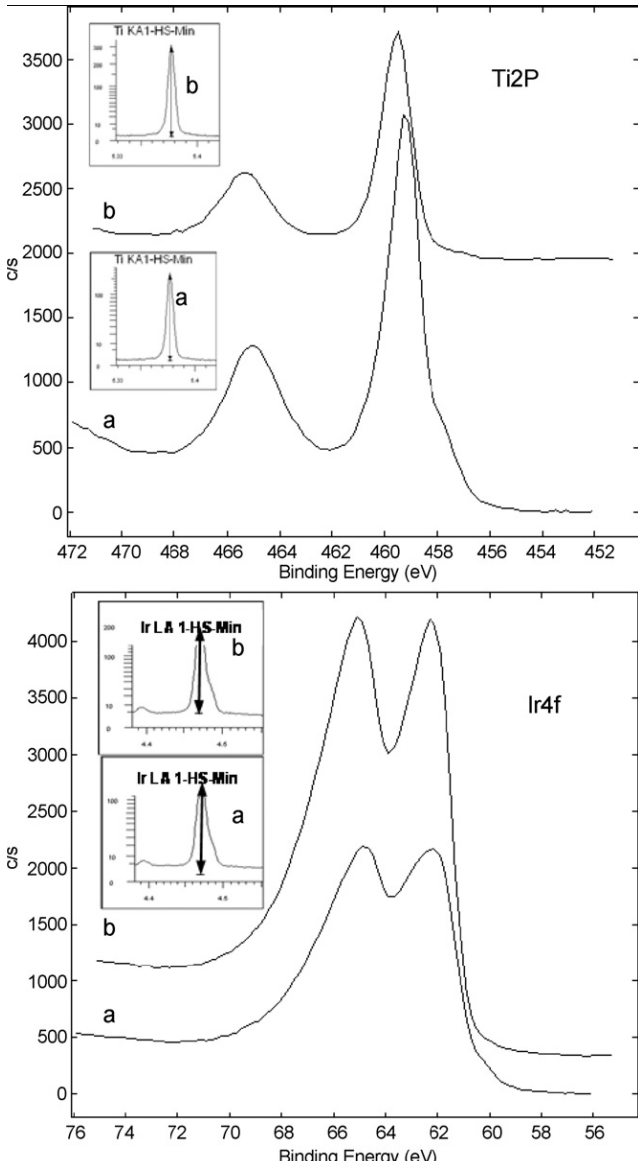

Figure 14. XPS spectra of Ti2p and Ir4f: (a) Ebonex®; (b) Ti_nO_{2n-1} (in-house)

The Ir4f and Ti2p photoelectron lines occurred at slightly higher B.E. for the in-house support based catalyst (Fig. 14) [34]. This indicated an increased level of electron-vacancies for both Ir and Ti in such a system. This aspect may be considered favourable in terms of oxygen evolution at the Ir sites in the in-house support based catalyst since they can easily accept electron donation from water molecules; whereas, in the case of the Ebonex® based catalyst the lower B.E. of Ti2p reveals a larger degree of sub-stoichiometry. This evidence is in agreement with the XRD analysis that showed a prevalence of a crystallographic structure with an O/Ti ratio of 1.8 in the commercial support and 1.88 in the in-house prepared Ti_nO_{2n-1}. Yet, although the B.E. of Ti for the in-house support (459.3 eV)

is not much dissimilar from that of Rutile and Anatase (459.2 eV) [34], the electronic conductivity and bulk characteristics (see structural analysis) are those of Ti-suboxides. Such aspects are of relevant interest for what concerns the resilience to the electrochemical corrosion. It is preferable for the support a refractory behaviour on the surface such as that of the insulating TiO_2 but also the presence of suitable electronic conductivity properties in the bulk. A deconvolution of the Ir4f photoelectron lines is shown in Fig. 15.

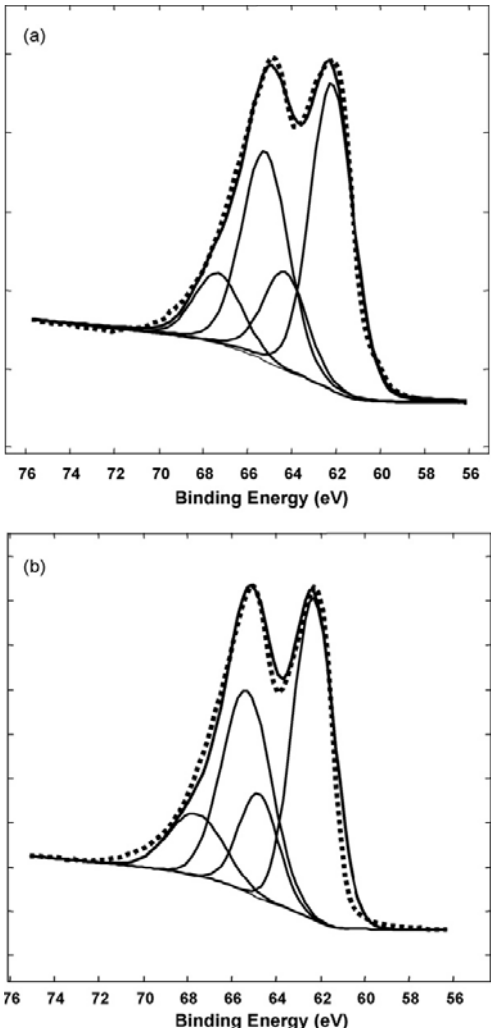

Figure 15. Deconvolution of the Ir4f spectra. (a) Ebonex®; (b) Ti_nO_{2n-1} (in-house)

The $4f_{7/2}$–$4f_{5/2}$ doublet occurring at B.E. 62.2–65.2 eV and 62.3–65.3 eV for IrO_2/Ebonex® and prepared in-house IrO_2/Ti_nO_{2n-1}, respectively, was assigned to Ir^{4+} species [35]. These values are not significantly different from those reported in the literature for the Ir (IV) species of Ir-oxide in a Ti supported system, e.g. 62.5–62.9 eV for 4f7/2 [36]. Another doublet with broader character is observed at B.E.

of 64.3–67.3 and 64.7–67.7 for IrO_2/Ebonex® and IrO_2/Ti_nO_{2n-1} prepared in-house, respectively. These species are due to the presence of higher oxidation states, probably Ir (VI) species, on the surface [35]. Their relative content is larger in the IrO_2/Ti_nO_{2n-1} prepared in-house confirming an increased level of electron-vacancies for the Ir sites in this sample.

5.4 Conclusions

The observed electrochemical performance for the catalyst based on the in-house prepared Ti-suboxide support favourably compared to the catalyst containing Ebonex®. The commercial amorphous IrO_2 phase used in the present work is generally considered

less performing with respect to a crystalline IrO_2 phase prepared at 400 ◦C. Thus, the supported catalysts could be further ameliorated in terms of specific and mass activity. The support prepared in-house revealed less degree of sub-stoichiometry than the commercial Ebonex® but larger surface area and surface roughness. These properties allowed a better dispersion of the IrO_2 phase on the support and a larger occurrence of the active sites on the surface. A larger voltammetric charge was measured for the catalyst prepared in-house with respect to the one based on Ebonex®. Such morphological characteristics together with the more favourable electrochemical properties determined a better electrocatalytic activity for the oxygen evolution in a SPE electrolyser for the catalyst based on the support prepared in-house with respect to the catalyst containing Ebonex®.

5.5 References

[1] A. Magneli, S. Anderson, B. Collen,U. Kuylenstierna, Acta Chem. Scand. 11 (1957) 1641.

[2] M. Marezio, P.D. Dernier, J. Solids State Chem. 3 (1971) 430.

[3] P.C.S. Hayfield, A. Hill, Int. J. Restorat. Build. Monuments 6 (2000) 647.

[4] P.C.S. Hayfield, R.L. Clarke, Performance of electrodes for industrial electrochemical processes, in: F. Hine, B.V. Tilak, J.M. Fenton, J.D. Lisius (Eds.), Proceedings, vol. 89–10, The electrochemical Society, Pennington, NJ, 1989, p. 87.

[5] R.L. Clarke, S.K. Harnsberger, Am. Lab. 20 (1988) 8.

[6] R.L. Clarke, Proceedings of the Second International Forum of Electrolysis in the Chemical Industry, Deer-field Beech, Fl, 1988.

[7] P.C.S. Hayfield, R.L. Clarke, The electrochemical characteristics and uses of Magneli phase titanium oxide ceramic electrodes, in: Electrochemical Society Spring Meeting, Los Angeles, 7–12 May, 1989.

[8] K. Ellis, A. Hill, J. Hill, A. Loyns, T. Partington, J. Power Sources 136 (2004) 366.

[9] G. Chen, S. Bare, T. Mallouk, J. Electrochem. Soc. 149 (2002) A1092.

[10] S. Song, H. Zhang, X. Ma, Z. Shao, R.T. Baker, B. Yi, Int. J. Hydrogen Energy 33 (2008) 4955.

[11] S. Trasatti, Electrodes of Conductive Metallic Oxides (part A), Elsevier, Amsterdam, 1980.

[12] L. Krusin-Elbaum, M.Wittmer, J. Electrochem. Soc. 135 (1988) 2610.

[13] A.C.C. Tseung, S. Jasem, Electrochim. Acta 22 (1977) 31.

[14] S. Trasatti, Electrochim. Acta 36 (1991) 225.

[15] L.A. Da Silva, V.A. Alves, M.A.P. Da Silva, S. Trasatti, J.F.C. Boodts, Electrochim. Acta 42 (1997) 271.

[16] A. Marshall, B. Børresen, G. Hagen, M. Tsypkin, R. Tunold, Electrochim. Acta 51 (2006) 3161.

[17] E. Rasten, G. Hagen, R. Tunold, Electrochim. Acta 48 (2003) 3945.

[18] A. Marshall, S. Sunde, M. Tsypkin, R. Tunold, Int. J. Hydrogen Energy 32 (2007) 2320.

[19] S. Trasatti, Electrodes of Conductive Metallic Oxides (Part B), Elsevier, Amsterdam, 1981.

[20] A. Benedetti, P. Riello, G. Battaglin,A. De Battisti, J. Electroanal. Chem. 376 (1994) 195.

[21] A. de Oliveira-Sousa, M.A.S. da Silva, S.A.S. Machado, L.A. Avaca, P. de Lima-Neto, Electrochim. Acta 45 (2000) 4467.

[22] Y. Shimizu, K. Uemura, H. Matsuda, N. Miura, N. Yamazoe, J. Electrochem. Soc. 137 (1990) 3430.

[23] Z. Hou, B. Yia, H. Zhang, J. Electrochem. Solid State Lett. 6 (2003) A232.

[24] W.T. Grubb, D.W. Mckee, Nature 210 (1966) 192 (London).

[25] A.C.C. Tseung, H.L. Bevan, J. Electroanal. Chem. 45 (1973) 429.

[26] M. Kato, S. Maezawa, K. Sato, Appl. Energy 59 (1998) 261.

[27] E.E. Frandon, D. Pletcher, Electrochim. Acta 42 (1997) 1281.

[28] G.R. Dieckmann, S.H. Langer, Electrochim. Acta 44 (1998) 437.

[29] E. Slavcheva, V. Nikolova, T. Petkova, E. Lefterova, I. Dragieva, T. Vitanov, E. Budevski, Electrochim. Acta 50 (2005) 5444.

[30] Lj.M. Vracar, N.V. Krstajic, V.R. Radmilovic, M.M. Jaksic, J. Electroanal. Chem. 587 (2006) 99.

[31] V. Antonucci, A. Di Blasi, V. Baglio, R. Ornelas, F. Matteucci, J. Ledesma-Garcia, L.G. Arriaga, A.S. Aricò, Electrochim. Acta 53 (2008) 7350.

[32] S. Ardizzone, G. Fregonara, S. Trasatti, Electrochim. Acta 35 (1990) 263.

[33] A.S. Aricò, V. Antonucci, V. Alderucci, E. Modica, N. Giordano, J. Appl. Electrochem. 23 (1993) 1107.

[34] J.F. Moulder, W.F. Stickle, P.E. Sobol, K.D. Bomben, Handbook of X-ray Photoelectron Spectroscopy, Physical Electronics Inc., 1995.

[35] R.S. Chen, H.M. Chang, Y.S. Huang, D.S. Tsai, S. Chattopadhyay, K.H. Chen, J. Crystal Growth 271 (2004) 105.

[36] L.A. da Silva, V.A. Alves, S.C. de Castro, J.F.C. Boodts, Colloids Surf. A: Physicochem. Eng. Aspects 170 (2000) 119.

[37] S. Siracusano, V. Baglio, C. D'Urso, V. Antonucci, A.S. Aricò. Preparation and characterization of titanium suboxides as conductive supports of IrO_2

electrocatalysts for application in SPE electrolysers. Electrochimica Acta 54 (2009) 6292–6299.

List of the publications and oral presentation related to the thesis

During the period of my thesis, I have produced the following publications:

1. S. Siracusano, T. Denaro, V. Antonucci, A. S. Arico`, C. Urgeghe, F. Federico, "Degradation of oxygen-depolarized ag-based gas diffusion electrodes for chlor-alkali cells" J. Appl. Electrochem. (2008) 38:1637-1646
2. S. Siracusano, A. Stassi, V. Baglio, A.S. Aricò, F. Capitanio, A.C. Tavares. Investigation of carbon-supported Pt and PtCo catalysts for oxygen reduction in direct methanol fuel cells. Electrochimica Acta 54 (2009) 4844–4850
3. S. Siracusano, V. Baglio, C. D'Urso, V. Antonucci, A.S. Aricò, "Preparation and characterization of titanium suboxides as conductive supports of IrO2 electrocatalysts for application in SPE electrolysers", Electrochimica Acta 54 (2009) 6292–6299
4. J. C. Cruz, V. Baglio, S. Siracusano, R. Ornelas, L. Ortiz-Frade, L.G. Arriaga, V. Antonucci, A. S. Aricò, "Nanosized IrO2 electrocatalysts for oxygen evolution reaction in an SPE electrolyser" J Nanoparticle Res. DOI 10.1007/s11051-010-9917-2
5. J. C. Cruz, V. Baglio, S. Siracusano, V. Antonucci, A. S. Aricò, R. Ornelas, G. Osorio-Monreal, L. Ortiz-Frade, L.G. Arriaga "Synthesis and characterization of RuO2 catalysts for oxygen evolution in a solid polymer electrolyte electrolyzer" Int. J Hydrogen Energy. Submitted
6. S. Siracusano, V. Baglio, A. Di Blasi, N. Briguglio, A. Stassi, R. Ornelas, E. Trifoni, V. Antonucci, A. S. Aricò "Electrochemical characterization of single cell and short stack PEM electrolyzers based on a nanosized IrO_2 anode electrocatalyst". Int. J Hydrogen Energy: 35(2010)5558-5568
7. P. Frontera, V. Modafferi, F. Frusteri, G. Bonura, M. Bottari, S. Siracusano, P.L. Antonucci. "Catalytic Features of Ni/Ba-Ce0.9-Y0.1 Catalyst to Produce Hydrogen for PCFCs by Methane Reforming". Int. J Hydrogen Energy. Accepted for publication.

Furthermore, I have contributed to the following conferences:

- C. Urgeghe, F. Federico, A.S. Aricò, V. Antonucci, T. Denaro, S. Siracusano. "Study of oxygen-depolarized Ag-based cathode catalysts for electrolysis in chlor-alkali cell". GEI- ERA, Cagliari, Luglio 2007
- C. Urgeghe, F. Federico, DeNora A.S. Aricò, V. Antonucci, T. Denaro, S. Siracusano. "Study of oxygen-depolarized Ag-based cathode catalysts for electrolysis in chlor-alkali cell". 58th annual meeting of ISE , Banff (Canada), Settembre 2007
- S. Siracusano, V. Baglio, C. D'Urso, V. Antonucci, A.S. Aricò, J.C. Cruz, L. Ortiz-Frade, L.G. Arriaga, R. Ornelas IrO2 electrocatalysts for oxygen evolution reaction in an SPE electrolyzer. WHTC 2009, 26-28 August, New Delhi, India.
- S. Siracusano, P. Frontera, V. Modafferi, F. Frusteri, G. Bonura, P. L. Antonucci. "Catalytic Features of Ni/Ba-Ce0.9-Y0.1 Catalyst to Produce Hydrogen for PCFCs by Methane Reforming". HYCELTEC 2009, II Iberian Symposium on Hydrogen, Fuel Cells and Advanced Batteries, Vila Real, 13-17 September 2009, Portogallo.
- S. Siracusano, V. Baglio, V. Antonucci, A. S. Aricò, R. Ornelas, J. C. Cruz, L. Ortiz-Frade, L.G. Arriaga. "Investigation of iridium oxide electrocatalysts for the O2 evolution reaction in solid polymer electrolyte water electrolysers". Hysydays 2009, Torino Expo - October 7-9, 2009